### LIBRARY Michigan State University

PLACE IN RETURN BOX to remove this checkout from your record. TO AVOID FINES return on or before date due.

DATE DUE	DATE DUE	DATE DUE

MSU Is An Affirmative Action/Equal Opportunity Institution c:/circ/datadus.pm3-p.1

### DIELECTRIC AND ELECTROCHEMICAL PROPERTIES OF SMECTITE CLAYS AND LAYERED DOUBLE HYDROXIDES

Вy

### Padmananda De Silva Kaviratna

### **A DISSERTATION**

Submitted to

Michigan State University

in Partial Fulfillment of the Requirements

for the Degree of

**DOCTOR OF PHILOSOPHY** 

Department of Chemistry

### **ABSTRACT**

### DIELECTRIC AND ELECTROCHEMICAL PROPERTIES OF SMECTITE CLAYS AND LAYERED DOUBLE HYDROXIDES

B y

### Padmananda De Silva Kaviratna

The main objective of this work is to identify and understand the fundamental relationships between the structural and dielectric properties of 2:1 layered silicates. The dielectric properties of oriented films of fluorohectorite, laponite and montmorillonite were measured as a function of relative water vapor pressure. Water sorption and frequency dependence (40-10<sup>5</sup> Hz) of the conductivity and dielectric constant of these materials have also been studied.

Both conductivity and dielectric constant of smectite clays increase with increasing layer charge density and decreasing q/r (q = charge, r = ionic radius) of gallery cations. They also increase non linearly with increasing water content. However, neither property changes substantially during the adsorption of the first monolayer, but, thereafter, both conductivity and dielectric constant increase rapidly as additional water beyond a monolayer is adsorbed. Very high dielectric constants are obtained. Conductivity increases with increasing frequency whereas dielectric constant decreases with increasing frequency.

### Padmananda De Silva Kaviratna

 $Ru(NH_3)6^{3+}$ -laponite films supported on graphite electrodes exhibited cyclic voltammograms with a well defined  $Ru(NH_3)6^{3+/2+}$  wave. The concentration and nature of the cation in the supporting electrolyte greatly affected the peak currents of the homoionic  $Ru(NH_3)6^{3+}$  clay, whereas the electroactivity of the ion paired  $Fe(bpy)_3^{2+}/SO_4^{2-}$  centers were not affected by the electrolyte cation. The decrease in the electroactivity of homoionic  $Ru(NH_3)6^{3+}$ -montmorillonite with increasing electrolyte concentration was attributable to the exchange of  $Ru(NH_3)6^{3+}$  by electrolyte cations. A mechanism has been suggested for maintaining electrical neutrality upon electron transfer in these clay films.

Although it is highly plausible that lattice iron can involve in the electrochemistry of clay modified electrodes, alternative mechanisms can be suggested because of the possible decomposition and demetalation of metal complexes on clay surfaces. Therefore, we further studied the system by using non ferruginous clays in order to determine whether such a clay can also participate in these catalytic reactions. It was found that only ferruginous clays exhibit electrocatalytic activity confirming the true lattice iron effect.

Dependency of the electroactivity on the pH of the supporting electrolyte was studied. It was clearly noticed that the electroactivity of  $Ru(NH_3)_6^{3+}$  is independent of the pH of the supporting electrolyte whereas that of  $Fe(bpy)_3^{2+}$  decreased with decreasing pH.

### Padmananda De Silva Kaviratna

Electrochemistry at clay modified electrodes depends upon the surface density of the clay coating. For Ru(NH<sub>3</sub>)<sub>6</sub><sup>3+</sup> pre-exchanged into laponite, electroactivity decreases beyond a certain surface density (about 500 μg cm<sup>-2</sup>) of the clay coating probably due to the increasing difficulty to maintain the electrical neutrality within the clay film. However, electrodes presoaked in the electroactive species solutions did not show a maximum within the densities studied (~25-3000 μg cm<sup>-2</sup>). This is probably due to the disordered structure of the clay coating upon prolonged soaking.

To my brother and guardian, Jayananda whose love and dedication made this possible.

And also in memory of my parents

### **ACKNOWLEDGEMENTS**

I would like to thank Dr. Thomas J. Pinnavaia for his guidance and financial support throughout this work. His deep understanding of chemistry as well as nature of the human being made me really comfortable working with him as a graduate student. I would also like to thank Dr. Peter A. Schroeder for his guidance. His dedication in writing of this manuscript is also acknowledged. I am grateful to Dr. Mercouri G. Kanatzidis for critically reading the manuscript. I am also thankful to Dr. Stanley R. Crouch for his commitment with the limited time offered.

It is always a pleasure to remember the work and amusement I had with Dr. Dimitris Petridis and Dr. Eiichi Narita during their stay at Michigan State University. Financial assistance from the Department of Chemistry, Center for Fundamental Materials Research and the National Science Foundation is also acknowledged.

Special thanks are due for my wife, Hema, and son, Lakmal, for their love, affection, help and constant encouragement. Thanks should also be extended to include all my friends, specially members of Dr. Pinnavaia's group and Dr. Schroeder's group for their help and friendship.

### **TABLE OF CONTENTS**

Chapter Page
LIST OF TABLESxi
LIST OF SCHEMESxiii
LIST OF FIGURESxiv
CHAPTER I. Introduction
I.a Objective and rationale1
I.b Structure and properties of smectite clays3
I.c Layered double hydroxides10
I.d List of references13
CHAPTER II. Dielectric properties of smectite clays16
II.a Background16
Dipolar relaxation22
Maxwell-Wagner effects27
Electrode polarization33
Double layer effects37

Chapter		Page
	Clay minerals in geological media	43
	Water adsorbed on smectite clays	44
	Dielectric properties of water adsorbed clay	50
II.b	Experimental	53
	Materials	53
	Instrumentation	54
II.c I	Results and discussion	57
	X-Ray analysis	57
	Water adsorption isotherms	62
	Effects of water and type of gallery cations on	
	dielectric properties	69
	Effects of layer charge	76
	Effects of frequency of the applied voltage	79
II.d(	Conclusions	79
II e l	List of references	84

Chapter	Page
CHAPTER III. Electrochemical properties of smectite clays	88
III.a Background	88
Cyclic voltammetry	100
Stirred-solution voltammetry	103
III.b Experimental	107
Synthesis of metal complexes	107
Construction of graphite working electrodes	108
Preparation of clay modified electrodes	109
Instrumentation	109
III.c Results and Discussion	110
Electroactive Ru(NH <sub>3</sub> ) <sub>6</sub> <sup>3+</sup> gallery cations in clay	<i>i</i>
modified electrodes	110
Confirmation of the electrocatalytic activity of	
lattice iron in clay modified electrodes	126
Effects of the electrolyte pH on the	
electrochemistry at clay modified electrodes	133

Chapter P	age
Effects of the surface density of clay coating on	
the electrochemistry at clay modified electrodes	.142
III.d Conclusions	146
III.e List of references	150
CHAPTER IV Layered double hydroxide modified	
lectrodes	163
IV.a Background	163
Polyoxometalates (POM)	.163
IV.b Experimental	164
Preparation of polyoxometalate intercalated	
layered double hydroxides	164
Preparation of LDH modified electrodes	166
IV.c Results and discussion	167
IV.d Conclusions	172
IV.e List of references	173

### LIST OF TABLES

Table	Page
I.1	Idealized structural formulae for representative 2:1  Phyllosilicates
II.1	A Comparison of physical properties of smectite clays and amorphous silica
II.2	Time scales for adsorbed water structure and the experimental methods used to measure the properties of adsorbed water
II.3	Comparison of physical properties of laponite,  montmorillonite and fluorohectorite
III.1	Dependence of initial peak current (µA) on supporting electrolytes for electroactive centers in montmorillonite-modified electrodes
III.2	Dependance of initial peak current (µA) on pH of the supporting electrolyte, 0.1 M sodium acetate and acetic acid buffer, for electroactive centers in montmorillonite-modified electrodes

Table	P	a g e
III.3	Dependance of initial peak current (µA) on pH of the supporting electrolyte, 0.1 M sodium trichloroacetate	
	and trichloroacetic acid buffer, for electroactive centers in montmorillonite-modified electrodes	.137
III.4	Dependance of initial peak current (µA) on pH of the soaking solution, 0.1 M sodium trichloroacetate and trichloroacetic acid buffer, for electroactive centers in montmorillonite-modified electrodes. supporting electrolyte was always a 0.1 M sodium acetate and acetic acid buffered at pH 7	129
	acetic acid buffered at pH 7	138

### LIST OF SCHEMES

Scheme	<b>e</b>	Page
I.I	Classification of clay minerals	2
III.1	Electrical neutrality mechanism	122
III.2	Proposed scheme for the catalytic reaction	134

### LIST OF FIGURES

Figure		Page
I.1	Idealized structure of a smectite clay mineral. Open circles, oxygen atoms; Filled circles, hydroxyl groups. Silicon and sometimes aluminum normally occupy tetrahedral positions in the oxygen framework. Aluminum, magnesium, iron or lithium may occupy octahedral sites. $M^{n+}$ . $xH_2O$ represents the interlayer exchange cation	
1.2	Structure of the basic layered double hydroxide, hydrotalcite, [Mg <sub>3</sub> Al(OH) <sub>8</sub> ][CO <sub>3</sub> ] <sub>0.5</sub> .2H <sub>2</sub> O	12
II.1	Real (E') and imaginary (E") parts of the complex dielectric constant of a suspension of polystyrene particles as a function of frequency	
II.2	Cole-Cole (ε" against ε') plot. The same data as presented in II.1	25
II.3	A simple equivalent circuit for modelling the Maxwell-Wagner effect in a clay sample	30

Figure	Page
II.4	Idealized view of the polarization due to dipoles and ions. (A) Unpolarized; (B) Orientation and conduction begins; (C) Fully polarized. In actual materials, both process can occur simultaneously34
11.5	Equivalent circuit that includes a blocking layer35
II.6	Theoretical Cole-Cole plots for various L/2t <sub>b</sub> 38
II.7	(A) Formation of a double layer around a charged spherical surface. Zero applied field. (B) An unchanged particle with no counter ions in an applied field. Polarization of the particle cause attraction of the charges as indicated producing a current. If I is in phase with E, the impedance, Z of the system is resistive and there is no effect on the dielectric constant. On the other hand if I has an out-of-phase component then the impedance, $Z = R + 1/i\omega C$ and the capacitive part enhances the dielectric constant.
II.8	Similar to the situation in Figure II.7.B. But with counter ions moving in phase with E and augmenting the dipolar distribution. Because of the counter ions, a larger out-of-phase current will be generated.  This causes a great enhancement in the dielectric

constant......41

11.9	Chew and Sen Model for the Enhanced Double Layer.
	A= Polarized charge, B= Double layer, C= Neutral
	diffusion cloud and D= Circumferential current.
	According to Chew and Sen the most important
	effect is the development of a neutral layer of
	charges consisting of equal negative and positive
	charges. Incoming current has two components (1).
	a normal ohmic current I $\propto$ E (2). diffusional current
	$I = \frac{dN}{dx}$ . The diffusional current is out-of-phase with
	the applied field causing the dielectric
	enhancement42
TT 10	
II.10	Spatial arrangement of water molecules solvating
	exchangeable Li <sup>+</sup> cations on hectorite as determined
	by IR spectroscopy. (A) section view in the plane
	ab; (B) plane view. M denotes the transition dipole
	moment for the symmetric (s) and asymmetric (as)
	stretching modes47
II.11	A Spatial arrangement of water molecules in the
	interlamellar or galley region of montmorillonite
	containing monovalent exchangeable cations, as
	determined by dielectric relaxation spectroscopy.
	(A) section view in the plane ab; (B) plane view. The
	shaded circles denote clay surface oxygen atoms49

Figure		Page
II.12	Schematic representation of the stereochemistry of hydrated Cu <sup>2+</sup> as determined by ESR spectroscopy.  (A) one layer of water; (B) two layers of water occupy the interlamellar regions	
II.13	A simplified circuit of the measuring bridge indicating the equivalent circuit elements $C$ and $G$ measured by the bridge, and the connection to the guard-ring. $C_S$ and $G_S$ are standard capacitances and conductances respectively. $D$ is a dual phase	
II.14	X-ray patterns of air dried films of Na+-	56
	fluorohectorite, Na+-montmorillonite and Na+- laponite	58
II.15	d-spacing versus relative water vapor pressure of Li+-fluorohectorite	
II.16	Water adsorption/desorption isotherm of Li+- fluorohectorite	
II.17	Water adsorption/desorption isotherm of Na+- fluorohectorite	65
II.18	Water adsorption/desorption isotherm of Cu <sup>2+</sup> - fluorohectorite	66
Figure		Page

II.19	d-spacing and water adsorption versus relative	
	water vapor pressure of Li+-fluorohectorite	67
II.20	d-spacing and water adsorption versus relative	
	water vapor pressure of Na+-fluorohectorite	68
II.21	Water adsorption/desorption isotherm of Na+-	
	montmorillonite	70
II.22	Water adsorption/desorption isotherm of Na+-	
	laponite	71
II.23	Water dependency of the relative permittivity of	
	Li <sup>+</sup> -fluorohectorite, Na <sup>+</sup> -fluorohectorite and Cu <sup>2+</sup> -	
	fluorohectorite. $M_b$ = Monolayer begins; $M_e$ =	
	Monolayer ends; $B_h$ = Bilayer begins; $B_e$ = Bilayer	
	ends	72
II.24	Water dependency of the conductivity of Li+-	
	fluorohectorite, Na+-fluorohectorite and Cu <sup>2+</sup> -	
	fluorohectorite. $M_b = Monolayer begins; M_e =$	
	Monolayer ends; $B_b$ = Bilayer begins; $B_e$ = Bilayer	
	ends	73
11.25	d-spacing of Li <sup>+</sup> -fluorohectorite and Na <sup>+</sup> -	
	fluorohectorite as a function of the percentage water	
	content of the clay	75
Figure	D	9 6 6

II.26	Water dependency of the relative permittivity of	
	Na+-fluorohectorite, Na+-montmorillonite and Na+-	
	laponite	77
II.27	Water dependency of the conductivity of Na+-	
	fluorohectorite, Na+-montmorillonite and Na+-	78
	laponite	
II.28	Cole-Cole (ε" Vs ε') of Na+-fluorohectorite	80
II.29	Frequency dependence of the relative permittivity	
	of Na+-fluorohectorite	81
11.30	Frequency dependence of the conductivity of Na+-	
	fluorohectorite	82
III.1	A simplified model for a surface modified electrode	89
III.2		
	electroactivity of Fe(bpy) <sub>3</sub> <sup>2+</sup> at clay modified	101
	electrodes	101
III.3	(A) An idealized cyclic potential sweep and (B) the	100
	resulting cyclic voltammogram	102
III.4	•	106
	solution voltammetry	105
Figure	P	226

An idealized concentration profiles in stirred solution voltammetry. (A) Unperturbed or $E_{app} << E^{0'}$ (B) $E_{app} = E^{0'}$ (C) $E_{app} >> E^{0'}$	.106
Homoionic Ru(NH <sub>3</sub> ) <sub>6</sub> <sup>3+</sup> loaded by pre-exchange in	
Na <sup>+</sup> -laponite. Supporting electrolyte was 0.05 M Na <sub>2</sub> SO <sub>4</sub> . Scan rate 100 mV Sec <sup>-1</sup>	111
Time dependency of normalized i <sub>pc</sub> of homoionic Ru(NH <sub>3</sub> ) <sub>6</sub> <sup>3+</sup> and ion paired Fe(bpy) <sub>3</sub> <sup>2+</sup> at montmorillonite-modified electrodes in 0.05 M CH <sub>2</sub> CO <sub>2</sub> Na supporting electrolyte buffered at pH 3.	
	112
Time dependency of normalized i <sub>pc</sub> of homoionic Ru(NH <sub>3</sub> )6 <sup>3+</sup> in different concentrations of Na <sub>2</sub> SO <sub>4</sub> supporting electrolyte. Scan rate 100 mV sec <sup>-1</sup>	115
Normalized peak current $i_p(t=24) / i_p(t=0)$ of homoionic Ru(NH <sub>3</sub> ) <sub>6</sub> <sup>3+</sup> and ion paired Fe(bpy) <sub>3</sub> <sup>2+</sup> in different concentrations of Na <sub>2</sub> SO <sub>4</sub> supporting electrolyte. Scan rate 100 mV sec <sup>-1</sup>	116
Time dependency of normalized $i_{pc}$ of homoionic $Ru(NH_3)6^{3+}$ in 0.01 M concentrations of different	
	solution voltammetry. (A) Unperturbed or $E_{app} \ll E^{0'}$ (B) $E_{app} = E^{0'}$ (C) $E_{app} \gg E^{0'}$

Figure

III.11	P. P.
	homoionic $Ru(NH_3)_6^{3+}$ and ion paired $Fe(bpy)_3^{2+}$ in
	0.01 M concentrations of different supporting
	electrolytes. Scan rate 100 mV sec <sup>-1</sup> 119
III.12	X-ray diffraction patterns of homoionic
	montmorillonite. (A) Na+-montmorillonite; (B)
	$Ru(NH_3)_6^{3+}$ -montmorillonite; (C) $Fe(bpy)_3^{2+}$
	montmorillonite; (D)Ru(NH <sub>3</sub> ) <sub>6</sub> <sup>3+</sup> -montmorillonite
	/glycerin; (E) Fe(bpy) <sub>3</sub> <sup>2+</sup> -montmorillonite/glycerin124
III.13	X-ray diffraction patterns of homoionic
	montmorillonite. (A) Na+-montmorillonite; (B)
	$Ru(NH_3)_6^{3+}$ -montmorillonite; (C) $Fe(bpy)_3^{2+}$ -
	montmorillonite; (D)Ru(NH <sub>3</sub> ) <sub>6</sub> <sup>3+</sup> -montmorillonite/0.1
	M NaCl; (E) Fe(bpy) <sub>3</sub> <sup>2+</sup> -montmorillonite/0.1 M NaCl125
III.14	Cathodic Limiting Currents for Stirred solution
	voltammograms: A) Bare graphite electrode in 0.05
	M CH <sub>3</sub> CO <sub>2</sub> Na pH 3 buffer electrolyte containing 10 <sup>-5</sup>
	M Ru(NH <sub>3</sub> ) $6^{3+}$ . B) Bare graphite electrode in 0.05 M
	CH <sub>3</sub> CO <sub>2</sub> Na pH 3 buffer electrolyte containing 10 <sup>-5</sup> M
	$Ru(NH_3)_6^{3+}$ and 0.1 M $H_2O_2$ . C) Na <sup>+</sup> -montmorillonite
	coated graphite electrode in 0.05 M CH <sub>3</sub> CO <sub>2</sub> Na pH 3
	buffer containing 10 <sup>-5</sup> M Ru(NH <sub>3</sub> ) <sub>6</sub> <sup>3+</sup> . D) Na <sup>+</sup> -
	laponite coated graphite electrode in 0.05 M

Figure

	CH <sub>3</sub> CO <sub>2</sub> Na pH 3 buffer containing 10-5 M	
	Ru(NH <sub>3</sub> ) <sub>6</sub> <sup>3+</sup> and 0.1 M H <sub>2</sub> O <sub>2</sub> . E) Na <sup>+</sup> -montmorillonite	
	coated graphite electrode in 0.05 M CH <sub>3</sub> CO <sub>2</sub> Na pH 3	
	buffer containing 0.1 M H <sub>2</sub> O <sub>2</sub> . F) Na+-	
	montmorillonite coated graphite electrode in 0.05 M CH <sub>3</sub> CO <sub>2</sub> Na pH 3 buffer containing 10-5 M	
	$Ru(NH_3)_6^{3+}$ and 0.1 M $H_2O_2$ . G) Na <sup>+</sup> -nontronite	
	coated graphite electrode in 0.05 M CH <sub>3</sub> CO <sub>2</sub> Na pH 3	
	buffer containing $10^{-5}$ M Ru(NH <sub>3</sub> ) <sub>6</sub> <sup>3+</sup> and 0.1 M	
	H <sub>2</sub> O <sub>2</sub> . A 1 % clay sample was used to coat the	
	electrodes (0.18cm <sup>2</sup> ). The amount of clay on the	
	electrode was found to be 4 X 10-4 g cm-2	128
III.15	Cyclic voltammograms of clay coated graphite	
	electrodes soaked in 1 mM Ru(NH <sub>3</sub> ) <sub>6</sub> <sup>3+</sup> for 24 hrs	
	and then rinsed with deionized water. The	
	electrolyte was 0.05 M CH <sub>3</sub> CO <sub>2</sub> Na in a pH 3 buffer.	
	a) Na+-laponite; b) Na+-montmorillonite and c) Na+-	
	nontronite	131
III.16	Cyclic voltammograms of graphite electrodes coated	
	with equivalent amounts of Na+-montmorillonite. a)	
	pre-reduced with 0.1 M Na <sub>2</sub> S <sub>2</sub> O <sub>4</sub> and then soaked in	
	1 mM Ru(NH <sub>3</sub> ) <sub>6</sub> <sup>3+</sup> for 30 mins. b) Pristine mineral	
	without pre-reduction or pre-oxidation. c) pre-	
	oxidized with 5 M H <sub>2</sub> O <sub>2</sub> and then soaked in 1 mM	

Figure

	$Ru(NH_3)_6^{3+}$ for 30 mins. The electrolyte solution	
	was 0.05 M CH <sub>3</sub> CO <sub>2</sub> Na in a pH 3 buffer	132
III.17	Cyclic voltammogram of Fe(CN)6 <sup>3-</sup> at a	
	montmorillonite coated graphite electrode pre-	
	soaked in 1 mM K <sub>3</sub> Fe(CN) <sub>6</sub> for 24 hrs. Supporting	
	electrolyte was 0.05 M sodium sulfate pH 7.0. $\nu$ =	
	100 mV sec <sup>-1</sup>	140
III.18	Cyclic voltammograms of Fe(CN)6 <sup>3</sup> at (A)	
	montmorillonite clay coated graphite electrode	
	soaked in 1 mM $Fe(CN)_6^3$ containing 0.1 M	
	CH <sub>3</sub> CO <sub>2</sub> Na pH 4 for 1 hr; (B) Bare graphite electrode	
	soaked in 1 mM Fe(CN) <sub>6</sub> <sup>3</sup> - containing 0.1 M	
	CH <sub>3</sub> CO <sub>2</sub> Na pH 4 for 24 hrs. (C) The same as (A) but	
	soaked for 24 hrs	141
III.19	Effect of the amount of clay added on cyclic	
	voltammetry of $Ru(NH_3)_6^{3+}$ pre-exchanged into	
	laponite	143
III.20	Effect of the amount of clay added on bulk	
	electrolysis of $Ru(NH_3)_6^{3+}$ pre-exchanged into	
	laponite	145
III.21	Effect of the amount of clay added on cyclic	
	voltammetry of $Ru(NH_3)_6^{3+}$ and $Fe(bpy)_3^{2+}$ at	
Figure		Page

laponite	coated graphite electrodes soaked in 1 mM solutions of Ru(NH <sub>3</sub> ) <sub>6</sub> <sup>3+</sup> and Fe(bpy) <sub>3</sub> <sup>2+</sup> 147
IV.1	Structure of (A) Keggin-type and (B) lacunary  Keggin-type polyoxometalates165
IV.2	Cyclic voltammogram of $SiW_{11}O_{39}^{8-}$ at a bare graphite and a hydrotalcite coated graphite electrode. Supporting electrolyte was 0.1 M sodium acetate buffer pH 5. $v=100$ mV sec <sup>-1</sup>
IV.3	Cýclic voltammogram of $SiW_{11}O_{39}^{8-}$ at a hydrotalcite coated graphite electrode (pre-soaked). Supporting electrolyte was 0.1 M sodium acetate buffer pH 5. $v=100$ mV sec <sup>-1</sup>
IV.4	Cyclic voltammogram of SiW <sub>11</sub> O <sub>39</sub> <sup>8-</sup> at a hydrotalcite coated graphite electrode (pre-exchanged). Supporting electrolyte was 0.1 M sodium acetate buffer pH 5. v= 100 mV sec <sup>-1</sup> 170
IV.5	Cyclic voltammogram of Fe(CN)6 <sup>3-</sup> at a hydrotalcite coated graphite electrode (pre-exchanged).  Supporting electrolyte was 0.05 M sodium sulfate.  V= 100 mV sec <sup>-1</sup>

### CHAPTER I

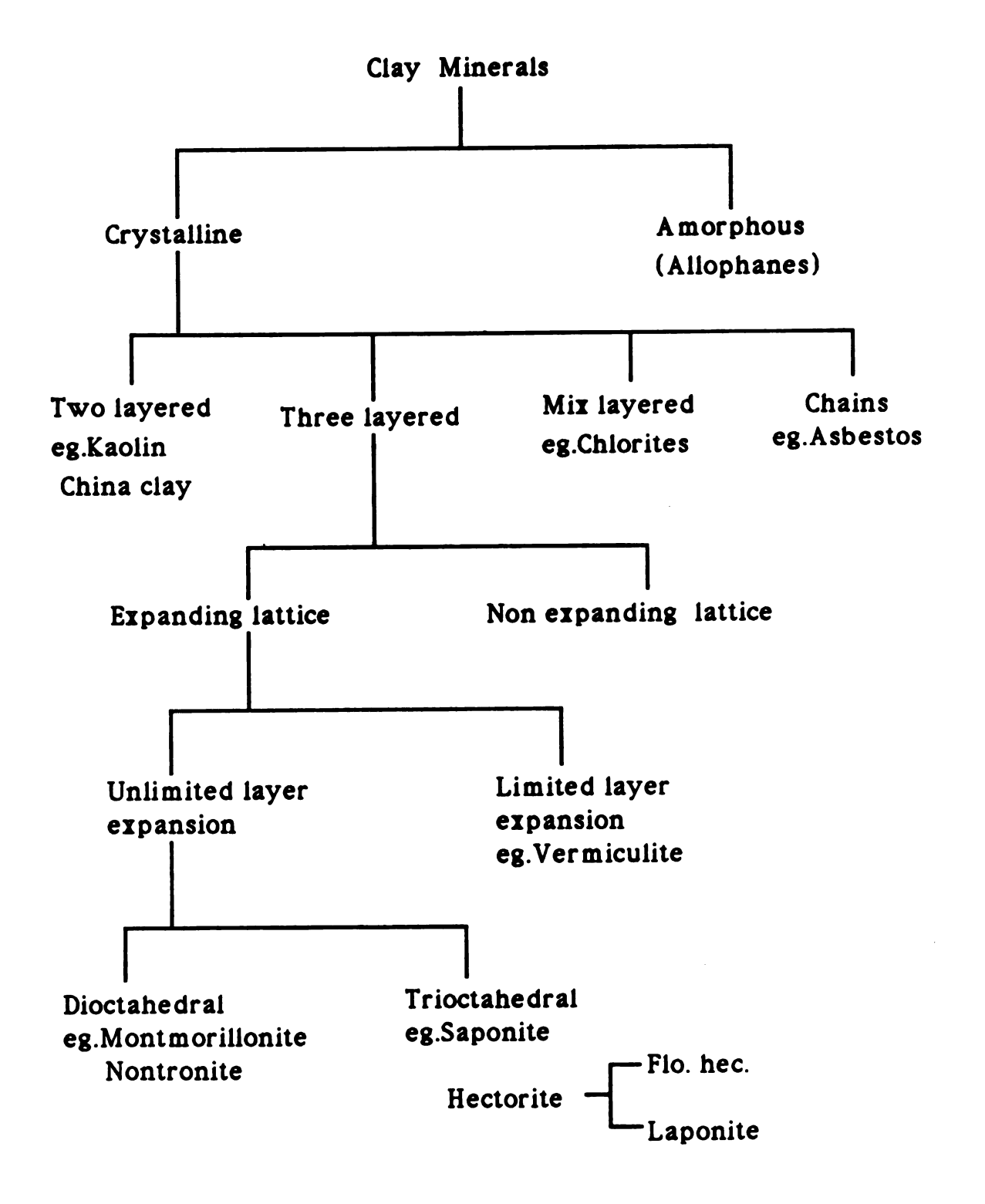
### INTRODUCTION

### I.a Objective and Rationale.

Complex layered alumino silicates, commonly known as clay minerals, and their derivatives are a major class of compounds that are currently being investigated for their fundamental materials properties. Scheme I.1 shows the vast variation of structural types among the clay minerals. They have a wide spectrum of forms varying from amorphous powder, chain structure, layered structure to single crystals. Among all the above clay minerals, 2:1 layered clays with an expanding lattice, known as smectites are the most widely studied clay minerals due to their wide range of chemical and physical characteristics. The intercalation properties of these clay minerals make available a vast variety of derivatives. The ability of these materials to swell and undergo pillaring is also a significance factor. Because of these properties and their ready availability, the smectites are being investigated for potential applications in modified electrodes<sup>1-4</sup>, heterogeneous catalysis<sup>5-6</sup>, composites<sup>7</sup>, ceramics<sup>8</sup>, electrical<sup>9</sup> and electronics<sup>10</sup> devices.

The main objective of this work was to identify and understand the fundamental relationships between the structural and dielectric properties of 2:1 layered silicates for possible applications as sensors. And also it is our aim to establish the dependence of the dielectric

Scheme I.1 Classification of Clay Minerals



properties on the layer charge density, nature of the gallery ions and percentage of water content. This fundamental knowledge could lead to important applications of these layered silicates in new generations of electronics materials. Smectite clays exhibit unusual dielectric properties including high dielectric breakdown voltages. Such physical properties are related to the structure and chemistry of these compounds and this interplay is an exciting area of fundamental study.

The second goal of this research was to understand the fundamentals that govern the electrochemistry at clay modified electrodes. Electrode surfaces containing a thin coating of smectite clay are potentially useful for electrocatalytic reactions and sensor applications. It is important to understand the electrochemical behavior of electroactive species in order to develop a sensor or to generate an electrocatalytic system.

The third aim of this study was to extend the electrochemistry of smectite clays to layered double hydroxides (anionic clays) with robust inorganic cluster anions such as polyoxometalates. 11-13 Polyoxometalates are known to exhibit very interesting and important electrocatalytic reactions. 14

### I.b Structure and Properties of Smectite Clays.

The idealized oxygen framework of a 2:1 clay is shown in Figure I.1. The oxyanion layer consists of two inverted silicate

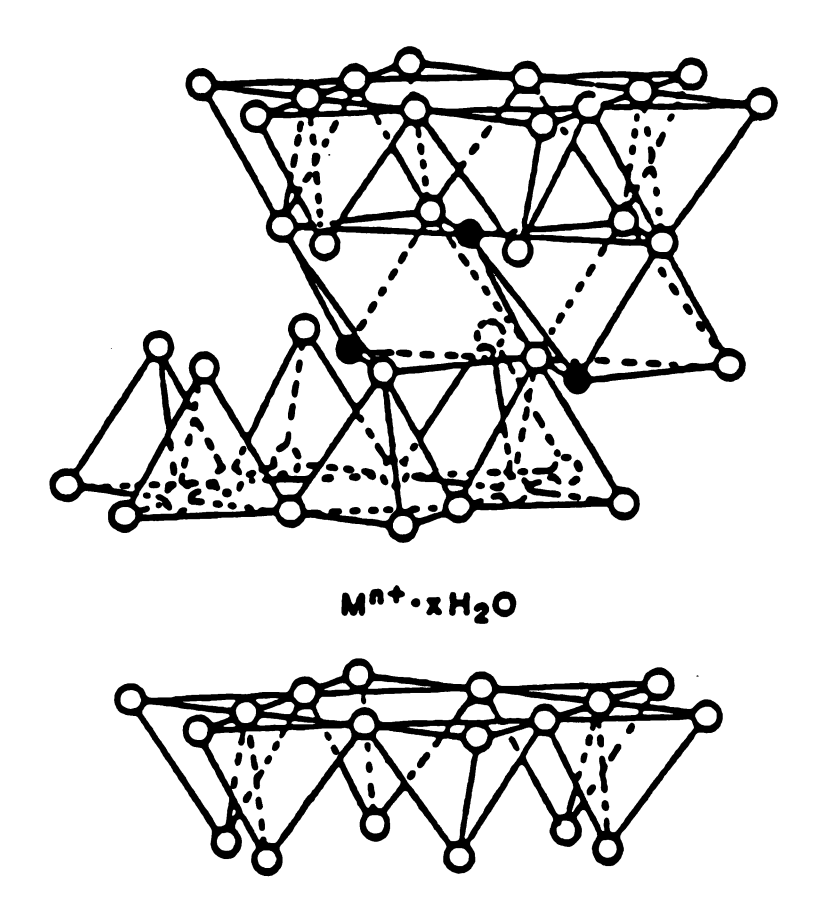


Figure I.1 Idealized structure of a smectite clay mineral. Open circles, Oxygen atoms; Filled circles, hydroxyl groups. Silicon and sometimes aluminum normally occupy tetrahedral positions in the oxygen framework. Aluminum, magnesium, iron or lithium may occupy octahedral sites.  $M^{n+}$ .  $xH_2O$  represents the interlayer exchange cation.

tetrahedral sheets sharing their apical oxygens with an octahedral The 2:1 relation between the tetrahedral and octahedral sheet. sheets within a layer allows these clays to be classified as 2:1 phyllosilicates. In a unit cell formed from twenty oxygens and four hydroxyl groups, there are eight tetrahedral sites and six octahedral sites along with four cavities surrounded by a six-membered oxygen ring on the surface. When two thirds of the octahedral sites are occupied by cations, the mineral is classified as a dioctahedral 2:1 A trioctahedral 2:1 phyllosilicate has all the phyllosilicate. octahedral sites filled with cations. Based on the magnitude of the layer charge per unit cell, 2:1 phyllosilicates are divided into five groups; talc-pyrophillite, smectite, vermiculite, mica and brittle mica. The members of each group are distinguished by the type and location of cations in the oxygen framework. The idealized chemical formulae of various kinds of 2:1 phyllosilicates are summarized in Table I.1.

In talc, all the tetrahedral and octahedral sites are filled by Si<sup>4+</sup> and Mg<sup>2+</sup> respectively, and the layers are electrically neutral. In pyrophyllite only two thirds of the octahedral sites are occupied by Al<sup>3+</sup> ions leaving a neutral aluminosilicate layer. Therefore, in crystals of these minerals the layers are coupled through relatively weak dipolar and van der Waals forces.<sup>15</sup> In contrast to talc and pyrophyllite, the layers in muscovite and phlogopite bear a net charge of 2 e<sup>-</sup> per Si<sub>8</sub>O<sub>20</sub> unit due to a positive charge deficiency which results from the substitution of Si<sup>4+</sup> by Al<sup>3+</sup> in tetrahedral positions. The charge deficiency is balanced by interlayer potassium

Table I.1 Idealized Structural	lized Structural Formulae for rej	Formulae for representative 2:1 Phyllosilicates. In each Formula
Parentheses and	Bracket Define Metal Ions in Te	Parentheses and Bracket Define Metal Ions in Tetrahedral and Octahedral Sites Respectively.
Mineral group	Dioctahedral	Trioctahedral
Pyrophyllite-Talc	lc Pyrophyllite [Al4](Si8)O <sub>20</sub> (OH)4	Talc [Mg <sub>6</sub> ](Si <sub>8</sub> )O <sub>20</sub> (OH)4
Smectite	Montmorillonite	Hectorite

 $\frac{x}{n} M^{n+} y H_2 O[A I_{4-x} Mg_x] (Si_8) O_{20} (OH)_4 \quad \frac{x}{n} M^{n+} y H_2 O[Mg_{6-x} Li_x] (Si_8) O_{20} (OH)_4$ 

(x = 0.4 - 1.2)

 $\frac{x}{n}$ M<sup>n+</sup> yH<sub>2</sub>O[Mg<sub>6-x</sub>] (Si<sub>8</sub>)O<sub>20</sub>(F)<sub>4</sub>

Fluorohectorite

## Table II.a Cont'd.

Beidellite	Saponite
$\frac{x}{n}M^{n+} yH_2O[AI_4] (Si_{8-x} AI_x) O_{20}(OH)_4$	$\frac{x}{n}$ Mn+ yH <sub>2</sub> O[ Mg <sub>6</sub> ] (Si <sub>8-x</sub> Al <sub>x</sub> )O <sub>20</sub> (OH) <sub>4</sub>
Nontronite	Laponite
$\frac{x}{n}M^{n+}$ yH <sub>2</sub> O[Fe <sub>4</sub> ] (Si <sub>8</sub> )O <sub>20</sub> (OH) <sub>4</sub>	$\frac{x}{n}M^{n+}yH_2O[Mg_{6-x}Li_x]$ (Sig)O <sub>20</sub> (OH)4

K<sub>2</sub>[Mg<sub>6</sub>] (Si<sub>6</sub>Al<sub>2</sub>)O<sub>20</sub>(OH)<sub>4</sub>

**Phlogopite** 

P
=
Ĕ
Con
_
a
II.a
4)
Ę
9
Table

•
<b>-</b>
=
=
ວ
•
Ξ
_
•
>
_

$$(x = 1.2 - 1.8)$$

### Vermiculite

$$\frac{x}{n}$$
Mn+ yH<sub>2</sub>O[Mg<sub>6</sub>] (Si<sub>8-x</sub>Al<sub>x</sub>)O<sub>20</sub>(OH)<sub>4</sub>

## Muscovite

## K<sub>2</sub>[Al<sub>4</sub>] (Si<sub>6</sub>Al<sub>2</sub>)O<sub>20</sub>(OH)<sub>4</sub>

### Clintonite

# Ca<sub>2</sub>[Mg<sub>4</sub>Al<sub>2</sub>] (Si<sub>2</sub>Al<sub>6</sub>)O<sub>20</sub>(OH)<sub>4</sub>

Ca<sub>2</sub>[Al<sub>4</sub>] (Si<sub>4</sub>Al<sub>4</sub>)O<sub>20</sub>(OH)<sub>4</sub>

Margarite

Brittle Mica

ions which are coordinated to the hexagonal arrays of oxygen atoms at the layer surface. Among the 2:1 layered phyllosilicates, the brittle mica group has the highest layer charge,  $4 e^-$  per  $Si_8O_{20}$  unit cell. The layer charge in vermiculite arises from the substitution of  $A1^{3+}$  for  $Si^{4+}$  in the tetrahedral layer. Vermiculite has a varying layer charge depending on the amount of substitution,  $1.2 - 1.8 e^-$  per  $Si_8O_{20}$  unit.

The charge on the layers of smectite is intermediate and varies from 0.4-1.2 e- per Si<sub>8</sub>O<sub>20</sub> unit.<sup>17</sup> To balance the layer charge, layers of hydrated cations are intercalated between the clay layers. The moderate layer charge in smectite clays, gives physical and chemical properties that are not found in the end members. In montmorillonite, the most familiar and common member of the smectite group, the layer charge originates from the substitution of octahedral Al3+ by Mg2+. Hectorite is also octahedrally charged with Li+ substituting for Mg<sup>2+</sup> in the octahedral sheet. Nontronite is a tetrahedrally charged smectite with Al3+ replacing Si4+ in the tetrahedral sheet and Fe<sup>3+</sup> replacing Al<sup>3+</sup> in the octahedral sheet. Laponite and fluorohectorite are synthetic hectorites and they represent two extremes in particle size and layer charge within the smectite group. Fluorohectorite has a particle size of up to about 2000 Å with a layer charge of 1.2 e- per SigO<sub>20</sub> unit and originates from the substitution of Li<sup>+</sup> for Mg<sup>2+</sup> in the octahedral layer while laponite has a particle size of 200 Å with a layer charge of 0.4 e<sup>-</sup> per SigO<sub>20</sub> unit as a results of substitution of Li<sup>+</sup> for Mg<sup>2+</sup> in the octahedral layer. In fluorohectorite, all the OH groups have been replaced by F. The layer charge in octahedrally charged clays is distributed over all oxygen in the framework. These clays tend to be turbostratic, that is the layers are randomly stacked with respected to the a-b planes of adjoining layers. The negative charge on the layers of the tetrahedrally charged smectites is more localized, and these derivatives tend to exhibit greater three dimensional order. 18-19

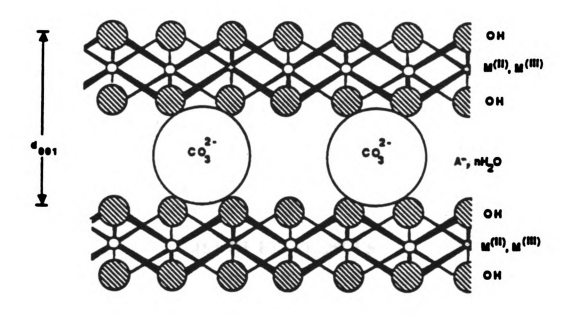
### I.c. Layered Double Hydroxides (LDHs).

Layered double hydroxides generally known as anionic clays are another class of materials that have been widely investigated for potential applications in catalysis<sup>20-22</sup> and medical applications.<sup>23-25</sup> They are also potentially useful candidates for the adsorption of environmentally hazardous anions from dilute aqueous waste streams.<sup>26</sup> The anion exchange characteristic of LDHs also allows them to be used as anion exchangers and electrode surface modifiers.<sup>27</sup>

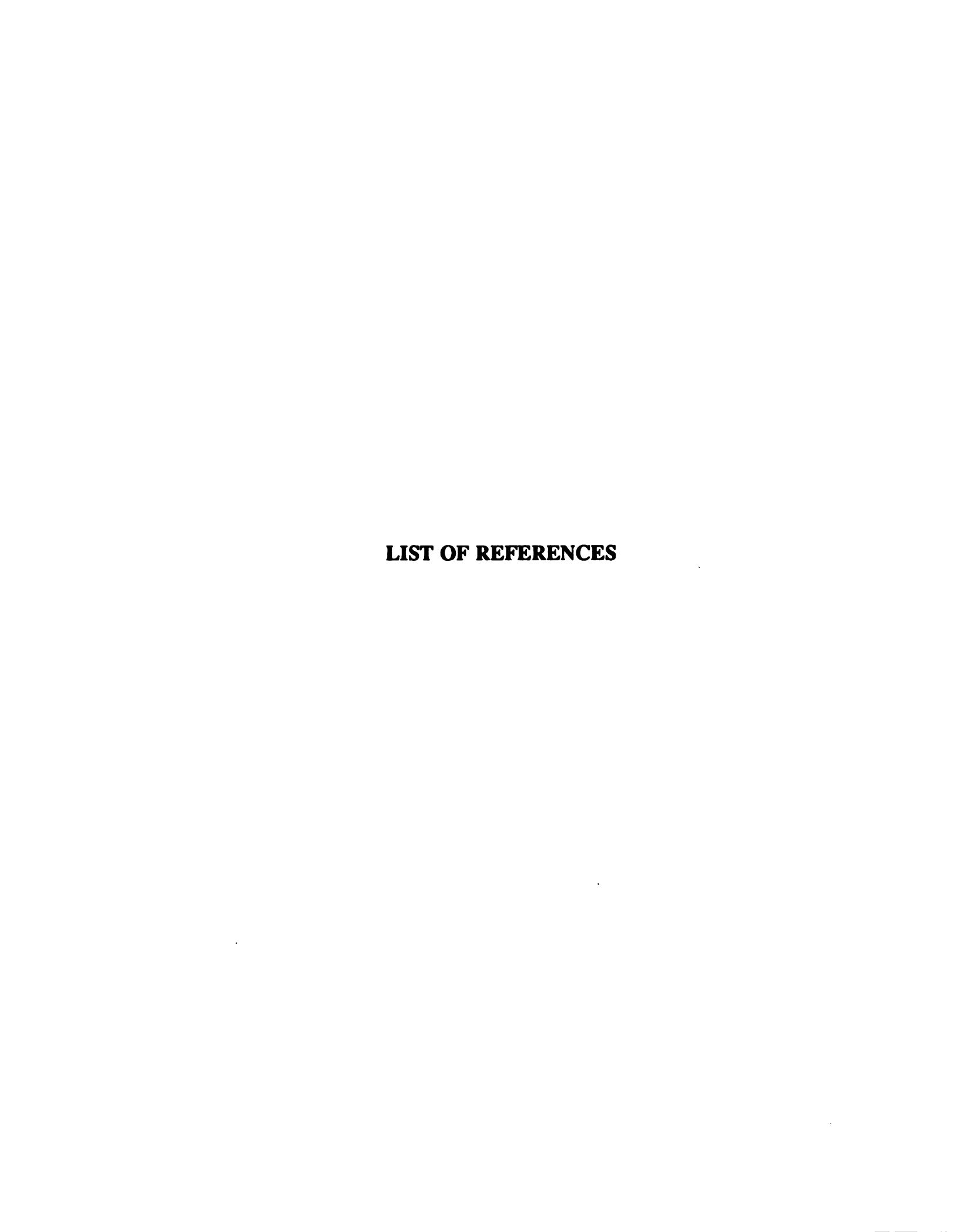
Layered double hydroxides and clays have several common features. They both consist of a layered structure with metal cations in an oxide (hydroxide) framework bearing a net charge distributed through the framework due to substitution of metal cations within the layers. Clay minerals have a net negative charge on the oxide-hydroxide framework whereas layered double hydroxides have a net positive charge. As in clay minerals the layer charge of LDH is neutralized by the counter ions intercalated within the interlayer

region. These interlayer anions of many LDH are exchangeable as in many clays.<sup>28</sup>

The layered double hydroxides are also known as hydrotalcite like  $^{29}$  or "Feitknecht" compounds.  $^{30}$  A large number of LDHs have been reported including both naturally occurring and synthetic members. Most of the LDHs have the general formula  $[M(II)_{1-x}M(III)_x](OH)_2[x/x]^2$ .  $[M(III)_x]^2$ , and consist of brucite-like octahedral sheets with the divalent metal cations periodically replaced by the trivalent cations (Figure I.2). This substitution leads to the net positive charge which is compensated by the intercalation of anions between the stacked hydroxide layers. Water molecules are also found in the interlayer region.



 $\label{eq:Figure I.2 Structure of the basic layered double hydroxide, hydrotalcite, $[Mg_3Al(OH)_8][CO_3]_{0.5}.2H_2O.$}$ 



#### LIST OF REFERENCES

- 1. Ghosh, P. K.; Bard, A. J. J. Am. Chem. Soc. 1983, 105, 5691.
- 2. Liu, H.-Y.; Anson, F. C. J. Electroanal. Chem. 1985, 184, 411.
- 3. King, R. D.; Nocera, G. D.; Pinnavaia, T. J. J. Electroanal. Chem. 1987, 236, 43.
- 4. Rong, D.; Kim, Y. I.; Mallouk, E. T. Inorg. Chem. 1990, 29, 1531.
- 5. Pinnavaia, T. J. Science 1983, 220, 365.
- 6. Kadkhodayan, A; Pinnavaia, T. J. J. Mol. Catal. 1983, 21, 109.
- 7. Xavier, S. F.; Sharma, Y. N. Polym. Compos. 1986 7 42.
- 8. Giunnelis, E. P. Clay Miner. Soc. 25th Meeting, 1988.
- 9. Abd-El-Nour, K. N.; Al-Ani, A. S.; Abdul-Mahdi, F. A. Z. Phys. Chemie. Leipzig 1983 264 S.577.
- 10. Bidadi, H.; Schroeder, P. A.; Pinnavaia, T. J. J. Phys. Chem. Solids 1988, 49, 1435.
- 11. Drezdzon, M. A. Inorg. Chem. 1988, 27, 4628.
- 12. Shaw, B.; Creasy, K. E. J. Electroanal. Chem. 1988, 243, 209.

- 13. Keita, B.; Nadjo, L. J. Electroanal. Chem. 1988, 240, 325.
- 14. Toth, J. E.; Anson, F. C. J. Am. Chem. Soc. 1989, 111, 2444.
- 15. Giese, R. F. Jr. Clay Miner. 1975, 23, 165.
- 16. Bailey, S. W. in Crystal Structure of Clay Minerals and Their X-Ray Identification. Brindley, G. W.; Brown, G. Eds.; 1980, Mineralogical Society London. Chapter 1.
- 17. Beson, G.; Mitsud, C. T.; Mering, J. Clays Clay Miner. 1974, 22, 379.
- 18. Brindley, G. W. in Crystal Structure of Clay Minerals and Their X-Ray Identification. Brindley, G. W.; Brown, G. Eds.; 1980, Mineralogical Society London. Chapter 2.
- 19. Suquet, H.; Calle, de la C.; Pezerat, H. Clays Clay Miner. 1975, 23,
- Herman, R. G.; Klier K.; Simons, G. W.; Finn, B. P.; Bulko, J. B.;
   Kobylinski, T. P. J. Catal. 1979, 56, 407.
- 21. Reichle, W. T. J. Catal. 1985, 94, 547.
- 22. Martin, K. J.; Pinnavaia, T. J. J. Am. Chem. Soc. 1986 108, 541.
- 23. Miyata, S.; Kagaku, G. MOL 1977, 15, 32.
- 24. White, J. L.; Hene, S. L. Ind. Eng. Prod. Res. Dell. 1983, 22, 665.
- 25. Miyata, S.; Takada, M.; Okada, A. Ger. Offen. 2,222,473; Chem. Abst. 1974 81 54438q.

- 26. Reichle, W. T. CHEMTECH 1986, 58.
- 27. Itaya, K.; Chang, C. H.; Uchida, I. Inorg. Chem. 1987, 26, 624.
- 28. Allmann, R. Chimia 1970, 24, 99.
- 29. Miyata, S.; Kumura, T. Chem. Lett. 1973, 843.
- 30. Beck, C. W. Amer. Mineral. 1950, 35, 985.

#### CHAPTER II

#### DIELECTRIC PROPERTIES OF SMECTITE CLAYS.

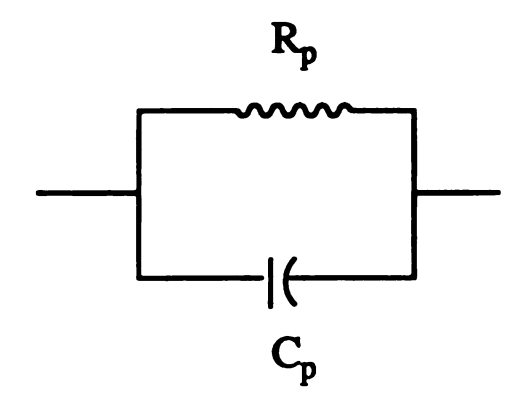
### II.a Background.

Originally the major driving force for the study of clay minerals in this work was their potential use as insulators in the semiconductor industry, replacing amorphous  $SiO_2$  ( $\alpha$ - $SiO_2$ ) as the gate oxide in MOS (Metal-Oxide-Semiconductor) devices. With the current individual component dimensions in microchips set at about 500 Å, amorphous  $SiO_2$  performs quite well as a gate oxide. However, as more compact devices are developed with component dimensions of the order of 100 Å or less, amorphous  $SiO_2$  will no longer be a satisfactory gate oxide due to a number of limiting reasons. It's breakdown voltage of  $10^8$  Vm<sup>-1</sup> will limit the applied voltages across an interface to  $\sim 0.5$  V, whereas 10-15 V are desired. The porosity of amorphous  $SiO_2$  on the 100 Å scale will lead to punch through of the metal to the semiconductor and result in short circuiting the device.

In addition to being nonporous on the 100 Å scale, 2:1 layered silicates have a typical breakdown voltage of  $10^9$  Vm<sup>-1</sup> and could easily sustain an applied voltage of 10-15 V. Furthermore, the amorphous structure of  $\alpha$ -SiO<sub>2</sub> generates a high density of electron

traps or interface states when it is bound to crystalline Si, whereas the crystalline nature of 2:1 layered silicates might lead to epitaxial bonding with a resulting low density of electron traps. Table II.1 summarizes these physical properties and justifies the potential applicability of 2:1 clay minerals in such devices.

A general Radio 1616 Capacitance Bridge was used to measure the impedance of a cell consists of a parallel plate capacitor with the samples between the plates. Various models of equivalent circuits for the system can be suggested, but the bridge always interprets the cell impedance in term of a parallel circuit as shown below.



It is a first approximation that  $C_p$  can be interpreted as the capacitance of the sample and  $G_p$ ,  $(1/R_p)$ , is the leakage conductance of the system. We now investigate in greater detail how these quantities are to be interpreted. For a lossless parallel plate capacitor with vacuum between the plates, the static capacitance,

Table II.1 A comparison of physical properties of smectite clays and amorphous silica,  $\alpha\text{-SiO}_2$ .

Physical property	Amorphous silica	Smectite clays
Dielectric strength	1 x 10 <sup>8</sup> V m <sup>-1</sup>	3 x 10 <sup>9</sup> V m <sup>-1</sup>
Electron traps	Many	Few
Transverse porosity	High	None
Deposition	High temperature	Room temperature
Ionic mobility	Moderate	~0
Epitaxy	Impossible	Possible

$$C_0 = \varepsilon_0 \frac{A}{d}$$

where A is the area of the plates, d is their separation and  $\varepsilon_0$  is the permittivity of the free space. For a dielectric material between the plates, the static capacitance C,

$$C = \varepsilon_0 \varepsilon_T \frac{A}{d}$$
$$= \varepsilon \frac{A}{d}$$

where  $\varepsilon_{\rm I}$  is the relative permittivity or the dielectric constant of the medium. For a dielectric material with leakage current and an alternating potential,

$$C^{*}(\omega) = \varepsilon^{*}(\omega) \frac{A}{d}$$

$$= \frac{A}{d} [\varepsilon'(\omega) - i \varepsilon''(\omega)]$$

$$= \frac{C_{0}}{\varepsilon_{0}} [\varepsilon'(\omega) - i \varepsilon''(\omega)] \qquad (1)$$

where  $C_0$  is the capacitance with an air or vacuum dielectric. The complex  $C^*$  and  $\epsilon^*$  correspond to the fact that current and voltage will generally be out of phase.  $C^*$  can also be defined as

$$\frac{1}{i \omega Z^*(\omega)}$$

where Z\* is the complex impedance of the sample cell. For the parallel equivalent circuit above

$$Z^*(\omega) = \frac{R_p}{(1 + i \omega C_p R_p)}$$

where

$$R_{p} = \frac{1}{G_{p}}$$

Hence C\* = 
$$\frac{1}{i \omega Z^*(\omega)}$$
, =  $C_p + \frac{1}{i \omega R_p}$   
=  $C_p - \frac{i G_p}{\omega}$  (2)

Comparing the Eq (1) with the Eq (2) we see that

$$C_{p} = \frac{C_{o}}{\varepsilon_{o}} \varepsilon'$$
 or 
$$\frac{C_{p}}{C_{o}} = \frac{\varepsilon'}{\varepsilon_{o}}$$
 (3)

and  $\frac{i G_p}{\omega} = i \varepsilon'' \frac{C_o}{\varepsilon_o}$ 

or  $\varepsilon'' = \frac{\varepsilon_0 G_p}{\omega C_o}$  (4)

To illustrate possible frequency dependences of  $\epsilon'$  and  $\epsilon''$  we consider two simple but important cases.

# (1) $G_p = DC$ conductance.

The conductivity  $\boldsymbol{\sigma}$  is derived from  $\boldsymbol{G}_p$  from the following relationship.

$$\sigma = \frac{G_p l}{A}$$

Where I and A are the thickness and the cross-sectional area of the clay film. However, it is important to notice that in an AC system  $G_p$  does not necessarily correspond with DC conductance. In the case where it does,  $G_p$  is a constant and  $\epsilon''$  decreases with frequency as  $1/\omega$  and  $\epsilon'$  is constant.

#### (2) Dipolar Relaxation.

Suppose we have a collection of permanent dipoles in a viscous fluid. In the absence of an applied field these are randomly distributed in angle. If a field is applied then after a long time the dipoles will be lined up in the direction of the field. On turning off the field they will randomize and polarization P will decay exponentially that is,

$$P = P_0 e^{-t/\tau}$$
 (5)

Where  $\tau$  is called the relaxation time. Where there is only one relaxation time, the equations for  $\epsilon'$  and  $\epsilon''$  as a function of  $\omega$  are:

$$\varepsilon'(\omega) = \varepsilon_{\infty} + \frac{\varepsilon_{s} - \varepsilon_{\infty}}{1 + \omega^{2} \tau^{2}}$$
 (6)

$$\varepsilon''(\omega) = \frac{(\varepsilon_s - \varepsilon_{\infty})\omega\tau}{1 + \omega^2 \tau^2} \tag{7}$$

Where  $\varepsilon_{\infty}$  is  $\varepsilon_{\rm T}$  at infinite frequency and  $\varepsilon_{\rm S}$  is  $\varepsilon_{\rm T}$  at very low frequency. Plots illustrating this behavior are shown in Figure II.11 At low frequencies dipoles orient in the direction of and in phase with the applied field and the dielectric constant is independent of frequency. As the frequency increases the polarization of permanent dipoles begins to lag behind the field and finally decreases to zero resulting in a decrease in the dielectric constant. The same information is frequently expressed by a Cole-Cole plot in which  $\varepsilon''$  is plotted against  $\varepsilon'$  for varying frequency (Figure II.2).

The distribution of electric charge in a water molecule is primarily dipolar.<sup>2</sup> Thus, if a water molecule is subjected to an applied ac field, the molecule will attempt to follow changes in the field direction by reorientating itself. The extent to which this is possible, depends on the constraints imposed on the molecule by its surrounding environment. The higher the degree of interaction the lesser the ability of water molecules to follow the fluctuating electric field. This has a major impact on the dielectric properties of water adsorbed on a solid surface.

The orientational motions of water molecules adsorbed on Na+and K+- montmorillonite are on the same time scale as those in liquid

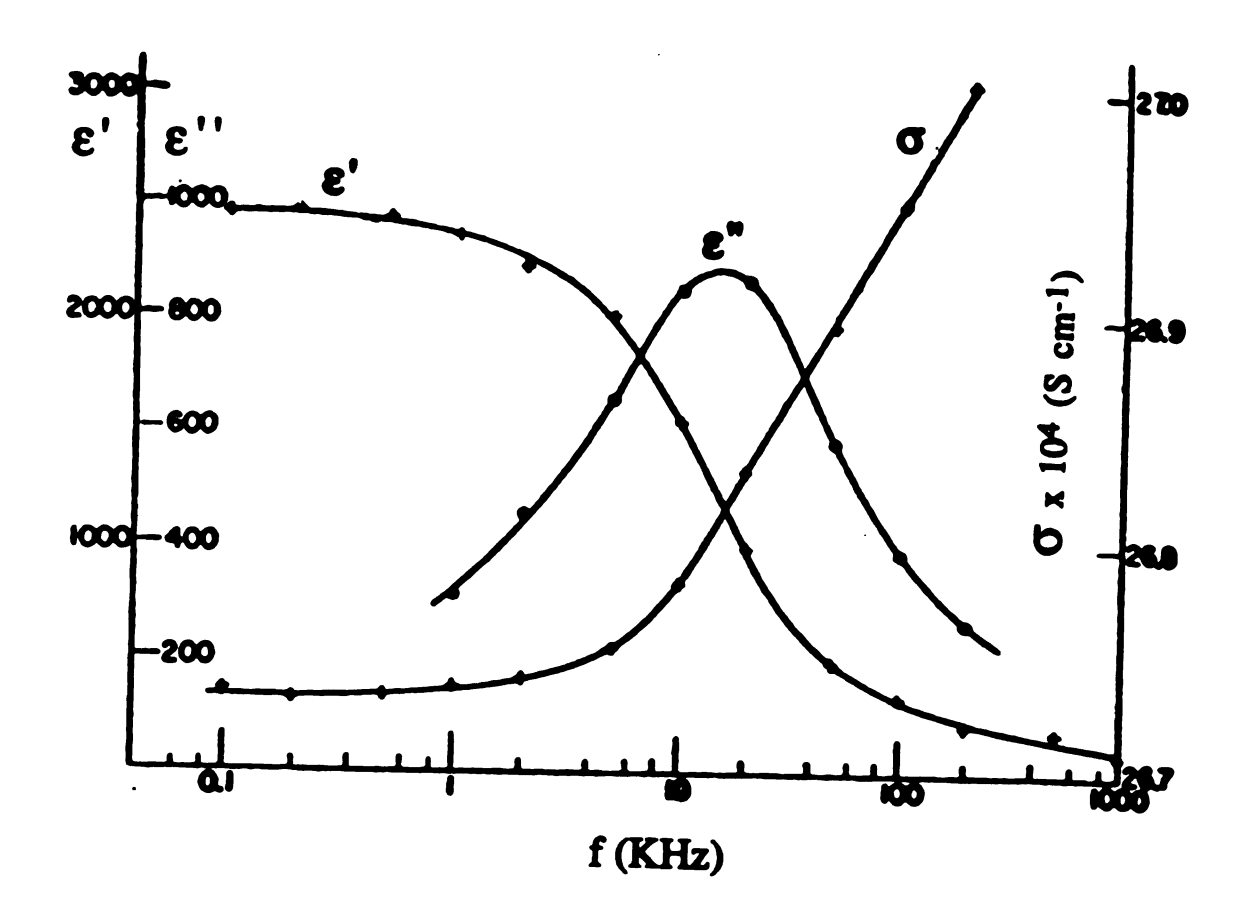


Figure II.1 Real ( $\epsilon$ ') and imaginary ( $\epsilon$ ") parts of the complex dielectric constant of a suspension of polystyrene particles as a function of frequency.

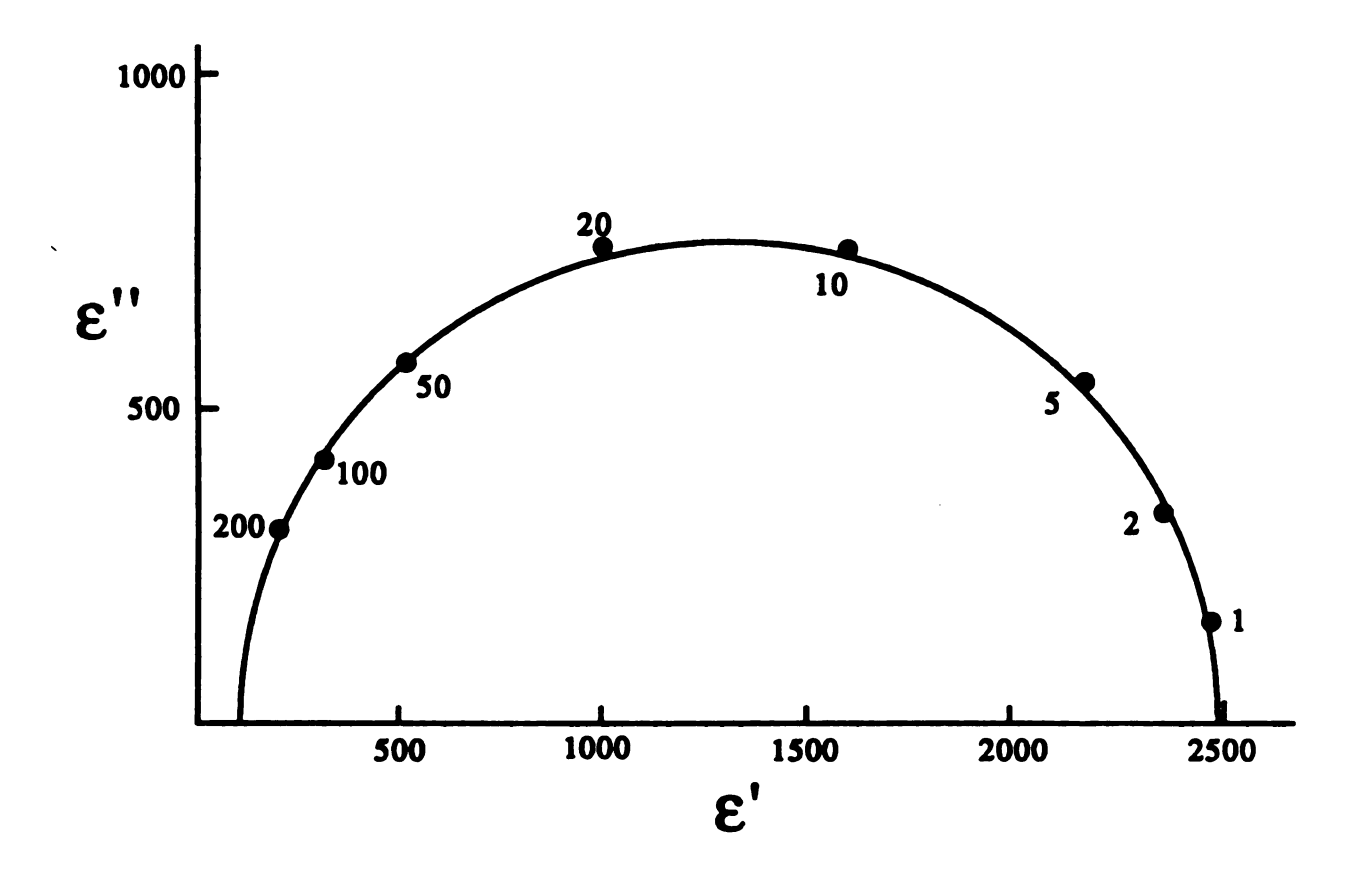


Figure II.2 Cole-Cole ( $\epsilon$ " vs  $\epsilon$ ') plot for the same data presented in Figure II.1.

water.<sup>3</sup> Therefore, the dipolar relaxation effect of Eq. 6 and 7 occurs at  $\sim 3 \times 10^{11}$  Hz and is well beyond our frequency range. On the other hand, the orientational motion of water molecules adsorbed on Li<sup>+</sup>-Mg<sup>2+</sup>- Ca<sup>2+</sup>- Sr<sup>2+</sup>- and Ba<sup>2+</sup>- montmorillonite is comparable to that of ice;  $\sim 6 \times 10^7$  Hz for Li<sup>+</sup>-montmorillonite and  $1 \times 10^5$  Hz for Mg<sup>2+</sup>-montmorillonite.<sup>3</sup> It is possible that this reflects the tendency of the latter exchangeable cations to bind solvation shell water molecules very strongly, thereby preventing an easy movement of their dipole moment vectors in response to an oscillating applied electric field. The relaxation times given above suggest that we will not observe these processes at the frequencies available to us. ie <  $10^5$  Hz.

#### Other Mechanisms.

The two systems mentioned above are the simplest mechanisms. For real systems both these may occur along with other effects which necessitate a detailed and complex analysis. We discuss our results in detail in Section II.c but for the moment we simply observe that the adsorption of small quantities of water results in very large changes in  $\varepsilon'$  and  $\varepsilon''$ . Having declared that we are unlikely to see the effect of dipolar relaxation, we go on to enumerate several effects which may contribute to the large observed values of  $\varepsilon'$  and  $\varepsilon''$ .

#### 1. Maxwell-Wagner Effect

The importance of geometrical arrangement on the dielectric constant of a mixture can be simply illustrated as discussed by Sen.<sup>4,5</sup> If an electric field is applied parallel to the interface of a layered medium, whose thicknesses are smaller than the electromagnetic wavelength, the effective dielectric constant is given by

$$\varepsilon_e = \sum f_i \varepsilon_i$$

where  $f_i$  denotes the volume fraction of the i<sup>th</sup> phase of dielectric constant  $\epsilon_i$ . But when the field is applied perpendicular to the interface of the layered medium,  $\epsilon_e$  is given by

$$\varepsilon_{e} = \frac{1}{\sum \frac{f_{i}}{\varepsilon_{i}}}$$

If one component is conducting and the other is not, then for the first case a non-zero DC conductivity,  $\sigma(0)$ , and for the second case zero  $\sigma(0)$  are obtained. Similarly, the dielectric constants are drastically different in the two cases. In the latter case a divergent

E' is obtained for a mixture of conductors and insulators. Effective mixing laws can handle simple situations in which the concentration of impurities is small or the contrast in the properties of constituents is small and the inclusions or the constituents have simple shapes.<sup>6</sup>

The low frequency dielectric constant of a material made up of a layer of insulating material covered with a layer of conducting material can be extremely large when the thickness of the insulating region becomes small.<sup>7</sup> This is known as the Maxwell-Wagner effect.<sup>8,9</sup> In this case the material as a whole could have a zero dc conductivity because the layer of insulating material blocks the current path. However, it is possible for such a system to have an enormously large dielectric constant even when the system remains conducting. 10 This idea is used in the theory of porous rocks containing water plus clay particles. Here there are two sources of enhancement of  $\epsilon'$  -namely surface double layer effects (see sec 3 under Other Mechanisms) and geometrical effects like the Maxwell-Wagner effect. In the porous rocks porous paths are interupted by clay particles and the resulting enhancement depends on the aspect ratio of these particles. The larger the aspect ratio the larger the dielectric constant. 10 The characteristic frequencies for the geometrical effects for rock water clay systems depend on the salinity of the mixture and are in and above the megahertz range.<sup>4</sup> Kenyon<sup>11</sup> has reported that the dielectric constant of calcite rock samples in the MHz frequency range depends on the relative amounts of platy-grain material in the sample. Spherical samples did not show any dielectric dispersion at this frequency range.

Working with air-dried, oriented montmorillonite clay films Bidadi et al.<sup>12</sup> have shown that the dielectric properties in the direction perpendicular to the clay sheets depend strongly on the amount of water takeup and on the type and concentration of the exchange cations in the clay gallery region. They have observed very large dielectric constants at low frequencies and found that at the same frequencies and at high water contents the capacitance, C is inversely and the conductance, G is exponentially proportional to the frequency. The authors have used a Maxwell-Wagner Effect to explain their results for the montmorillonite/water system.

According to Badadi et al.<sup>12</sup> there are easy conducting paths through the interstices of the clay. These paths are interrupted by thin insulating barriers, clay platelets for example, which act as capacitors with large capacitances because of the thinness of the insulating plates. The equivalent circuit of this system is shown in Figure II.3. The easy conducting paths are represented by R<sub>1</sub> and C<sub>1</sub> which both are small. The barriers are represented by a large R<sub>2</sub> and C<sub>2</sub>. The mathematical analysis of this circuit yield the following result.<sup>13</sup>

$$\epsilon' = \frac{1}{C_0(R_1+R_2)} \frac{\tau_1+\tau_2-\tau+\omega^2\tau_1\tau_2\tau}{1+\omega^2\tau^2}$$

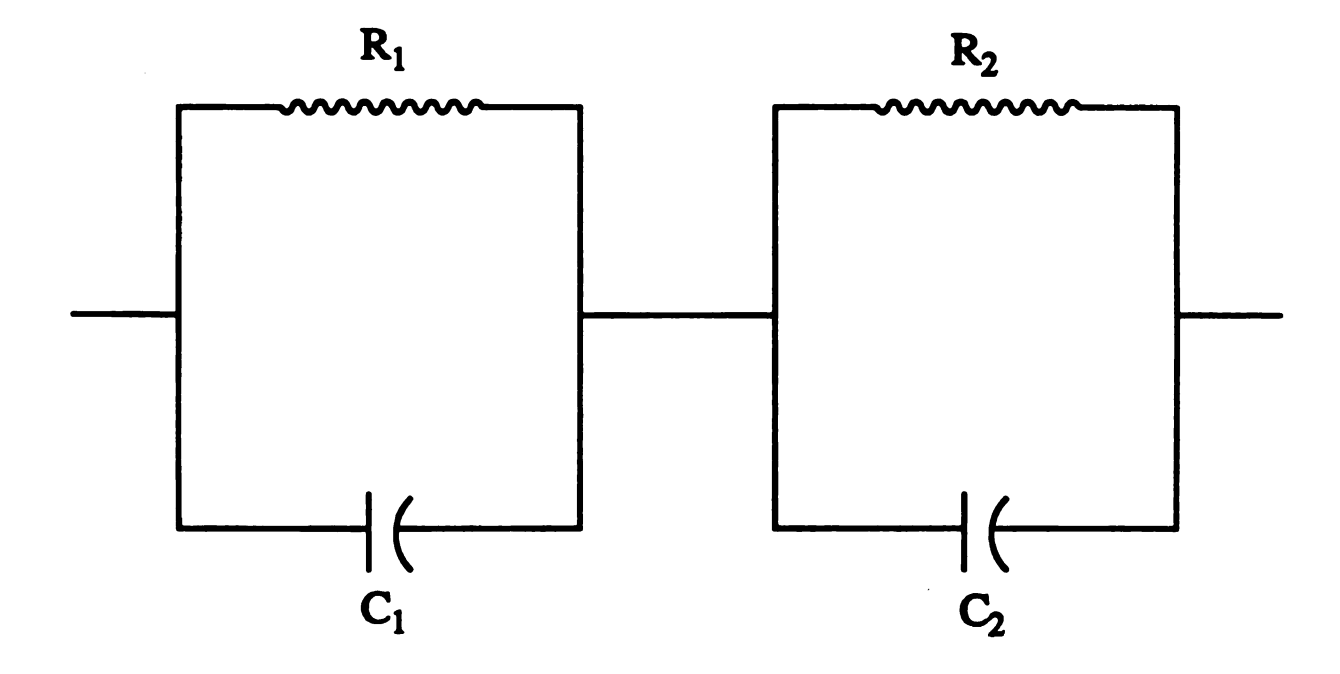


Figure II.3 A simple Equivalent Circuit for Modelling the Maxwell-Wagner Effect in a Clay Sample.

where 
$$C_0 = \frac{A}{(d_1+d_2)}$$
 and  $\tau = \frac{\tau_1\tau_2}{(\tau_1+\tau_2)}$ 

At 
$$\omega = 0$$
 and for  $\tau_2 >> \tau_1$ ,  $\epsilon' \rightarrow \epsilon'_s = \frac{C_2}{C_0}$ 

which may be very large because of the large value of  $C_2$  possible for a thin insulating barrier.

At 
$$\omega = \infty$$
 and for  $\tau_2 >> \tau_1$ ,  $\epsilon' \to \epsilon_{\infty}' = \frac{C_1}{C_0}$ 

which may be very small because of the small value of  $C_1$  associated with a conducting path. Therefore, the Maxwell-Wagner model qualitatively explains the correct frequency dependence and the high dielectric constant at low frequencies and decaying to a small one at higher frequencies. A more quantitative comparison can be made by observing that

$$\varepsilon' = \varepsilon'_{S} + \frac{D(\varepsilon'_{\infty} - \varepsilon'_{S})}{D + \frac{C}{\omega}}$$

where, 
$$C = C_0 R_2$$
 and  $D = C_0 R_1^2 R_2 C_2^2$ ,

and 
$$\varepsilon'' = \frac{1}{\omega C_0(R_1 + R_2)} + \frac{(\varepsilon_{\infty}' - \varepsilon_{s}')\omega \tau}{(1 + \omega^2 \tau^2)}$$

The theory gives a frequency dependence close to that observed. However, the underlying model needs justification.

Another case of dielectric enhancement somewhat similar to the above occurs in inhomogeneous mixtures of metals and insulators<sup>5</sup> when the conducting metal phase is close to a percolation threshold.

$$\sigma = \sigma_{\rm m} (\phi - \phi_{\rm c})^{\rm a}$$
 for  $\phi > \phi_{\rm c}$ 

$$\sigma = 0$$
 for  $\phi < \phi_c$ 

Where  $\sigma_m$  is the conductivity of the conducting phase and  $\phi$  is the volume fraction of metal. The real part of the dielectric constant diverges as  $\phi$  approaches  $\phi_c$ .

$$\varepsilon' = \varepsilon'_i |\phi - \phi_c|^{-b}$$

Where  $\epsilon_i'$  is the dielectric constant of the insulating medium.

#### 2. Electrode Polarization.

Figure II.4 indicates the electrode polarization at a parallel plate cell as illustrated by Day et al. 14 The sample is initially uncharged and unpolarized. When an electric field is applied, polarization of the material proceeds by dipole orientation (the normal permittivity mechanism) and polarization of the blocking electrodes proceeds by ionic conduction. The ions accumulate at the electrodes, forming a charge layer which is qualitatively similar to the layer of bound charge generated by the dipole orientation. However, the ionic polarization can have a much greater charge density than that ause by the dipole orientation. 14 Thus, the observed cap. citance can be much larger than that which would result from the dipoles alone.

An equivalent circuit including blocking layers is depicted in Figure II.5 as proposed by Day.<sup>14</sup> The two charged layers are combined into a single blocking capacitor C<sub>b</sub> with a plate spacing of

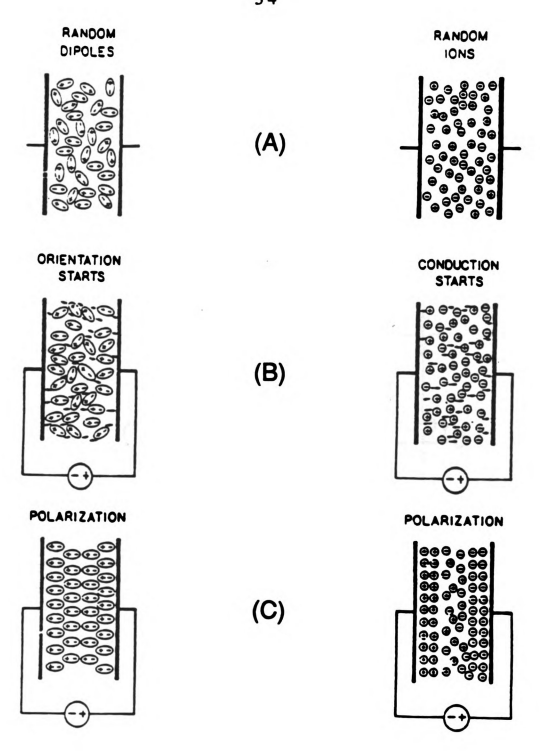


Figure II.4 Idealized view of the polarization due to dipoles and ions. (A) Unpolarized; (B) Orientation and conduction begins; (C) Fully polarized. In actual materials, both process can occur simultaneously.

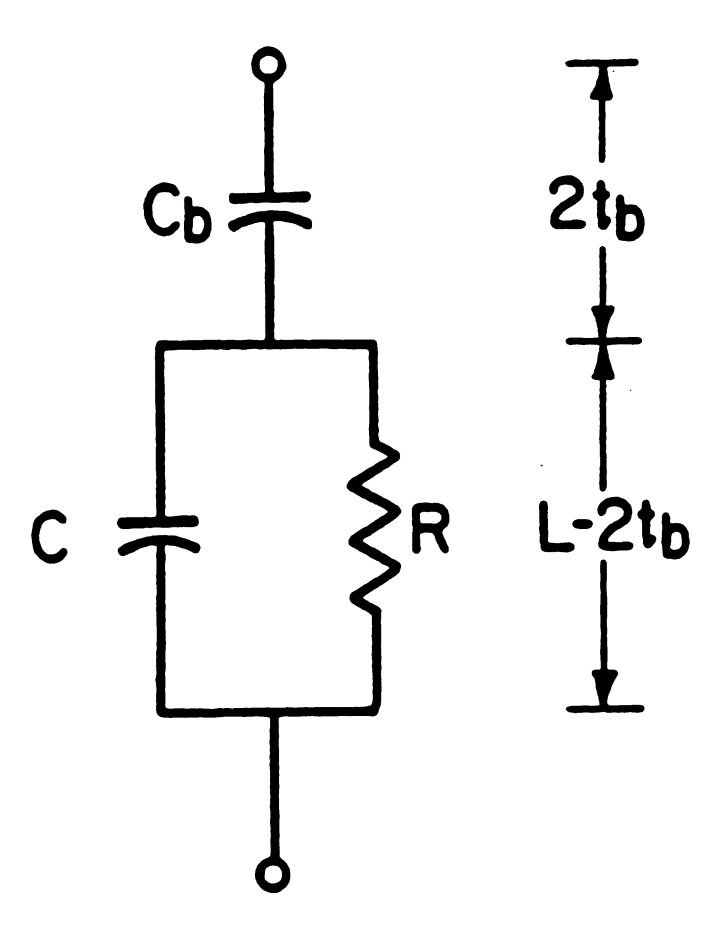


Figure II.5 Equivalent circuit that includes a blocking layer.

 $2t_b$ . When the conductivity is large, the impedance of R becomes less than that of C,  $(1/\omega C)$ . Then the charging of  $C_b$  through R becomes the dominant behavior of the circuit. Under these circumstances, the relative impedances of R and  $C_b$  determine whether or not a significant charging of  $C_b$  can take place at the frequency of measurement. If R represents the larger of the two impedances, then charging of  $C_b$  or the electrode polarization is not significant. However, when  $R < 1/\omega C_b$ , the charging of  $C_b$  becomes important. <sup>14</sup> According to Day et al <sup>14</sup>  $\epsilon$ ' and  $\epsilon$ " for the blocking electrode model can be expressed as given below.

$$\varepsilon_{x}' = \varepsilon' \frac{L}{2t_{b}} \left[ \frac{(\tan \delta)^{2} + \left(\frac{L}{2t_{b}}\right)}{(\tan \delta)^{2} + \left(\frac{L}{2t_{b}}\right)^{2}} \right]$$

$$\varepsilon_{x}^{"} = \varepsilon^{"} \frac{L}{2t_{b}} \left[ \frac{\left(\frac{L-2t_{b}}{2t_{b}}\right)}{(\tan \delta)^{2} + \left(\frac{L}{2t_{b}}\right)^{2}} \right]$$

$$\tan \delta_{x} = \frac{\varepsilon_{x}''}{\varepsilon_{x}'} = \tan \delta \left[ \frac{\left(\frac{L}{2t_{b}} - 1\right)}{(\tan \delta)^{2} + \left(\frac{L}{2t_{b}}\right)} \right]$$

or 
$$\tan \delta = \frac{\sigma}{\omega \epsilon_0 \epsilon'}$$

Where  $\epsilon_x'$  and  $\epsilon_x''$  are the experimental values of  $\epsilon'$  and  $\epsilon''$  calculated using the equations

$$C = \frac{\varepsilon' \varepsilon_0 A}{L}$$
 and  $R = \frac{L}{w A \varepsilon' \varepsilon_0}$ 

When there is no blocking layer or  $L >> 2t_b$ , the equations become  $\varepsilon_x' = \varepsilon'$  and  $\varepsilon_x'' = \varepsilon''$ . Theoretical curves for  $\varepsilon'$  versus  $\varepsilon''$  (ColeCole Plots) with increasing  $t_b$  are shown in Figure II.6.<sup>14</sup> For an infinitesimally thin blocking layer compared to the interelectrode spacing ( $L >> 2t_b$ ), the Cole-Cole diagram approaches a vertical line which intersects the  $\varepsilon_x'$  axis at the bulk or the dipolar permittivity  $\varepsilon'$ . As the ratio  $L/2t_b$  decreases, either due to a smaller interelectrode spacing or a thicker blocking layer, the Cole-Cole diagram becomes semicircular, with one  $\varepsilon_x'$ -axis intercept at the bulk permittivity and the second intercept at the bulk permittivity multiplied by  $L/2t_b$ .

## 3. Double Layer Effects

Surface double layer effects become important at frequencies in the kilohertz range and contribute to the large values of dielectric constant. 1,4,15 A charged particle, such as a clay particle, immersed

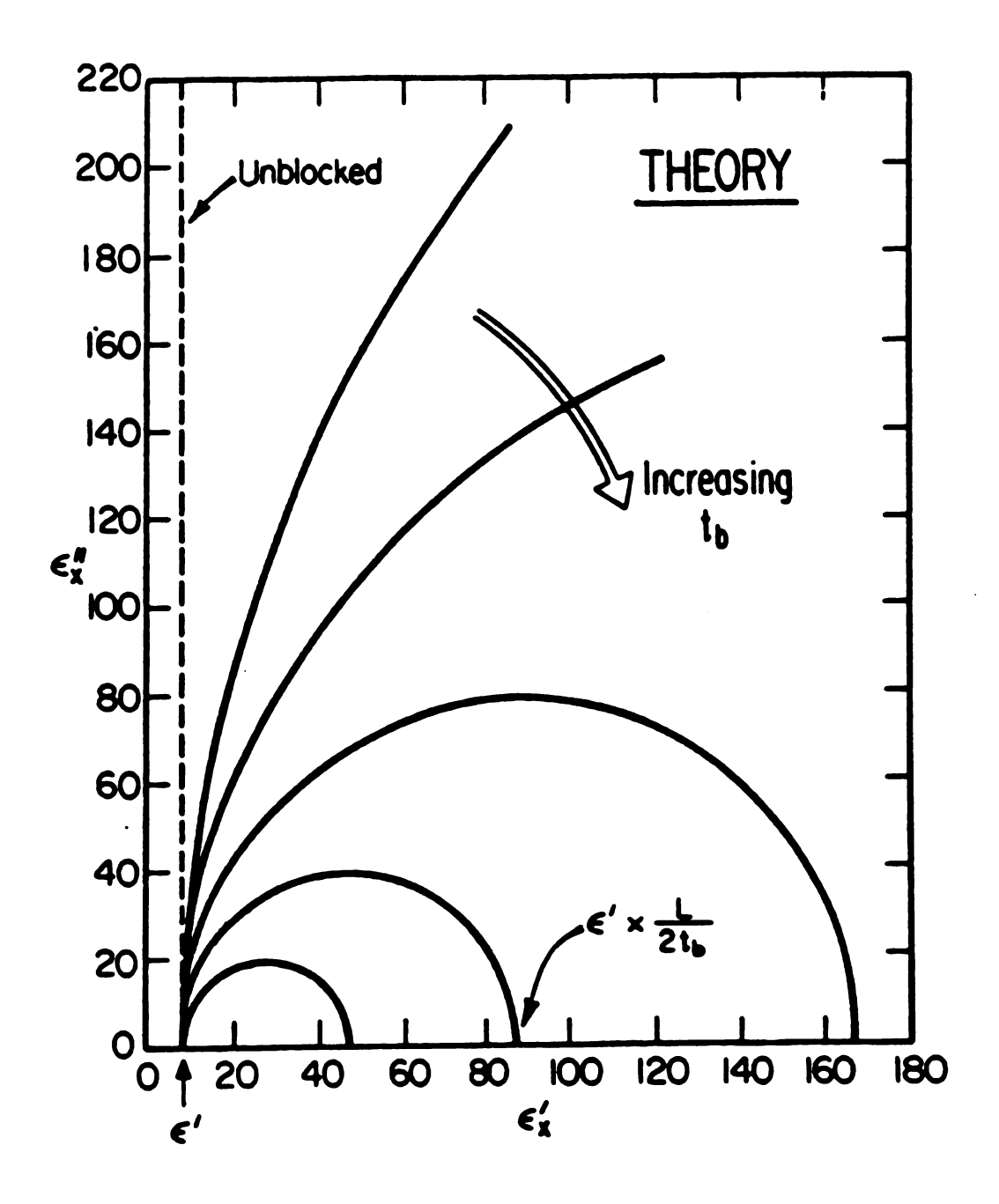


Figure II.6 Theoretical Cole-Cole plots for various  $\frac{L}{2t_b}$ .

in an electrolyte solution acquires a charge cloud, known as the electrochemical double layer. 16-20 Polarization of this double layer in an external electric field has been invoked as the mechanism responsible for the large low frequency dielectric constant in rocks containing clay particles, as well as in other colloidal systems. theory of electrode double layer polarization, as described by Schwarz<sup>1</sup>, is illustrated in Figures II.7 and II.8. Sen et al.<sup>4</sup> have shown that the enhancement depends critically on an induced diffusion cloud that extends far beyond the original double layer proposed by Schwarz. This is schematically shown in Figure II.9. At low frequencies, a large diffusion cloud is set up by the diffusion The diffusion current in the diffusion cloud is out-of-phase with the applied field. This out-of-phase diffusion current affects the circumferential current in the double layer and causes the circumferential current to be out-of-phase. This out-of-phase current leads to a large dielectric constant. On the other hand, when the frequencies are high, the rapid oscillation of circumferential current in the double layer does not allow the build up of a large diffusion cloud out side the double layer. In fact, the diffusion cloud is smaller, both in extent and in amplitude. Hence the out-of-phase component of the circumferential current in the double layer is small, resulting in little or no enhancement.

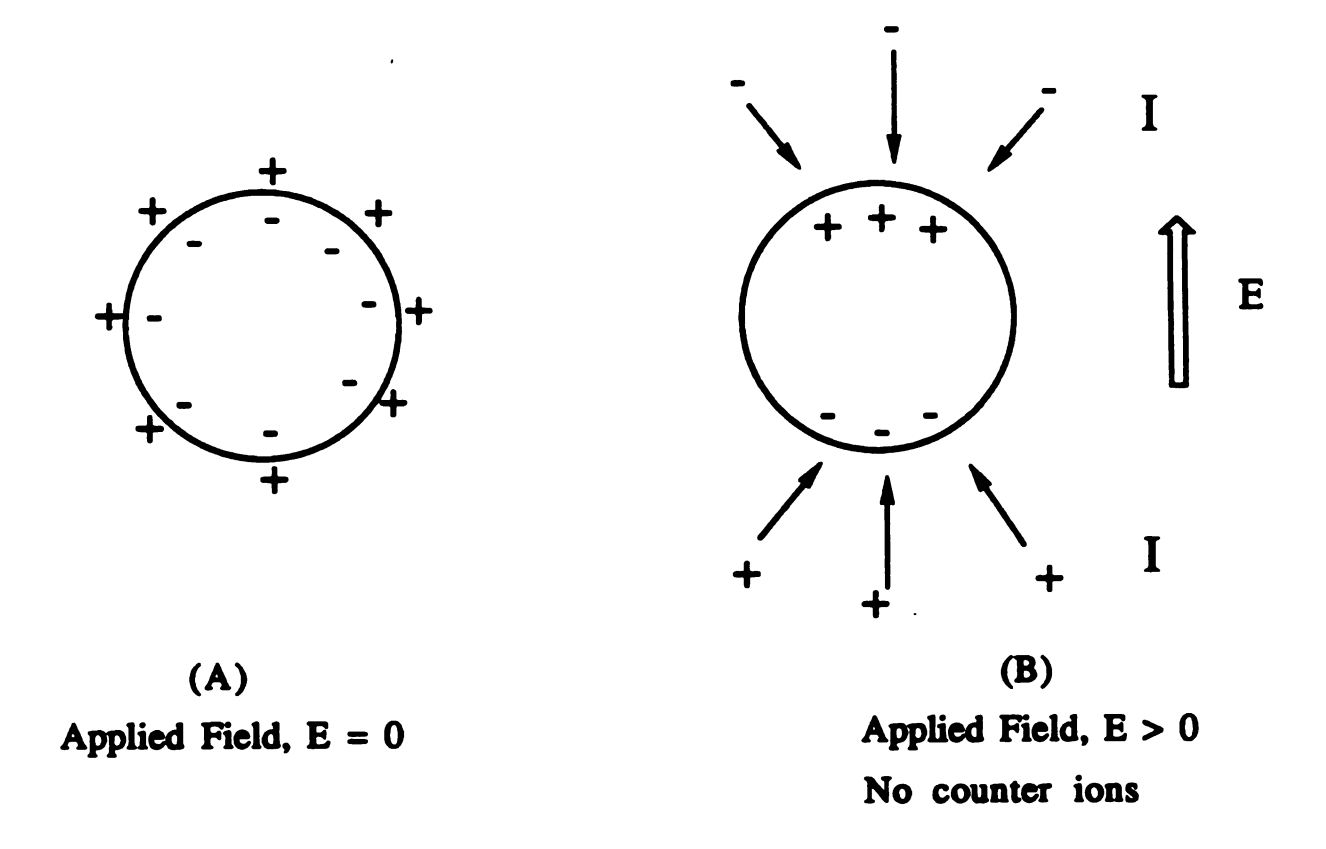


Figure II.7 (A) Formation of a double layer around a charged spherical surface. Zero applied field. (B) An unchanged particle with no counter ions in an applied field. Polarization of the particle cause attraction of the charges as indicated producing a current. If I is in phase with E, the impedance, Z of the system is resistive and there is no effect on the dielectric constant. On the other hand if I has an out-of-phase component then the impedance,  $Z = R + 1/i\omega C$  and the capacitive part enhances the dielectric constant.

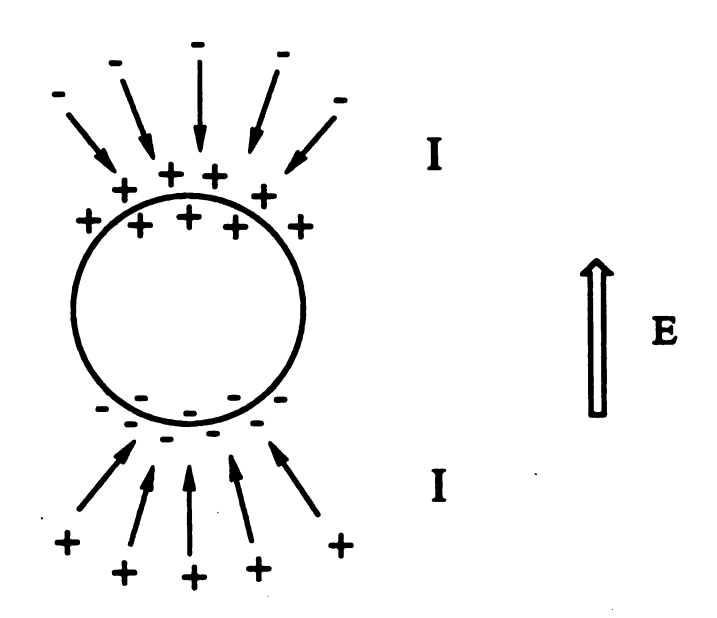


Figure II.8 Similar to the situation in Figure II.7.B. But with counter ions moving in phase with E and augmenting the dipolar distribution. Because of the counter ions, a larger out-of-phase current will be generated. This causes a great enhancement in the dielectric constant. This is the theory of Schwarz.

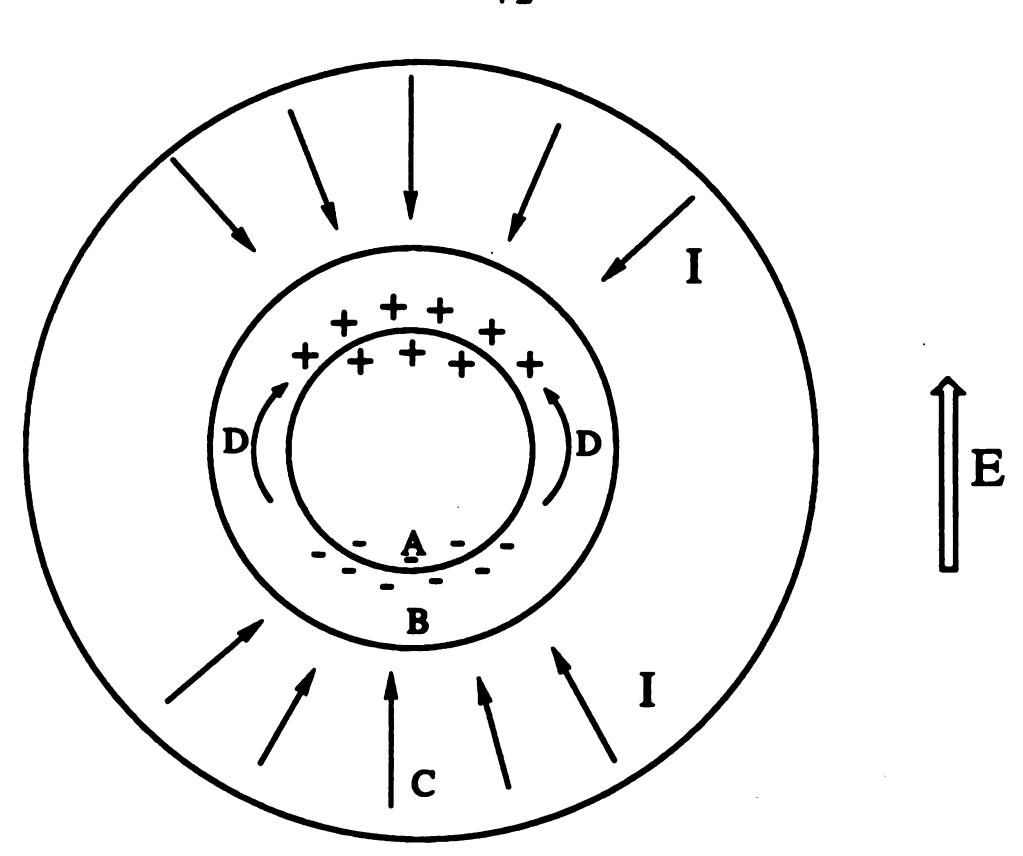


Figure II.9 Chew and Sen Model for the Enhanced Double Layer.

A= Polarized charge, B= Double layer, C= Neutral diffusion cloud and D= Circumferential current. According to Chew and Sen the most important effect is the development of a neutral layer of charges consisting of equal negative and positive charges. Incoming current has two components

- 1. a normal ohmic current I « E
- 2. diffusional current  $I = \frac{dN}{dx}$

The diffusional current is out-of-phase with the applied field causing the dielectric enhancement.

#### Previous Work On Clay Water Systems.

A large number of publications are found in literature on dielectric measurements of clay-water systems. 12,21-27 However, most of the work has dealt with clay slurries or clay suspensions, that is, water content of the samples was very high (>90 %). A systematic study of relatively dry clay/water systems with a very low percentage of water (<20 %), is needed in order to evaluate the significance of clay layer charge density, particle size or the nature of the gallery cation on the dielectric properties of these materials.

#### Clay Minerals in Geological Media

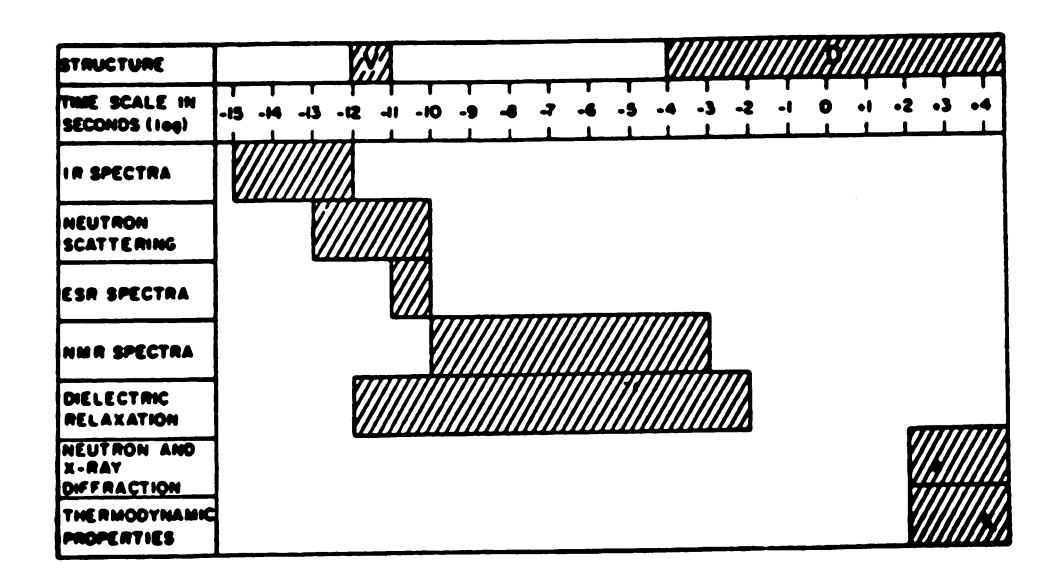
Clay minerals occur in sedimentary rocks and greatly affect the conductivity and the dielectric properties of rocks.  $^{28-30}$  This has a major impact on the commercially important determination of hydrocarbon (oil) content of reservoir rocks. If not properly accounted for, the presence of clay can lead to incorrect estimation of hydrocarbon content. Large dielectric constants, as high as  $10^6$ , for brine saturated rocks in the kilohertz range have been reported.  $^{10,28}$  This is remarkably high when compared to the dielectric constant of individual constituents, 10 for rocks and 80 for brine; these figures being largely independent of frequency for f < 1 GHz. On the other hand, the brine saturated rocks show a great deal of frequency dependence.  $^{10}$ 

#### "Dry" Clay Water Systems

## Water Adsorbed on Smectite Clays

According to Eisenberg and Kauzmann, the molecular structure of bulk liquid water is dynamic.<sup>32</sup> On a time scale which is long relative to the period of vibration of a hydrogen bond in liquid water ( $\sim 10^{-13}$  sec) but short relative to the time required for a water molecule to diffuse a distance equals to its diameter (~ 10-11 sec), a water molecule in liquid water experiences a spatial arrangement of its neighbors that is called the "vibrationally averaged structure" (Vstructure).<sup>3</sup> This structure will include only the effects of vibrational motions of water molecules and it can be probed by infrared and neutron scattering (Table II.2).3 On the other hand, on a time scale that is longer than that for a water molecule to diffuse a nominal distance in liquid water, a molecule experiences a surrounding spatial arrangement that is called the "diffusionally averaged structure" (D-structure).<sup>3</sup> This structure includes the effects of vibrational, rotational and translational motions of the water molecules. The D- structure can be probed by neutron scattering and X-ray diffraction experiments (Table II.2), and it provides a basis in molecular structure for thermodynamic properties. Between the time domains of the V and D-structures, there is a transition region that can be investigated by neutron scattering, magnetic resonance and dielectric relaxation spectroscopy.<sup>3</sup> Thus, it is clear that the structure of liquid water is dynamic one and the same should be true for the water adsorbed by smectite clays.<sup>3</sup> In the case of water

Table II.2 Time scales for adsorbed water structures and the experimental methods used to measure the properties of adsorbed water.



adsorbed on smectites an additional complexity is provided by the exchangeable cations, whose vibrational and translational motions take place in the transition region between the V and D-structures.<sup>33</sup>

At a given water content, the water adsorbed by smectite clays can be found in two different states. This includes the water solvating the exchangeable cations in the interlamellar space and the water in external regions such as edge surfaces and micropores.<sup>34</sup> The interaction of adsorbed water molecules with the smectite clays gives rise to a significant modification of the IR spectra of the individual species. As the clay mineral is hydrated, a shift of the stretching mode (from 3680 cm<sup>-1</sup> to 3690 cm<sup>-1</sup>) and of the bending mode (from 655 cm<sup>-1</sup> to 645 cm<sup>-1</sup>) of the structural OH groups of Li<sup>+</sup>-hectorite has been reported.<sup>34</sup> It has been reported by Prost that the dehydration of Li<sup>+</sup>-hectorite under 0.01 torr produces a state corresponding to three water molecules per Li+ cation (Figure II.10).<sup>34</sup> According to the author the lone-pair orbitals of the oxygen atoms in each water molecule are directed toward the Li+ cation and one of the protons in each molecule lies along an axis normal to the clay surface. This proton can perturb the structural OH groups of the clay mineral onto which it is adsorbed. Similar arrangement of the water molecules around exchangeable Na+ and Ca<sup>2+</sup> cations in hectorite at low water contents has been reported suggesting that the structure illustrated in Figure II.10 apply generally to alkali-metal and alkaline-earth metal cations.<sup>3</sup> However, when there is a significant deficit of positive charge in the tetrahedral sheet, the

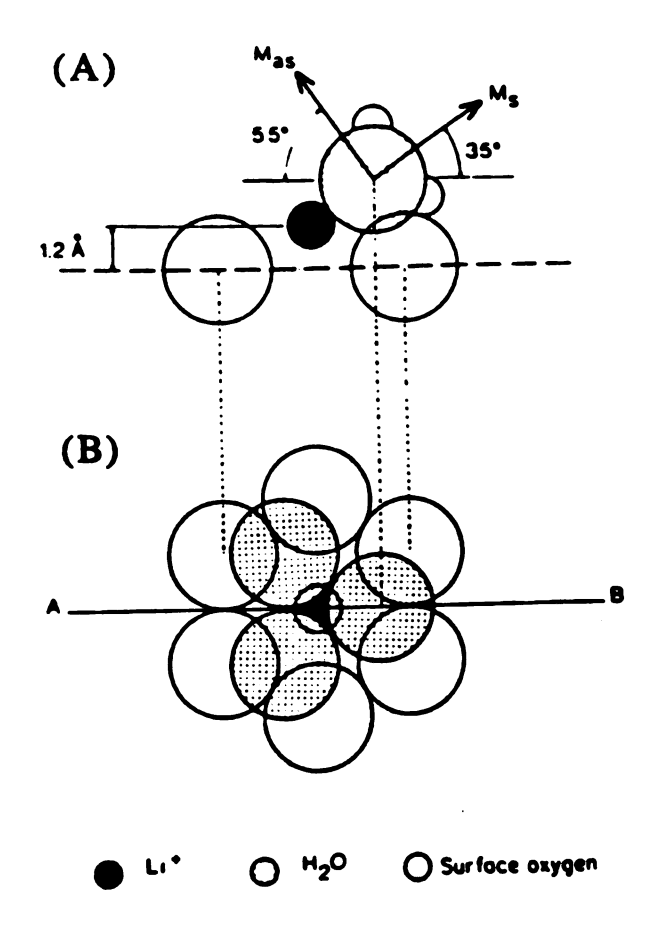


Figure II.10 Spatial arrangement of water molecules solvating exchangeable Li<sup>+</sup> cations on hectorite as determined by IR spectroscopy.<sup>3</sup> (A) section view in the plane ab; (B) plane view. M denotes the transition dipole moment for the symmetric (s) and asymmetric (as) stretching modes.

adsorbed water molecules will form strong hydrogen bonds with the surface oxygen atoms near sites of isomorphous substitution.<sup>35</sup>

Infrared studies by Prost<sup>34,36</sup> have revealed that the first stage of water adsorption by the smectite clays is the solvation of the exchangeable cations by either three (monovalent ions) or more (bivalent cations) water molecules. The second stage of hydration is the formation of either an octahedral solvation complex for the monovalent exchangeable cations or a second solvation sheath for the bivalent exchangeable cations.<sup>34</sup> The stage of hydration depends only on the ability of the exchangeable cations to solvate themselves. Therefore, it is not necessarily accompanied by the formation of a complete monolayer of water molecules in the interlamellar space. Prost has also shown that the fraction of interlamellar surface covered by water molecules at a given water content depends strongly on the nature of the exchangeable cation. The greater the hydration energy of the exchangeable cation the greater the amount of internal surface hydrated. According to Prost a monolayer of water molecules in Na+-hectorite surface corresponds to a 20% of water by weight.<sup>36</sup>

Mamy<sup>37</sup> has suggested that in montmorillonite the one-layer hydrate consists of water molecules arranged in an ice-like configuration with bonds formed both with intermolecular interactions and with oxygen atoms in the silicate surface as shown in Figure II.11. In this structure there are five water molecules assignable to each exchangeable cation. The stereochemistry of hydrated Cu<sup>2+</sup> in hectorite, montmorillonite and saponite has been

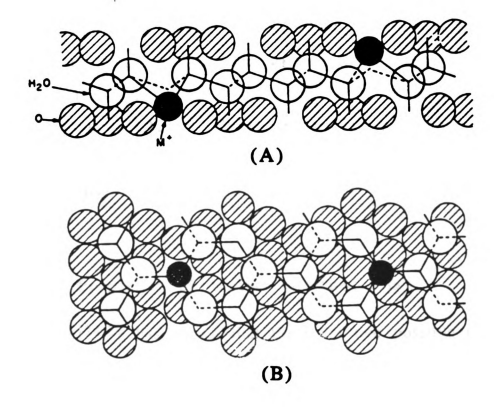


Figure II.11 A Spatial arrangement of water molecules in the interlamellar or galley region of montmorillonite containing monovalent exchangeable cations, as determined by dielectric relaxation spectroscopy.<sup>37</sup> (A) section view in the plane ab; (B) plane view. The shaded circles denote clay surface oxygen atoms.

investigated by Clementz et al.<sup>38</sup> According to the authors, when a monolayer of water occupies the interlamellar space the hydrated Cu<sup>2+</sup> cation is most likely coordinated to four water molecules in the ab plane and two silicate oxygens along the c axis. If two layers of water molecules are present, the hydrated Cu<sup>2+</sup> ion is in an axially elongated tetragonal field of six water molecules and the symmetry axis is inclined with respect to the silicate layers at an angle about 45 degrees (Figure II.12).<sup>38</sup> When several layers of water molecules occupy the interlamellar region, the hexa-hydrated Cu<sup>2+</sup> ion starts to tumble rapidly.

# Dielectric Properties of Water Adsorbed Clay

Calvet<sup>24,39</sup> has shown that there are two possible conductivity phenomena for montmorillonite. One of these conductivities dominates at low temperatures (< -100 °C) and the other dominates at high temperatures (above -100 °C). At low temperatures the conductivity is characterized by a low activation energy (1-3 Kcal mol<sup>-1</sup>) and is probably due to the migration of protons by tunnel effects. The conductivity at higher temperatures is characterized by a higher activation energy (5-10 Kcal mol<sup>-1</sup>) and is due to the migration of hydrated cations.<sup>24</sup> He has also shown that the conductivity of the hydrated clay mineral depends on the nature of the exchangeable cation and is much greater for Na<sup>+</sup> clay than any bivalent cation studied (Mg<sup>2+</sup>, Ca<sup>2+</sup>, Sr<sup>2+</sup> and Ba<sup>2+</sup>). It also depends on the water content which determines both the nature of the

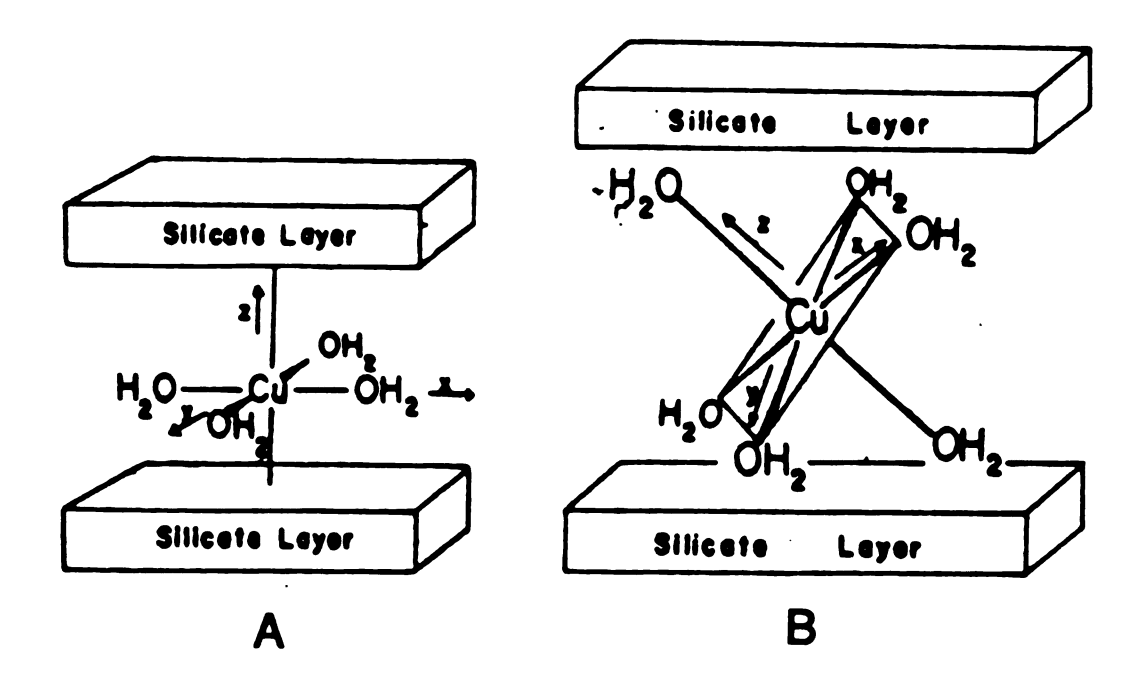


Figure II.12 Schematic representation of the stereochemistry of hydrated Cu<sup>2+</sup> as determined by ESR spectroscopy.<sup>38</sup> (A) one layer of water; (B) two layers of water occupy the interlamellar regions.

influence of the cation and the intensity of the phenomenon. Conductivity of the cation series Mg<sup>2+</sup>, Ca<sup>2+</sup>, Sr<sup>2+</sup> and Ba<sup>2+</sup> is inversely related to the layer d-spacing of the montmorillonite clay when the clay contains less than 14% of water.<sup>24</sup> However, at water contents greater than 20%, the increase in layer d-spacing is smaller even though the conductivity increases very much. With the hydration step clay layers are brought to an expansion in the interlamellar region. As the hydration proceeds a fraction of the newly adsorbed molecules occupy the space left by the hydrated cations on the accessible internal and the external surfaces. 18 These molecules are termed as 'filling molecules'.<sup>24</sup> For a given water content below 20%, the swelling increases in the order Ba<sup>2+</sup> < Sr<sup>2+</sup> < Ca<sup>2+</sup> < Mg<sup>2+</sup>. Therefore, it is possible that the number of filling molecules follows the inverse order. Based on the above facts Calvet has concluded that the high conductivity is probably due to the presence of a large number of filling molecules. As discussed by Calvet<sup>24</sup>, with increasing water content the exchangeable cations in clay begin to move relatively freely near the clay surface. motion provides a dominant contribution to the imaginary part of  $\epsilon^*(\omega)$ . However, at water contents below 15 %, the contribution of the exchangeable cations to  $\varepsilon^*(\omega)$  can be neglected.<sup>24,37</sup>

Fripiat et al. have reported that the electrical conduction in montmorillonite clays is related to the mobility of water molecules in the adsorbed monolayer.<sup>21</sup> The ac conductivity  $(2 \times 10^2 - 2 \times 10^4 \text{ Hz})$  exponentially increases with the surface coverage of clay by water molecules. They also have observed that both  $\varepsilon'$  and  $\varepsilon''$  decrease

with increasing frequency and were more pronounced at higher hydration. According to Freyman and Soutif this phenomenon is an indication of conduction by free charge carriers.<sup>40</sup> Nuclear Magnetic Resonance studies performed by Ducross and Dupont<sup>41</sup> have shown that the degree of dissociation of water in montmorillonite clay is three orders of magnitude larger than that of liquid water. Because of the higher conductivity of Na<sup>+</sup> and Ca<sup>2+</sup> montmorillonite compared to silica gel and powdered window glass, and the above NMR studies, Fripiat et al have concluded that the migrating ions in these materials are protons.

The higher conductivity of montmorillonite, compared to silica gel and window glass, could be a result of the availability of exchangeable cations in montmorillonite clay. Such free charge carriers are either not found in silica gel or window glass, or if available their concentration is very small compared to the cation concentration in the montmorillonite clay. Therefore, it is necessary to further study these systems in detail in order to determine the migrating ion.

# II.b Experimental.

#### Materials

Sodium montmorillonite was obtained from the Clay Repository, University of Missouri, Columbia, MO. The mineral was purified first by sedimenting to collect the  $< 2 \mu m$  fraction and then

treating the clay with sodium acetate buffered at pH 5 and then with sodium dithionite to remove carbonates and free iron oxides respectively. Homoionic sodium montmorillonite was prepared by treating with 1 M sodium chloride; finally washed until free from Cland then freeze dried. Laponite was purchased from Laporte Industries Ltd Widnes, England and washed to remove any excess water soluble impurities and freeze dried. Lithium fluorohectorite was obtained from Corning, Inc. and the sodium and the cupric forms were prepared by treating with sodium chloride and cupric chloride respectively. After washing to remove adsorbed Cl- the samples were freeze-dried.

## Instrumentation

Clay samples for dielectric measurements were deposited from a 4% suspension of the appropriate clay platelets, to form self-supporting sheets about 0.05 mm thick. These thin films became the dielectric in a circular parallel plate capacitor made of stainless steel with 1 cm in diameter. Sample films were kept under vacuum (10<sup>-3</sup> torr) for twenty four hours before the actual measurements were begun. This allowed us to remove most of the adsorbed water from the clay films. Measurements were always made in the direction perpendicular to the plane of the clay film. Measurements of the capacitance, C and the parallel conductance, G<sub>p</sub> were made on a General Radio 1616 Capacitance Bridge in the frequency range 40-10<sup>5</sup> Hz with a bias voltage of 5V, as a function of water vapor

pressure. Water adsorption/desorption isotherms as well as layer d-spacings were also measured as functions of water vapor pressure. The water adsorption measurements allowed us to report capacitance and conduction as a function of the content of water in these clays as a weight percentage. To clearly define the capacitance and more importantly to avoid leakage around the edges of the dielectric, one plate of the capacitor had a concentric guard-ring connected as shown schematically in Figure II.13. At balance the guard-ring and the main capacitor plate are at the same potential and any leakage current is diverted to ground. This bridge sees the capacitance cell as a parallel combination of capacitance, C and conductance, G.

Water adsorption/desorption isotherms were obtained using a McBain balance equipped with a quartz glass spring and bucket. Four such balances were connected to a vacuum line so that four samples can be studied at a time. Samples were outgassed at room temperature under vacuum, 10-3 Torr for 24 hrs. After the end of the isotherms, samples were outgassed at an elevated temperature (150 °C) for 24 hrs to determine the amount of water retained in samples after outgassing at room temperature for 24 hrs.

X-ray powder diffraction patterns of oriented thin films were recorded using a Rigaku diffractometer equipped with a rotating copper anode and a Ni filtered Cu Kα radiation source. Quartz was used as the standard, and the tube was operated at 45 KV and 80 mA. A thin layer of clay coating was prepared on the stage of a special cell developed with a thin aluminum window (1.2 x 10<sup>-5</sup> cm) for the determination of d-spacings at different water vapor

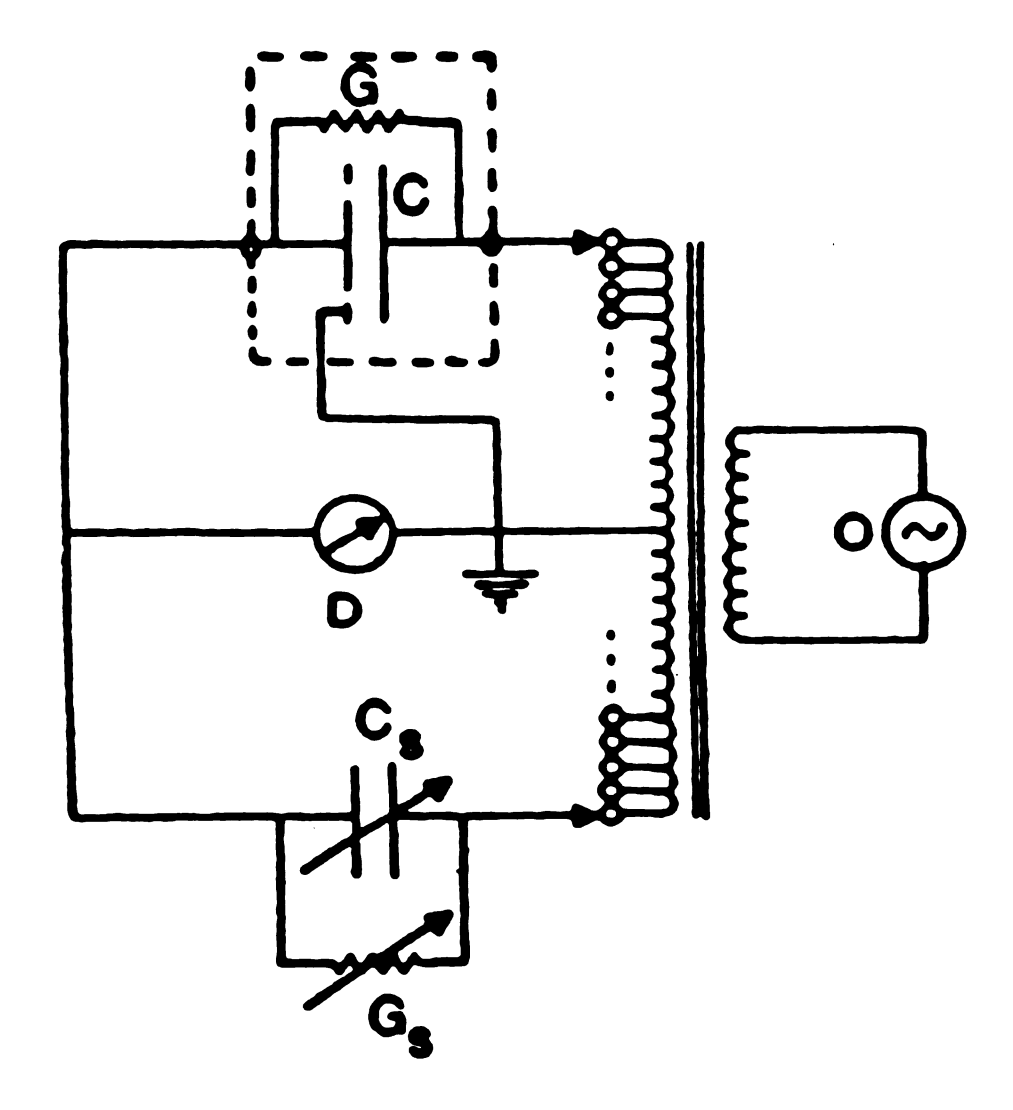


Figure II.13 A simplified circuit of the measuring bridge indicating the equivalent circuit elements C and G measured by the bridge, and the connection to the guard-ring.  $C_s$  and  $G_s$  are standard capacitances and conductances respectively. D is a dual phase sensitive detector.

pressures. At the beginning samples were outgassed for 24 hrs, as in the case of dielectric measurements or water adsorption isotherms, in order to remove the adsorbed water.

BET surface of the clay samples was measured using a Quantasorb Jr. Sorption Analyzer, Quantachrome Corporation Model QSJr. Samples were outgassed at 150 °C to remove all the adsorbed water molecules. Nitrogen was used as the adsorbate.

### II.c Results and Discussion

To study the effect of cation type, measurements were made of the series Li<sup>+</sup>, Na<sup>+</sup> and Cu<sup>2+</sup>-fluorohectorite. To study the effect of layer charge, measurements were made on Na<sup>+</sup>-fluorohectorite, Na<sup>+</sup>-montmorillonite and Na<sup>+</sup>-laponite.

# X-Ray Analysis

X-ray patterns of the air dried oriented clay films are shown in Figure II.14. They suggested that the structure of the fluorohectorite and montmorillonite films are similar, layers of more or less parallel platelets; laponite on the other hand forms disordered films. This disordered nature of the laponite clay films is probably a result of its smaller aspect ratio. Dependency of the d-spacing of Li+fluorohectorite on the relative water vapor pressure is depicted in Figure 15. As little as 3% of water by weight could expand the layers

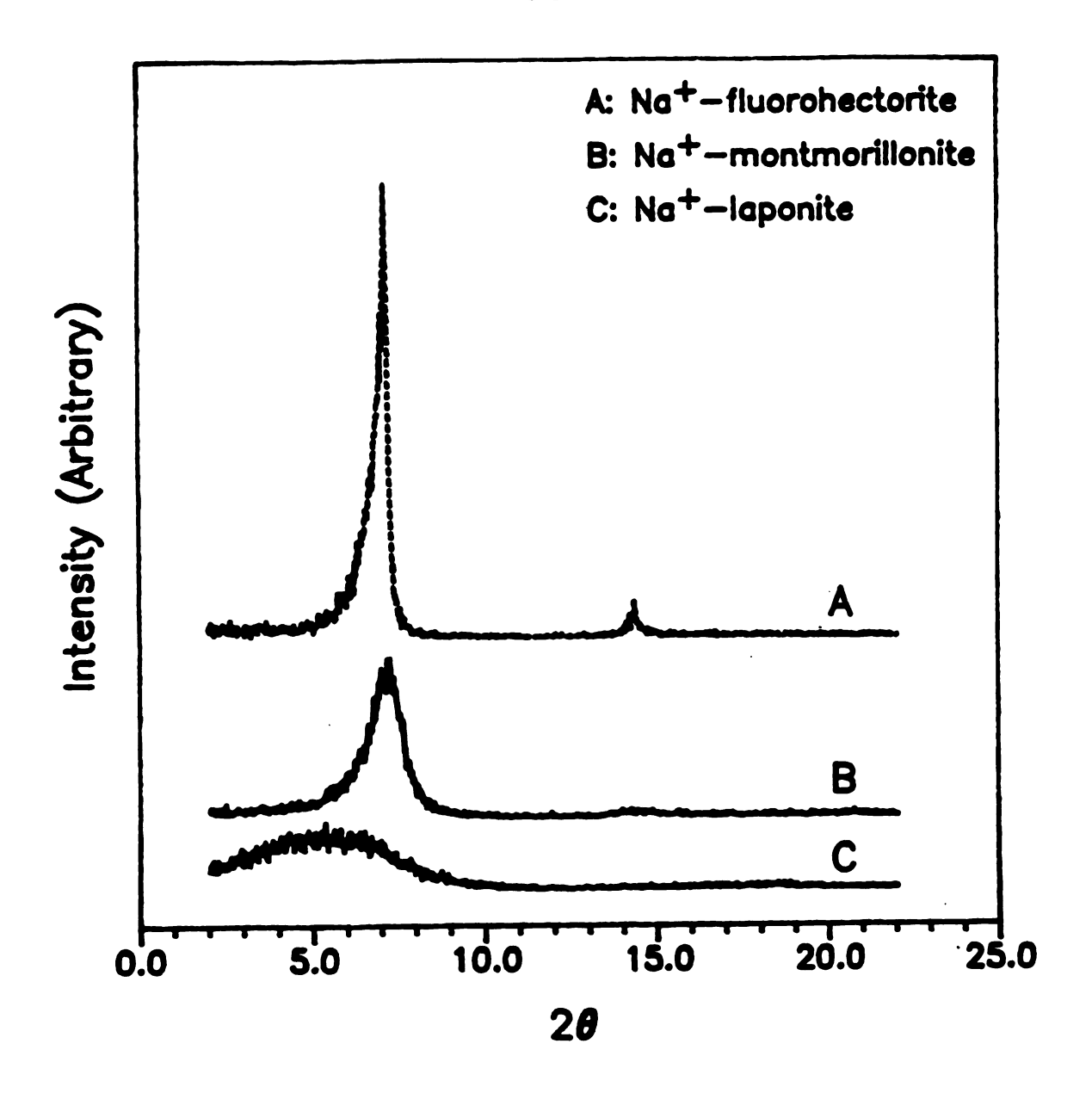


Figure II.14 X-ray patterns of air dried films of Na+fluorohectorite, Na+-montmorillonite and Na+-laponite.

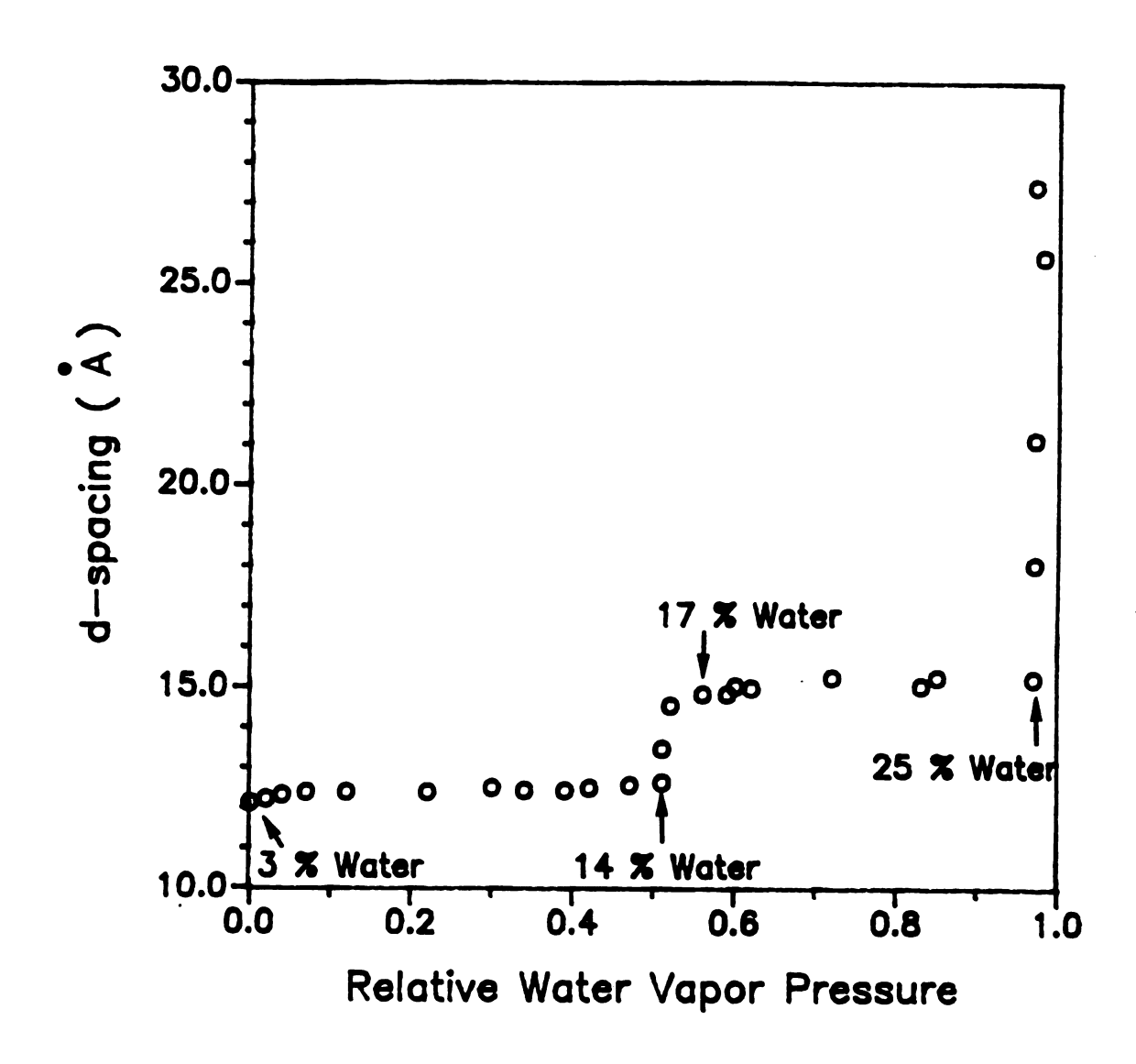


Figure II.15 d-spacing versus relative water vapor pressure of Li+-fluorohectorite.

by about 3 Å. This is because of the rigidity of the clay layers. A monolayer of water is completed when the water content is about 14% by weight, and with the adsorption of another 3% of water clay layers are separated by 3 Å more. By the end of the adsorption of the second layer, about 41% of water is found in the clay.

Another distinct difference between laponite, montmorillonite and fluorohectorite is their surface area. Table II.3 summarizes this and some other physical properties of these three different clays. The surface area of laponite is much higher than that of either montmorillonite or fluorohectorite. This is again a consequence of the difference in their particle size. Surface area of a non pillared layered material which contain a simple exchangeable cation such as Li<sup>+</sup> or Na<sup>+</sup>, is totally due to the external surfaces. This is because of the inaccessibility of the gallery or the interlamellar region due to the collapsing of layers upon degassing to remove the adsorbed The small aspect ratio of laponite particles gives the highest edge to face stacking upon the dehydration exposing most of the basal surface. On the other hand, because of the large aspect ratio, the fluorohectorite particles, favor the face to face stacking leading to a completely collapsed structure. As a result of this, only a very small external surface area is available. Intermediate size of the montmorillonite particles cause a moderate edge to face stacking generating an appreciable surface area.

Table II.3 Physical properties of laponite, montmorillonite and fluorohectorite.

Clay	Particle Size (Å)	CEC (meq/100g)	BET Surface Area (m <sup>2</sup> /g)	Charge Density (e/unit cell)
Laponite	200	48	300	0.4
Montmorillo	2,000	90	80	0.6
Fluorohecto-	20,000	122	3	1.2

## Water Adsorption Isotherms

Water adsorption isotherms were used to determine the percentage by weight of water content in clays. It is well known that clays frequently adsorb water or any other adsorbate in a stepwise fashion and hysteresis is exhibited in the complete adsorption desorption cycle.42-49 However, the stepwise adsorption is prominent only in moderately highly charged clays. According to Barrer, water adsorption in these clays seems to be dominated by the interlayer cations.<sup>50</sup> Layer charge as well as the type of cations in the galleries of a clay determine the extent of water adsorption and thereby control the swelling of the material.<sup>50</sup> If the layer charge is very high as in muscovite mica, the swelling properties of the material is hindered due to the greater electrostatic interaction between layers and the gallery cations. A simple hydration process can not bring, in this case, a lower energy state for the system than that which the material already has. Therefore, highly charged clays tend to stay unhydrated. When the layer charge is low, it is easy to push the layers away from their exchangeable cations by adsorbing a polar solvent such as water. However, the gallery cations still play an important role in this process. Energy of solvation of the gallery cations as well as the interaction with the hydrophilic clay layer surfaces may be the leading driving forces in this phenomenon.

## Isotherms

Water adsorption isotherms of Li<sup>+</sup>-fluorohectorite, Na<sup>+</sup>fluorohectorite and Cu<sup>2+</sup>-fluorohectorite are shown in Figures II.16, They all indicated a stepwise water II.17 and II.18 respectively. adsorption and exhibited a hysteretic behavior, which is characteristic of a porous material, upon desorption. This stepwise water adsorption is very characteristic of a swelling clay with a high layer charge such as vermiculite.<sup>42</sup> It is important to notice that according to X-ray analysis, Li<sup>+</sup>-fluorohectorite and Cu<sup>2+</sup>fluorohectorite samples retained a monolayer of water upon degassing at room temperature for 24 hrs. However, Na+fluorohectorite sample seems to loose almost all the inter-layer water upon the same treatment. The d-spacing obtained from X-ray analysis and the adsorption branch of the data water adsorption/desorption isotherm are shown in Figures II.19 and II.20 for Li<sup>+</sup> and Na<sup>+</sup>-fluorohectorite. At low relative water vapor pressure the first layer of water is completed and the second layer of water starts to build up at relative water vapor pressure of about 0.5 for Li<sup>+</sup>-fluorohectorite and 0.8 for Na<sup>+</sup>-fluorohectorite. When the relative water vapor pressure was about 0.9 multilayer adsorption begins to take place for Li<sup>+</sup>-fluorohectorite (Figure II.19). The water adsorption in Cu<sup>2+</sup>-fluorohectorite is very different from that of Li<sup>+</sup> and Na<sup>+</sup>-fluorohectorite. The steps are very weak and almost absent in the desorption branch. The hysteretic loop is very narrow and closes at a relative humidity of about 0.5. This difference may probably arise from the much higher q/r ratio (which determines the

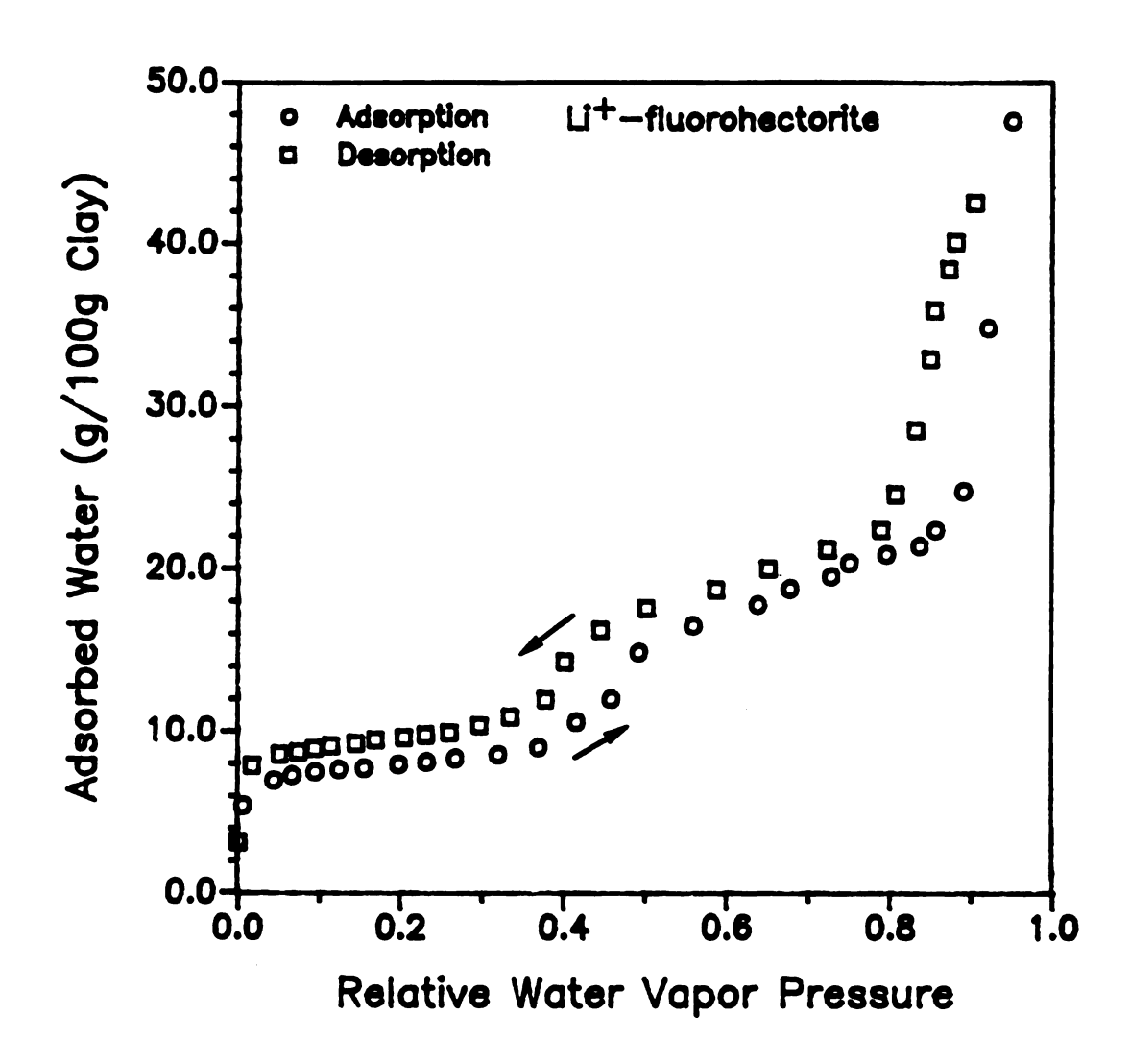


Figure II.16 Water adsorption/desorption isotherm of Li+fluorohectorite.

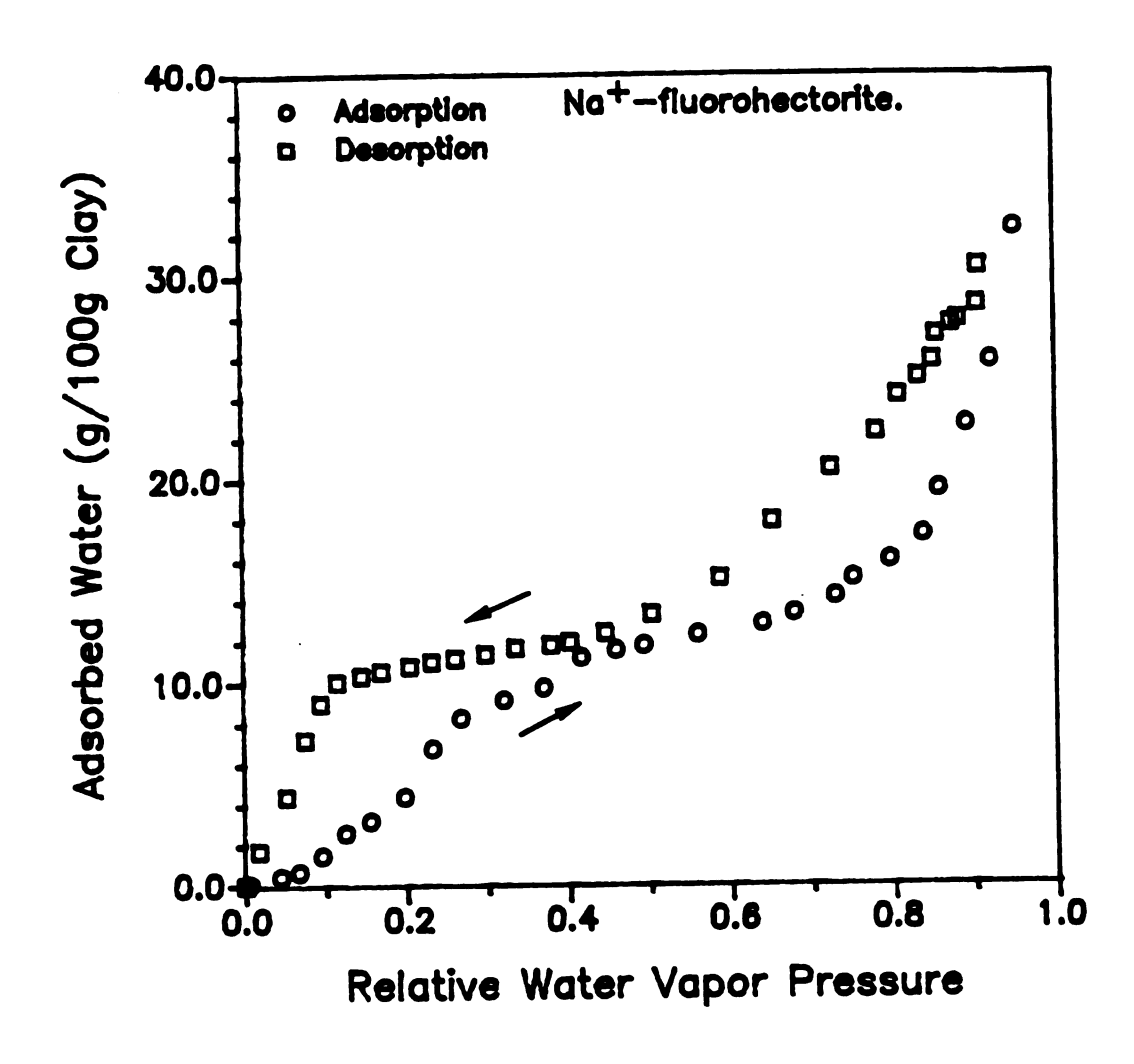


Figure II.17 Water adsorption/desorption isotherm of Na+fluorohectorite.

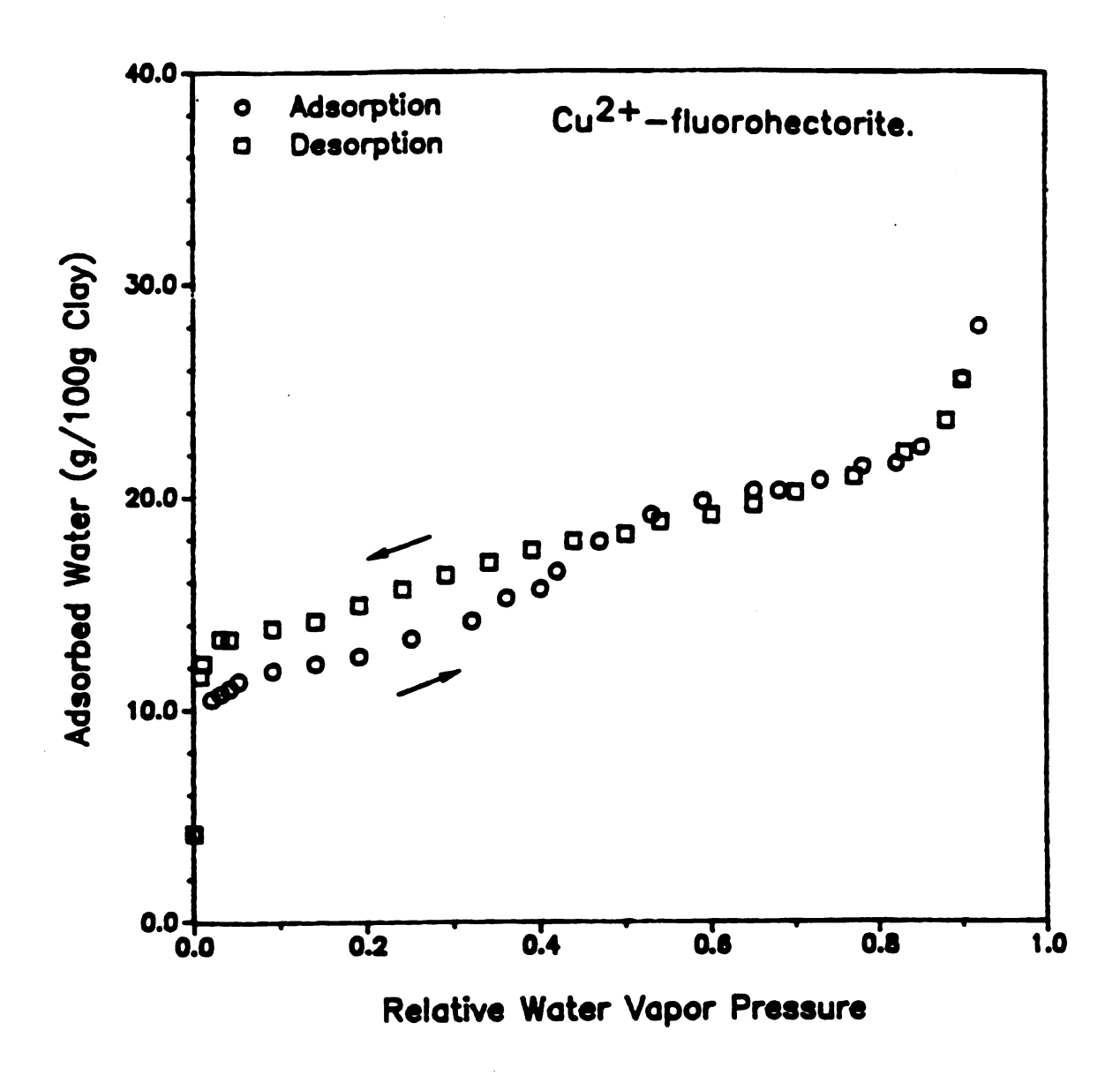


Figure II.18 Water adsorption/desorption isotherm of Cu<sup>2+</sup>-fluorohectorite.

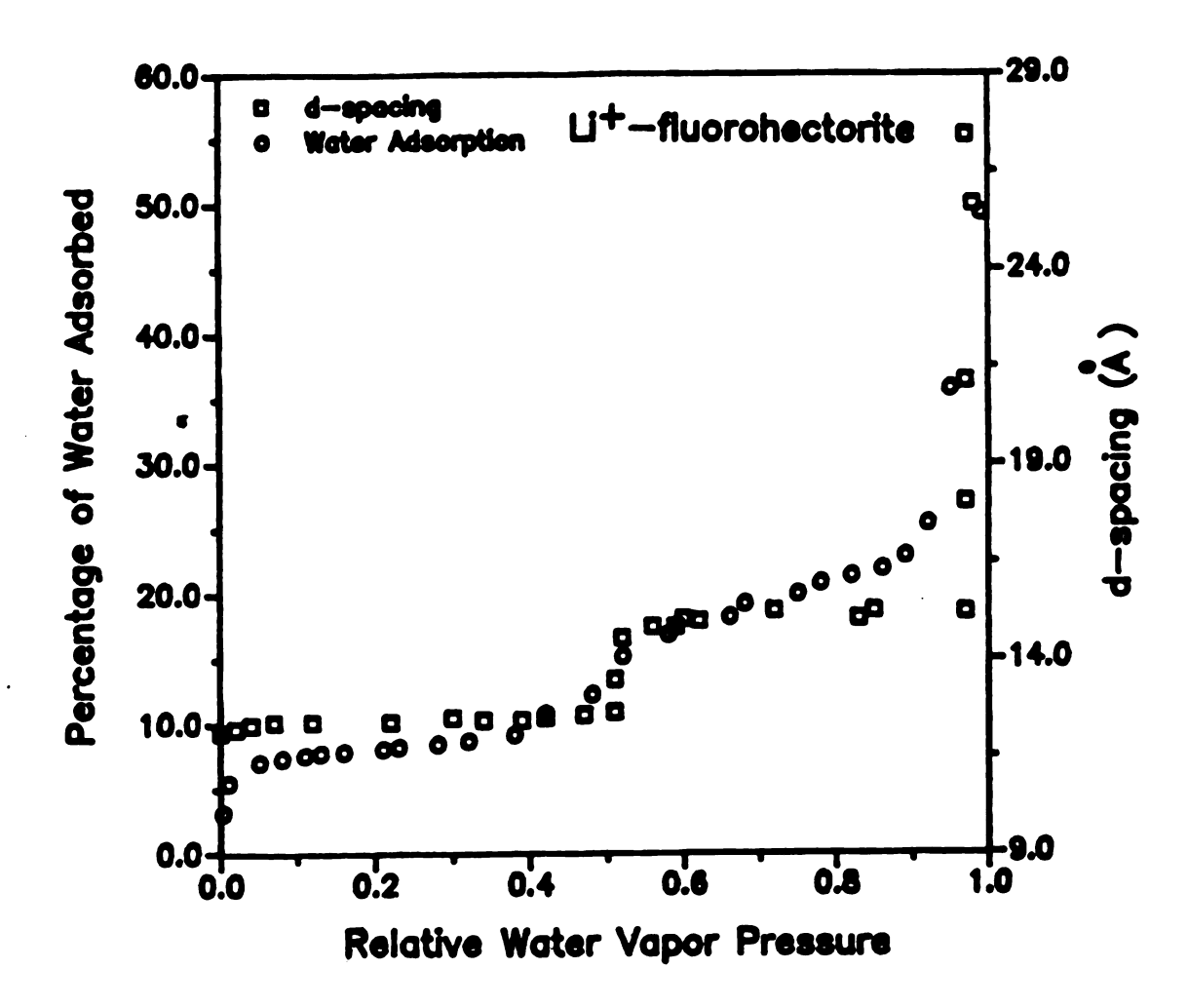


Figure II.19 d-spacing and water adsorption versus relative water vapor pressure of Li<sup>+</sup>-fluorohectorite.

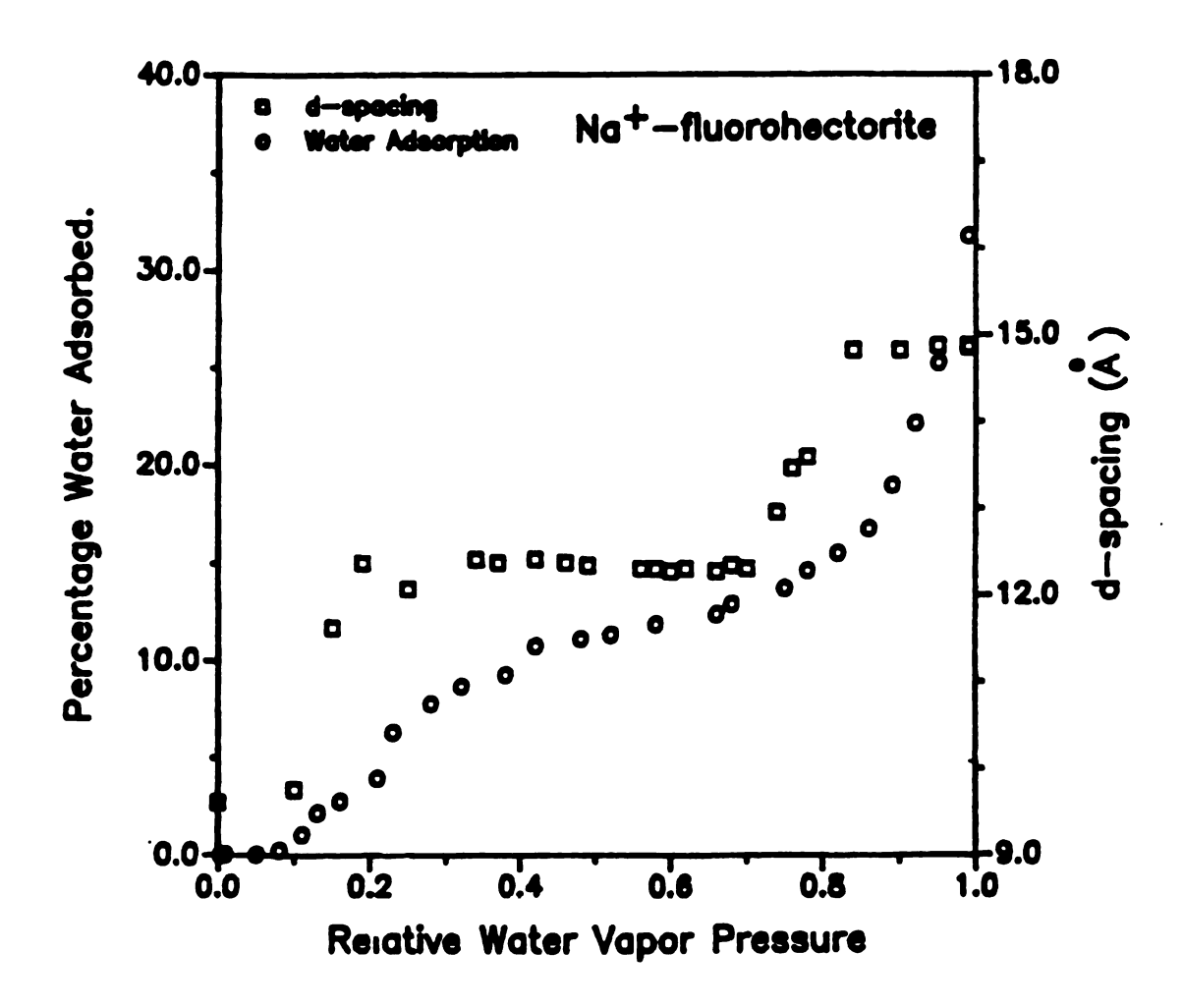


Figure II.20 d-spacing and water adsorption versus relative water vapor pressure of Na<sup>+</sup>-fluorohectorite.

extent of hydration) of Cu<sup>2+</sup> compared to Li<sup>+</sup> or Na<sup>+</sup>. Condensation of water begins near saturation vapor pressures. Water adsorption isotherms for Na<sup>+</sup>-montmorillonite and Na<sup>+</sup>-laponite are shown in Figures II..21 and II.22 respectively. Even though, they both exhibited a hysteretic isotherm, no clear indication for a stepwise adsorption was found. This may result from the simultaneous adsorption of both monolayer and bilayer ie second layer of water starts to build up before the first layer is completed. Laponite sample adsorbed more water than montmorillonite or fluorohectorite because of the higher external surface area of the material.

# Effects of Water and type of Gallery Cations on Dielectric Properties.

Relative permittivity and conductivity at 1 kHz as functions of percentage water content for Li<sup>+</sup>, Na<sup>+</sup> and Cu<sup>2+</sup> -fluorohectorites are depicted in figures II.23 and II.24 respectively. They indicate that there is no appreciable enhancement of either the relative permittivity or the conductivity by the first layer of adsorbed water. However, with the adsorption of the second layer of water both the relative permittivity and the conductivity start to increase sharply and the increase is prominent in the case of Na<sup>+</sup>-fluorohectorite. Relative permittivity as well as conductivity is in the order Cu<sup>2+</sup>-fluorohectorite < Li<sup>+</sup>-fluorohectorite < Na<sup>+</sup>-fluorohectorite. We interpret these data in the following way. This order of conductivity and the relative permittivity is in the decreasing order of q/r (q =

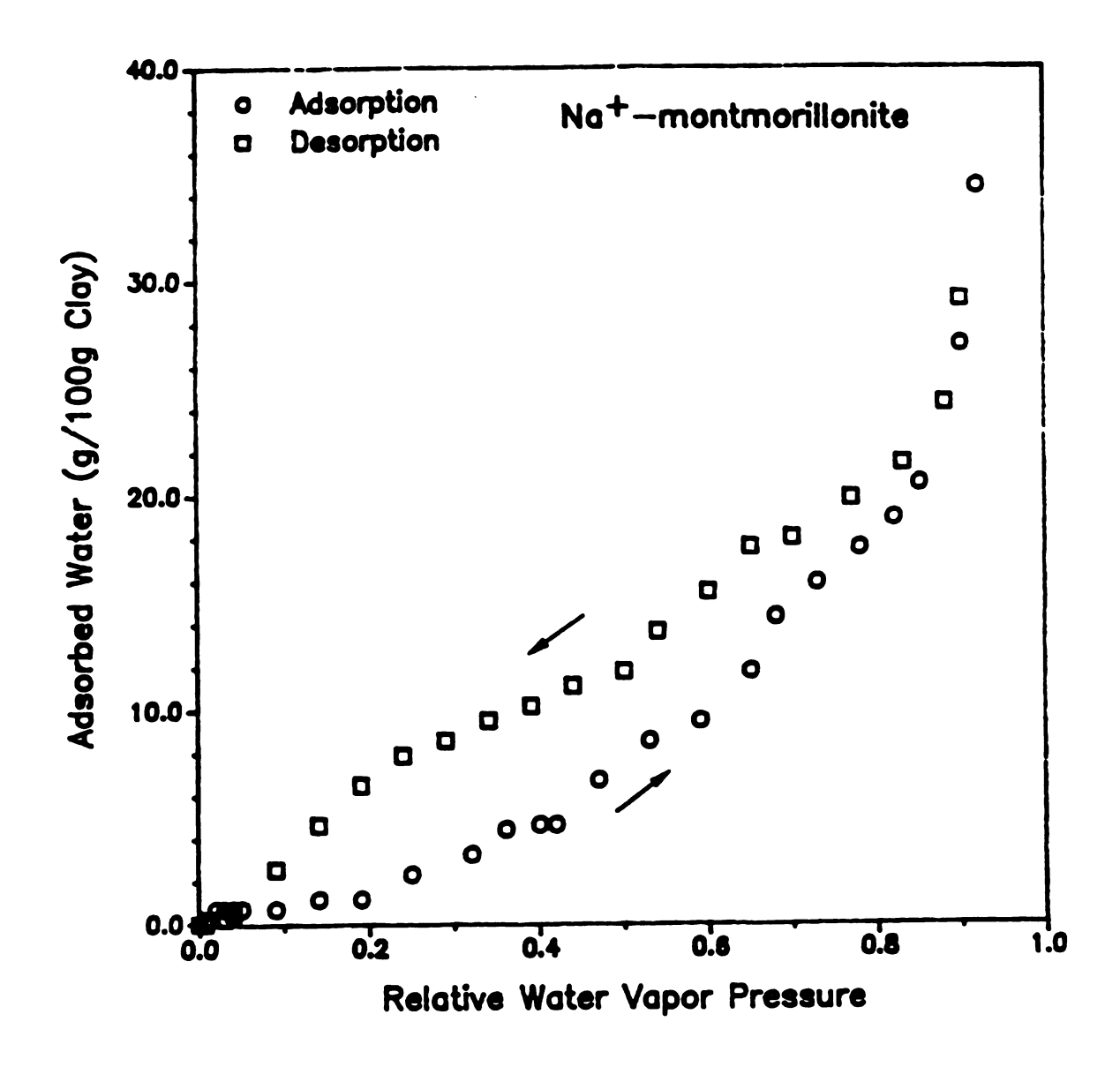


Figure II.21 Water adsorption/desorption isotherm of Na+montmorillonite.

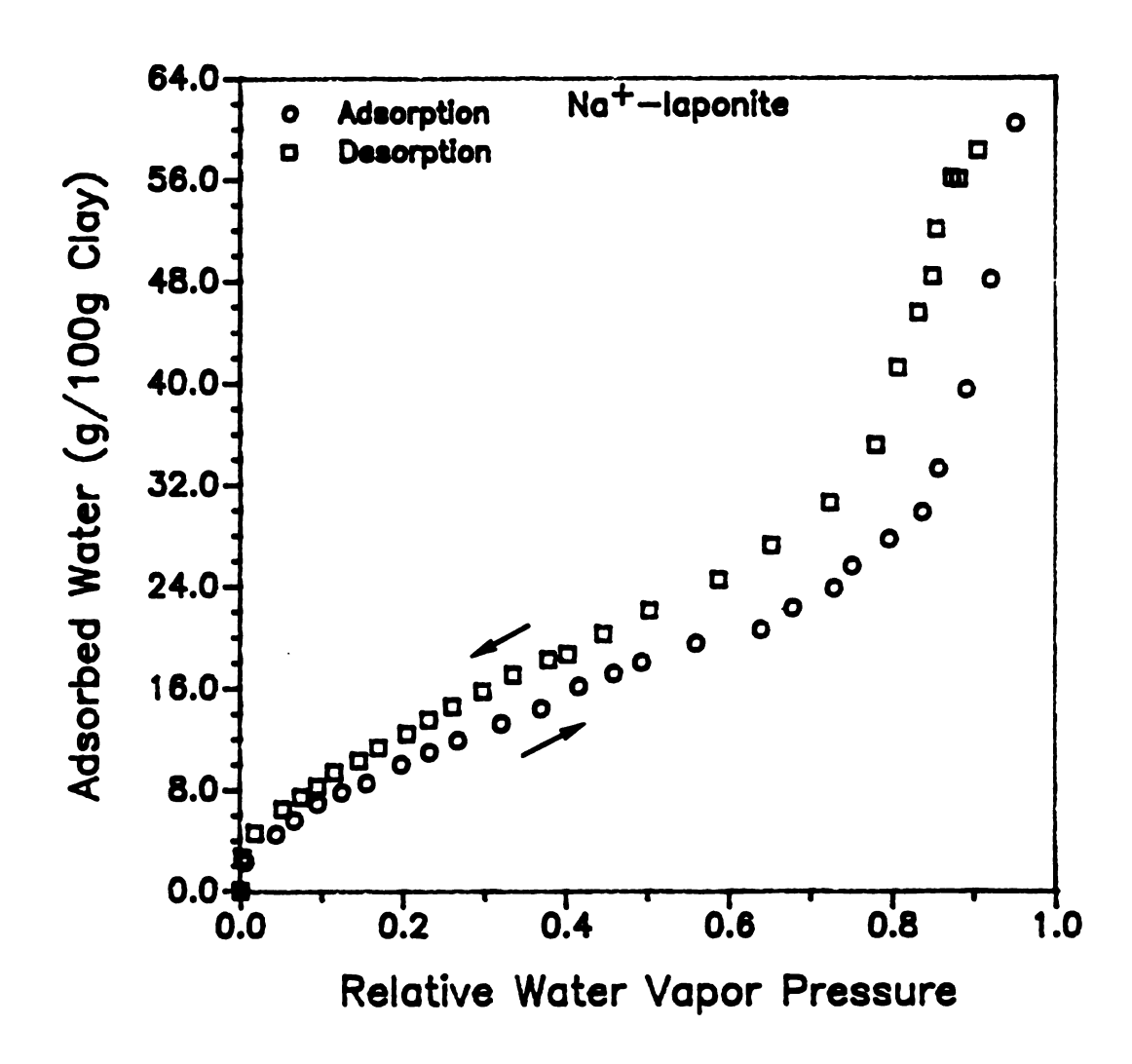


Figure II.22 Water adsorption/desorption isotherm of Na+-laponite.

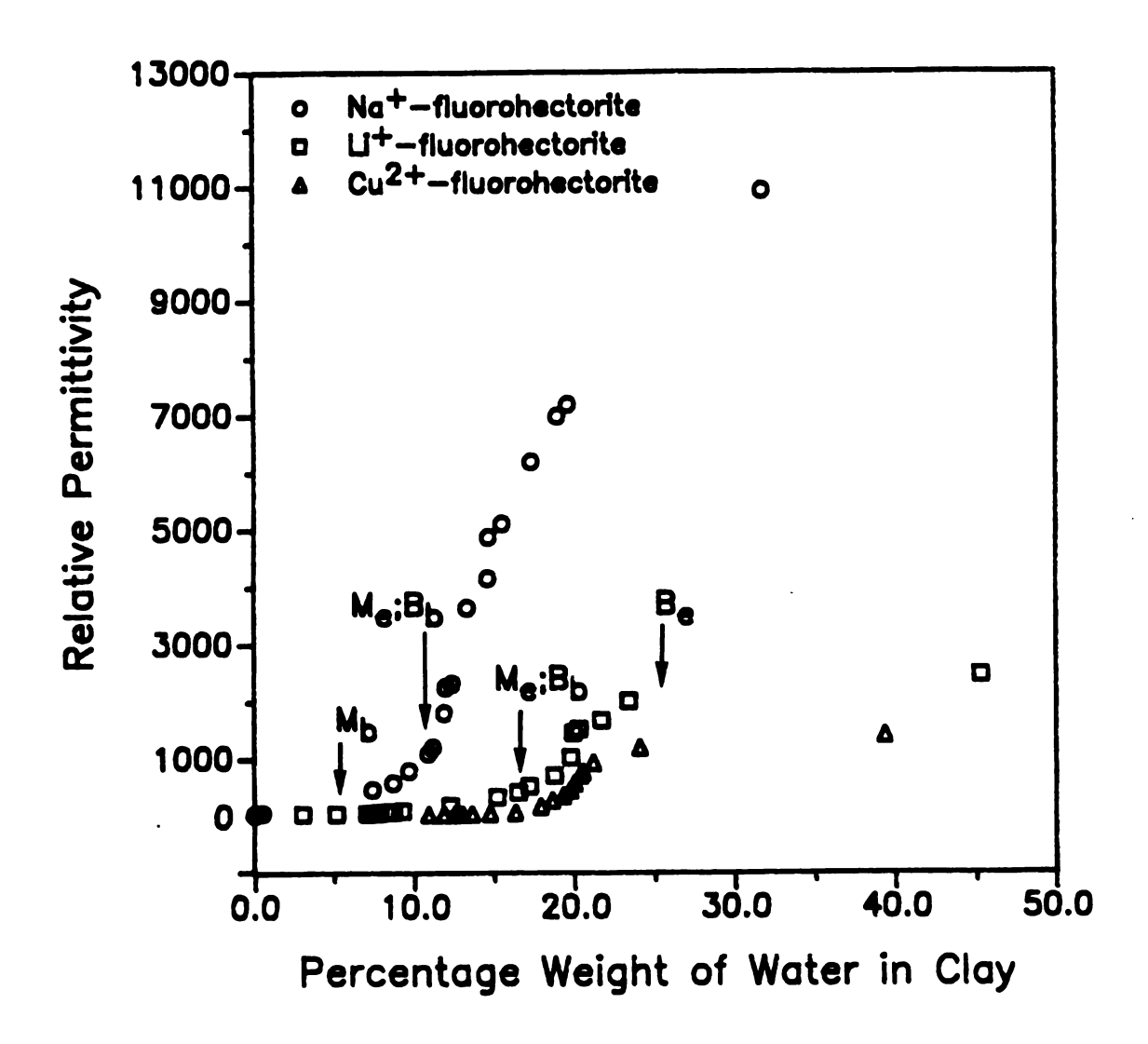


Figure II.23 Water dependency of the relative permittivity of Li<sup>+</sup>-fluorohectorite, Na<sup>+</sup>-fluorohectorite and Cu<sup>2+</sup>-fluorohectorite.  $M_b$  = Monolayer begins;  $M_e$  = Monolayer ends;  $B_b$  = Bilayer begins;  $B_e$  = Bilayer ends.

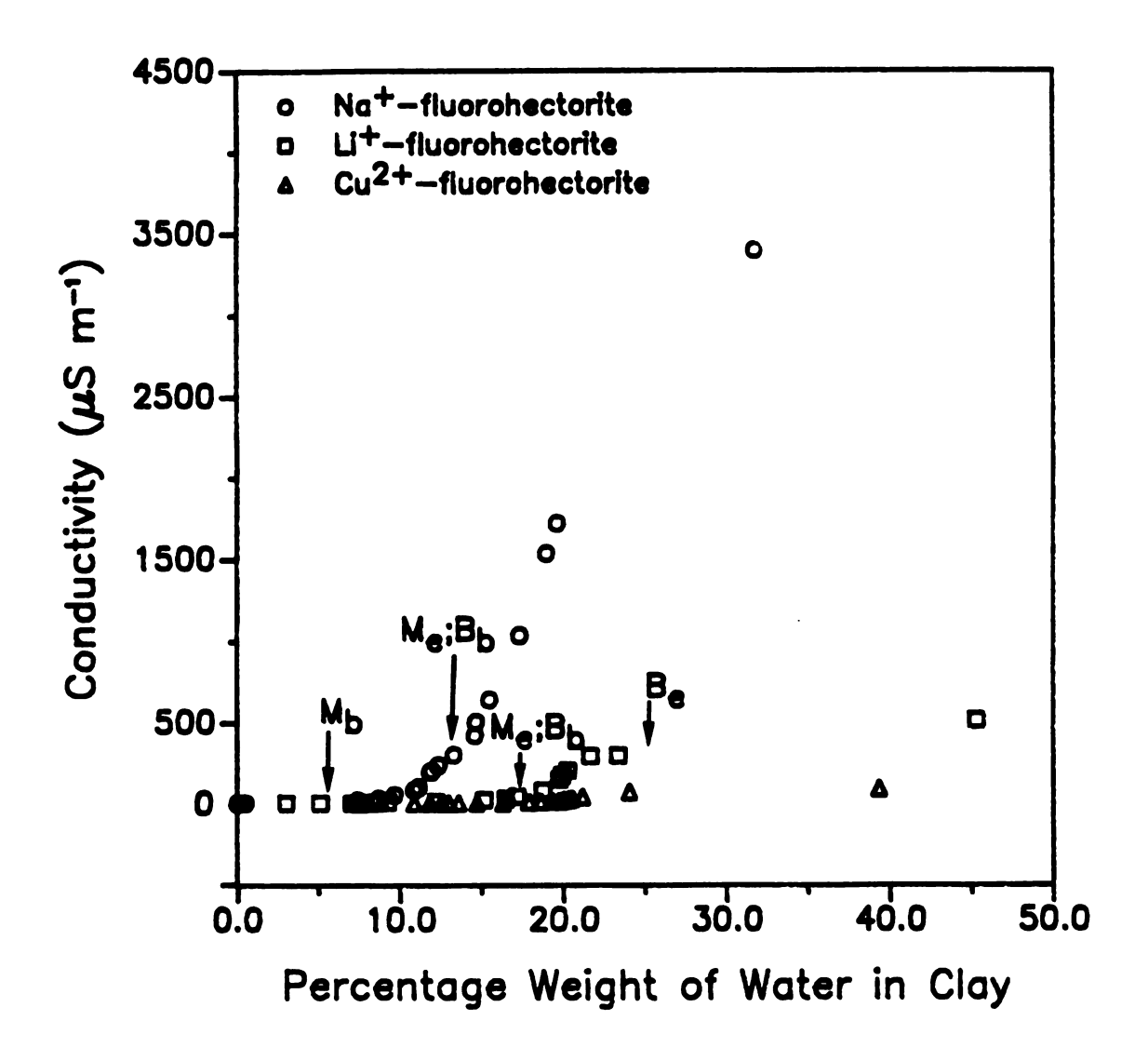


Figure II.24 Water dependency of the conductivity of Li<sup>+</sup>-fluorohectorite, Na<sup>+</sup>-fluorohectorite and Cu<sup>2</sup>+-fluorohectorite.  $M_b$  = Monolayer begins;  $M_e$  = Monolayer ends;  $B_b$  = Bilayer begins;  $B_e$  = Bilayer ends.

charge, r = radius) of the anhydrous gallery cation (Cu<sup>2+</sup>, r = 0.72 Å; Li<sup>+</sup>, r = 0.78 Å; Na<sup>+</sup>, r = 0.98 Å).<sup>51</sup> However, in order to have this order with q/r for the hydrated cation, which is the responsible species for the observed conductivity, the hydration of Li<sup>+</sup> and Na<sup>+</sup> cations at a given water content must be the same within these clay samples, at least in the range of relative water vapor pressure studied. In fact the X-ray analysis of these clays indicated that they have the same stage of hydration through out the range used for dielectric measurements (Figure II.25). As the q/r ratio increases the electrostatic binding of the cation to the negatively charge clay layers increases. As a result of this conductivity decreases with increasing q/r. On the other hand, when the cations are completely dehydrated, the electrostatic attraction to the negatively charged clay layers hinders the cations from moving back and forth. When the first layer of hydration occurs all the water molecules are in the ab plane of the clay layer. This leaves the axes perpendicular to the clay layers exposed to the electrostatic field of the negatively charged clay platelets. Therefore, the first layer of hydration does not effectively screen the cations from the negatively charged clay layers. When the second layer of hydration occurs each cation is surrounded by a sheath of water molecules. This arrangement of the water molecules leads to a more effective screen of cations from the negatively charged clay layers. This causes the enhancement of conductivity with the adsorption of the second layer of hydration. Furthermore, the above order of conductivity suggests that the migrating species is the hydrated cation rather than the protons originating from the dissociation of water molecules. In fact if the

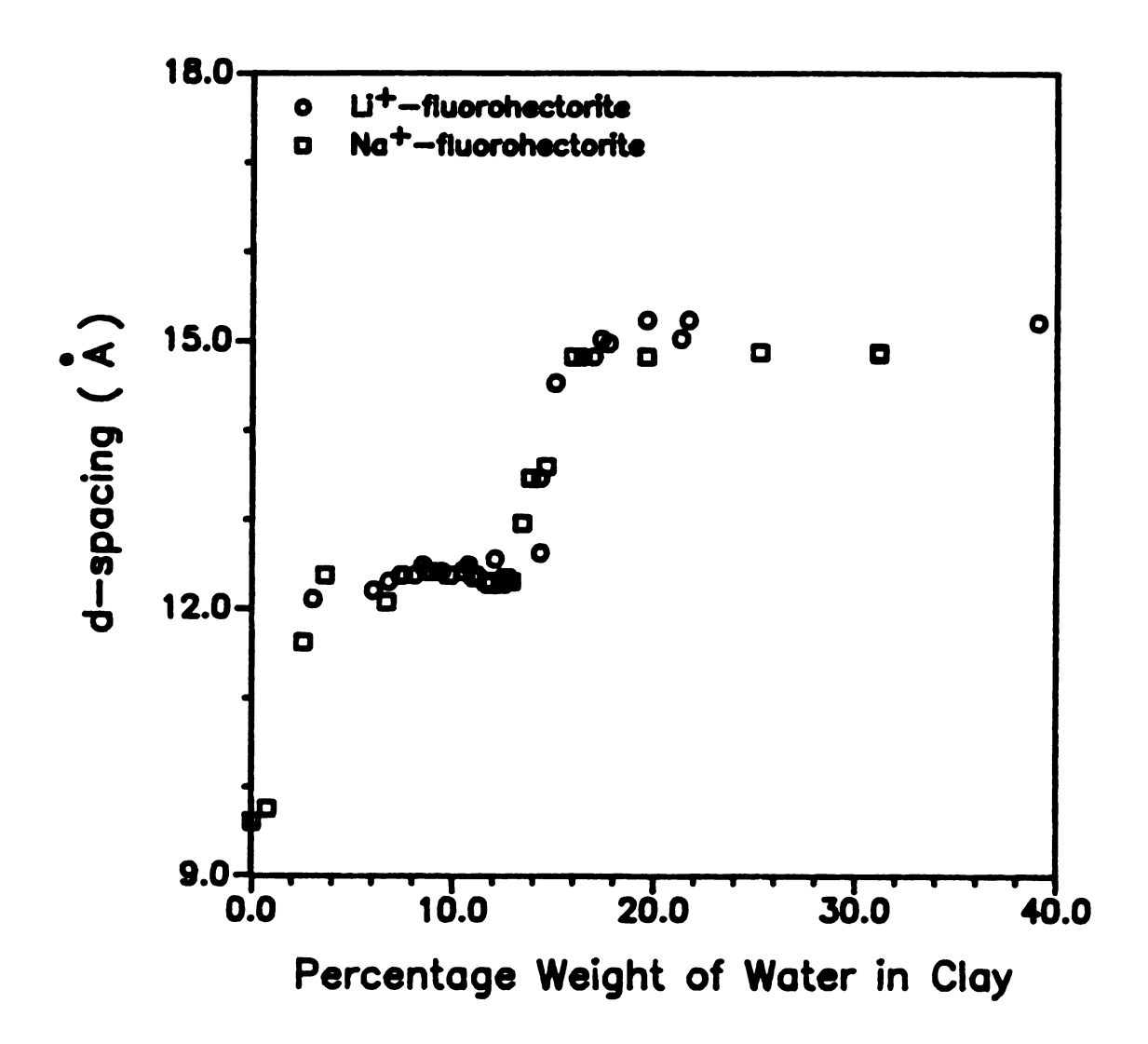


Figure II.25 d-spacing of Li<sup>+</sup>-fluorohectorite and Na<sup>+</sup>-fluorohectorite as a function of the percentage water content of the clay.

migrating species are predominantly protons the highest conductivity could be anticipated for Cu<sup>2+</sup>-fluorohectorite simply because the high q/r ratio of Cu<sup>2+</sup> should generate more protons than Li<sup>+</sup> or Na<sup>+</sup> and exhibit a higher conductivity than that of either Li<sup>+</sup> or Na<sup>+</sup> fluorohectorite.

# Effects of Layer Charge.

Relative permittivity and conductivity of Na<sup>+</sup>-fluorohectorite, Na<sup>+</sup>-montmorillonite and Na<sup>+</sup>-laponite at 1 kHz are shown in Figures II.26 and II.27 respectively. Both the cation exchange capacity and the particle size increase in the order laponite < montmorillonite < fluorohectorite ( see Table II.3). Assuming the migrating species is the hydrated cations, on the basis of the cation exchange capacity the conductivity of these three clays should be in the order laponite < montmorillonite < fluorohectorite. Relative permittivity could also vary in the same order because of the increase in the polarization of water molecules with increasing charge density. However, the results indicate that it is not the case. This may be due to the difference in the texture of these clay films. For instance, laponite has a disordered film structure but montmorillonite and fluorohectorite have more ordered film structure.

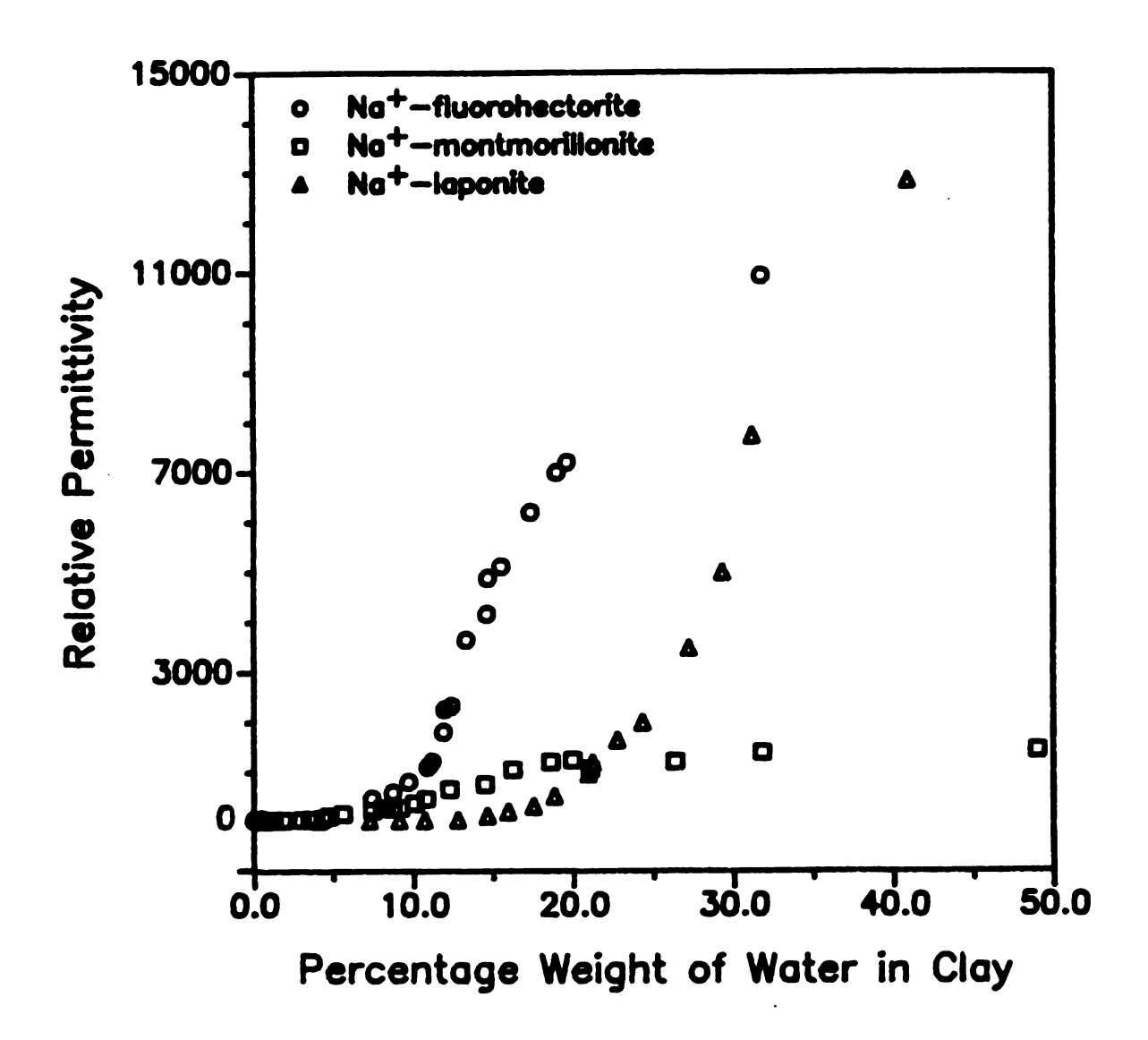


Figure II.26 Water dependency of the relative permittivity of Na+-fluorohectorite, Na+-montmorillonite and Na+-laponite.

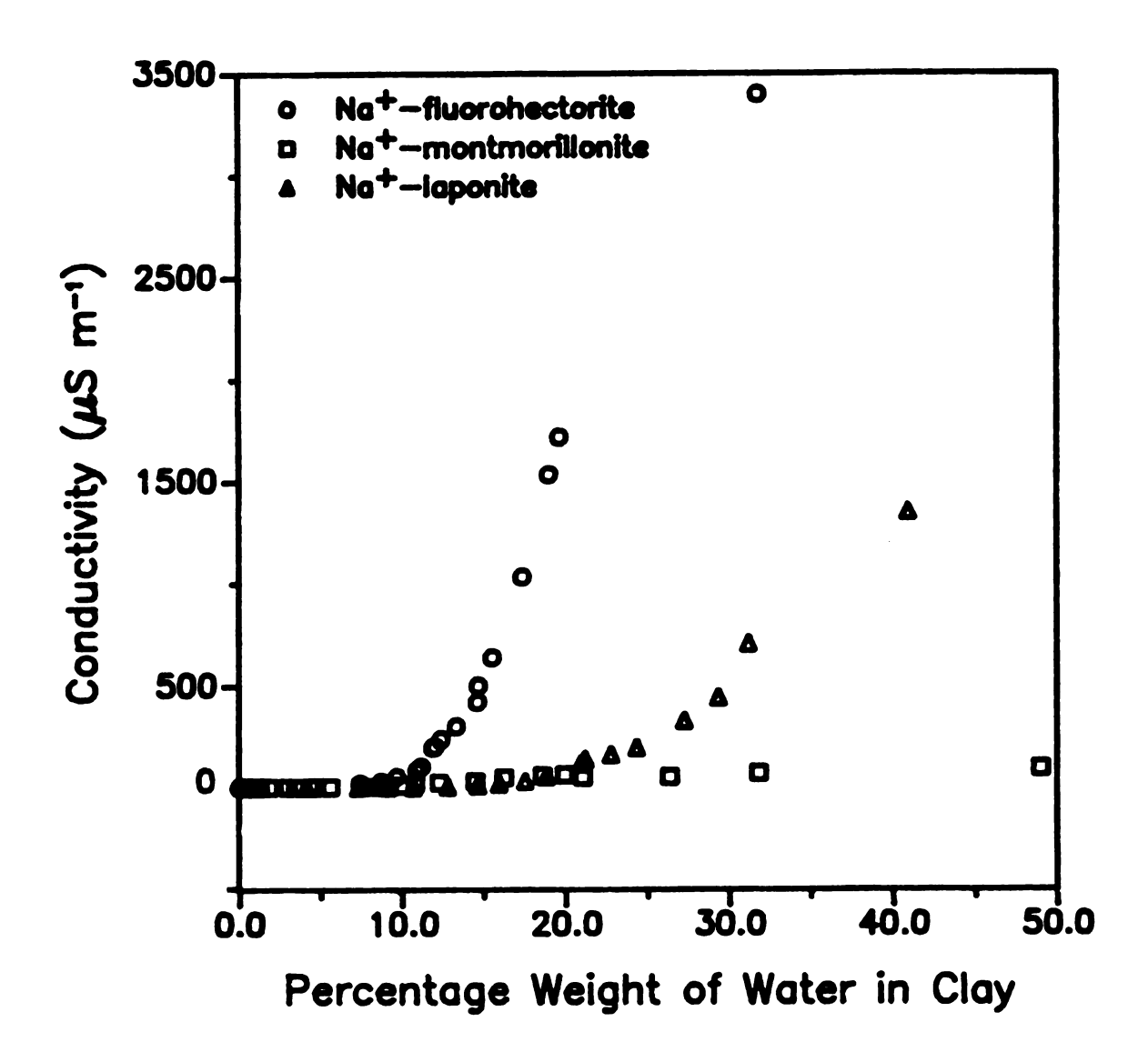


Figure II.27 Water dependency of the conductivity of Na<sup>+</sup>-fluorohectorite, Na<sup>+</sup>-montmorillonite and Na<sup>+</sup>-laponite.

## Effects of Frequency of the Applied Voltage

Cole-Cole plot for Na<sup>+</sup>-fluorohectorite is shown in Figure II.28. All the other clay samples studied also showed the very similar behavior. No evidence of dipolar relaxation is found. However, some evidence for the electrode polarization is observed. The relative permittivity and the conductivity of Na<sup>+</sup>-fluorohectorite are plotted against the frequency of the applied voltage at different water contents (Figures II.29 and II.30 respectively). Relative permittivity decreases rapidly with increasing frequency of the applied voltage. The decrease is prominent in the case of higher water content as observed by Fripiat et al.<sup>21</sup>. Conductivity increases dramatically with increasing frequency of the applied voltage. Again the increase is more rapid at higher water contents. Similar trends were found in every clay sample studied.

### II.d Conclusions.

- 1. Conductivity of clays is due to the migration of hydrated exchangeable cations and increases with decreasing charge to radius ratio of the hydrated gallery cation.
  - 2. No evidence for the dielectric relaxation was found.
- 3. Cole-Cole plots were somewhat similar to Figure II.6 indicating the electrode polarization effect.

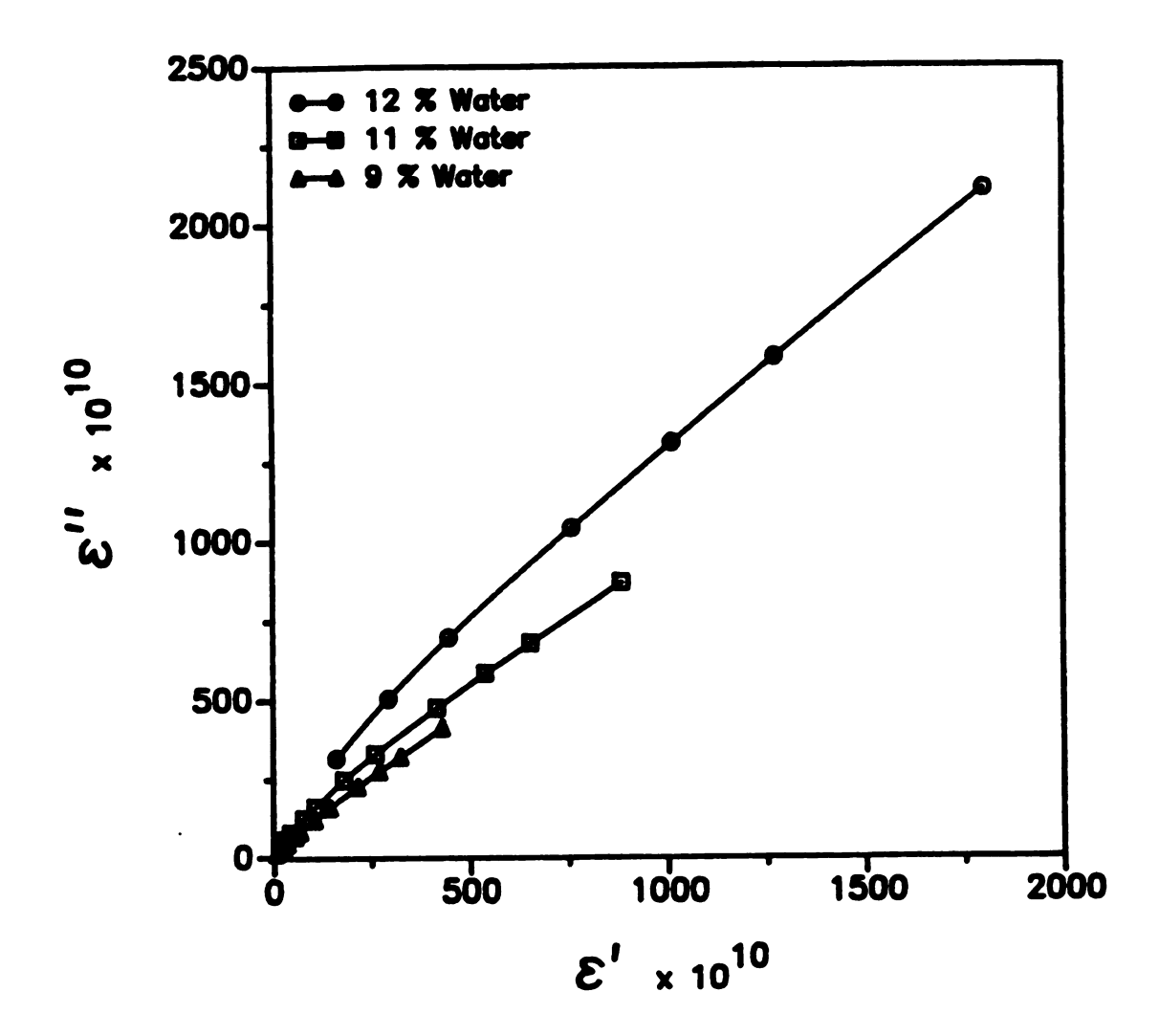


Figure II.28 Cole-Cole ( $\epsilon$ " Vs  $\epsilon$ ') of Na<sup>+</sup>-fluorohectorite.

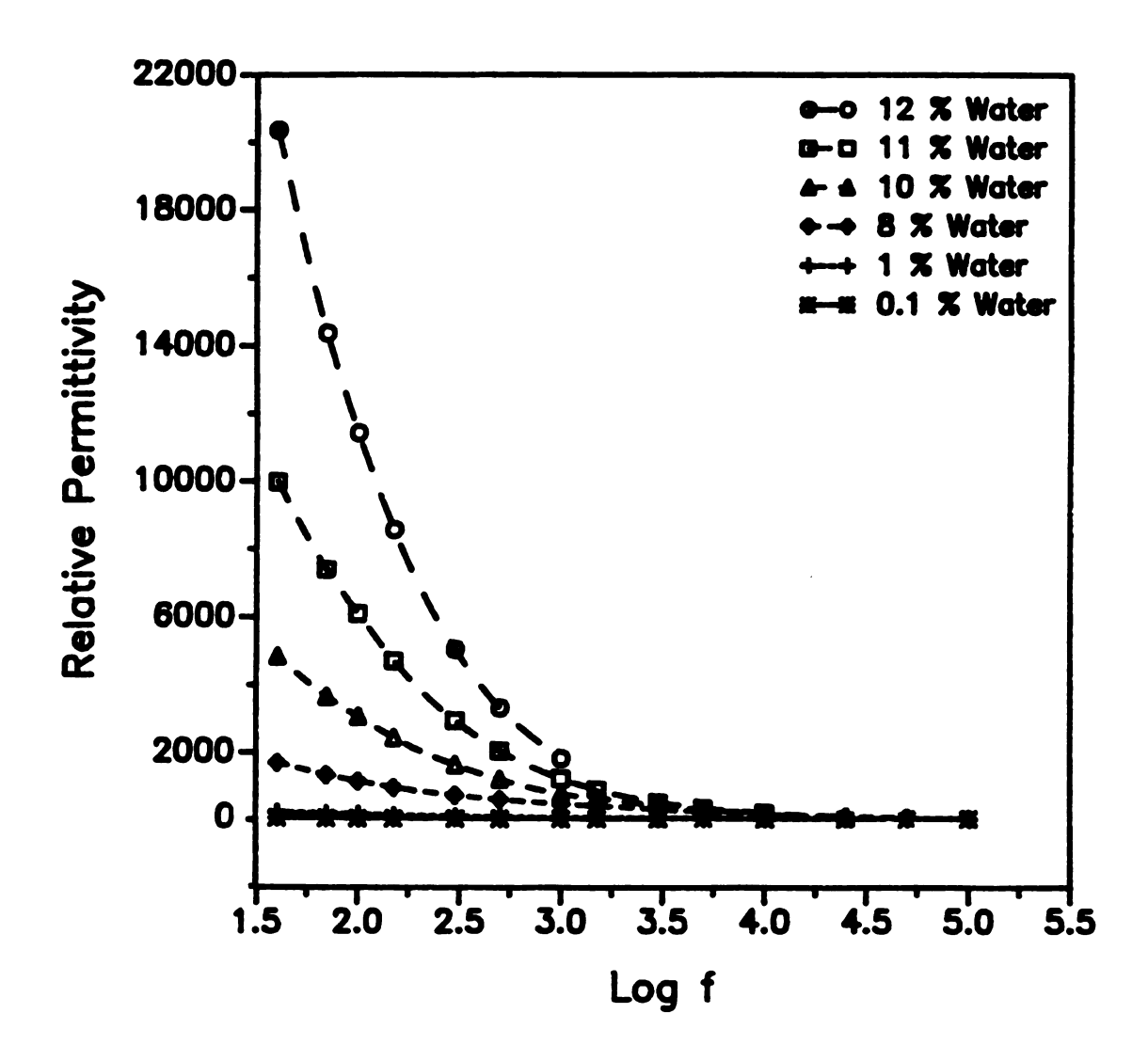


Figure II.29 Frequency dependence of the relative permittivity of Na<sup>+</sup>-fluorohectorite.

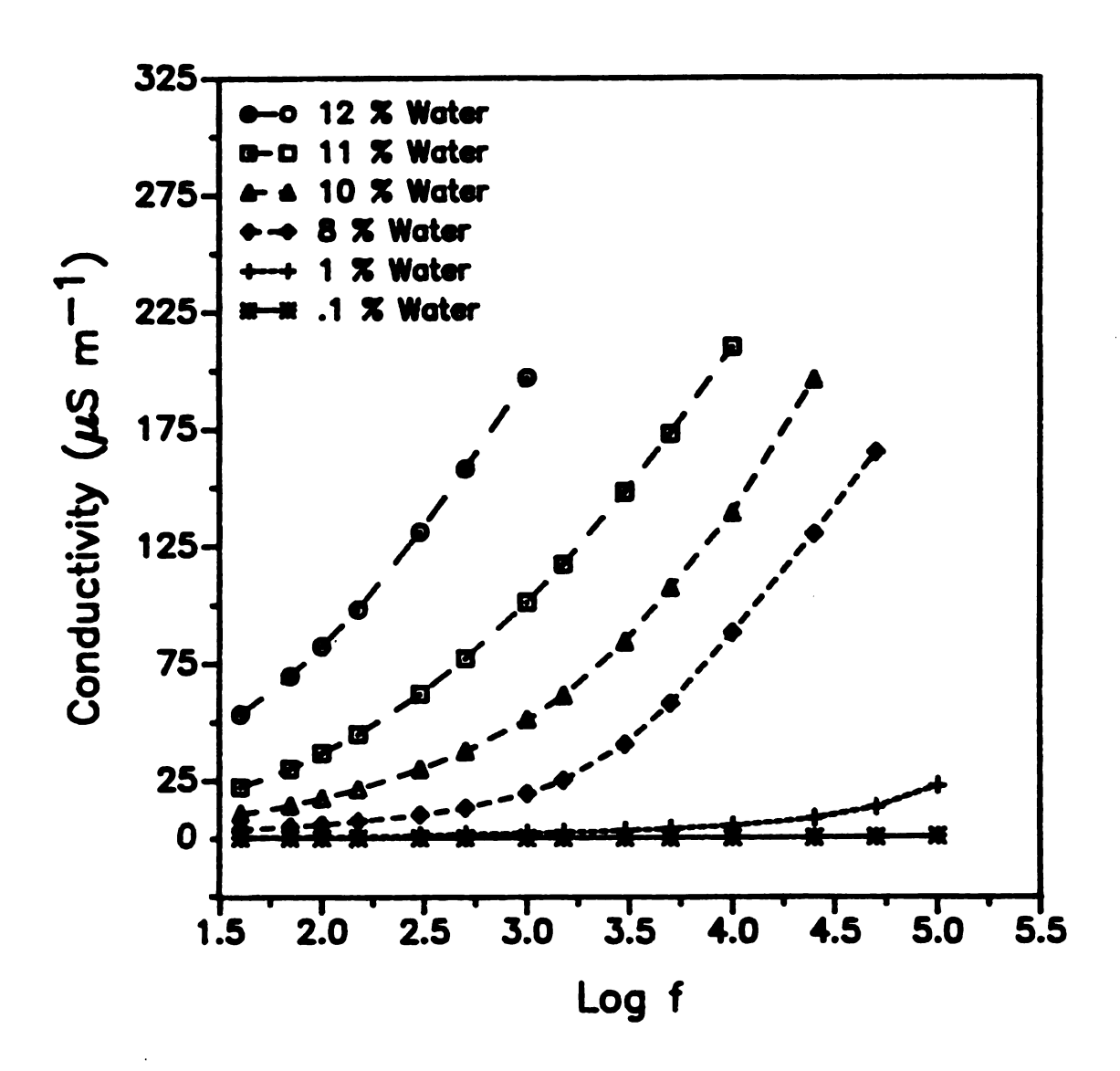
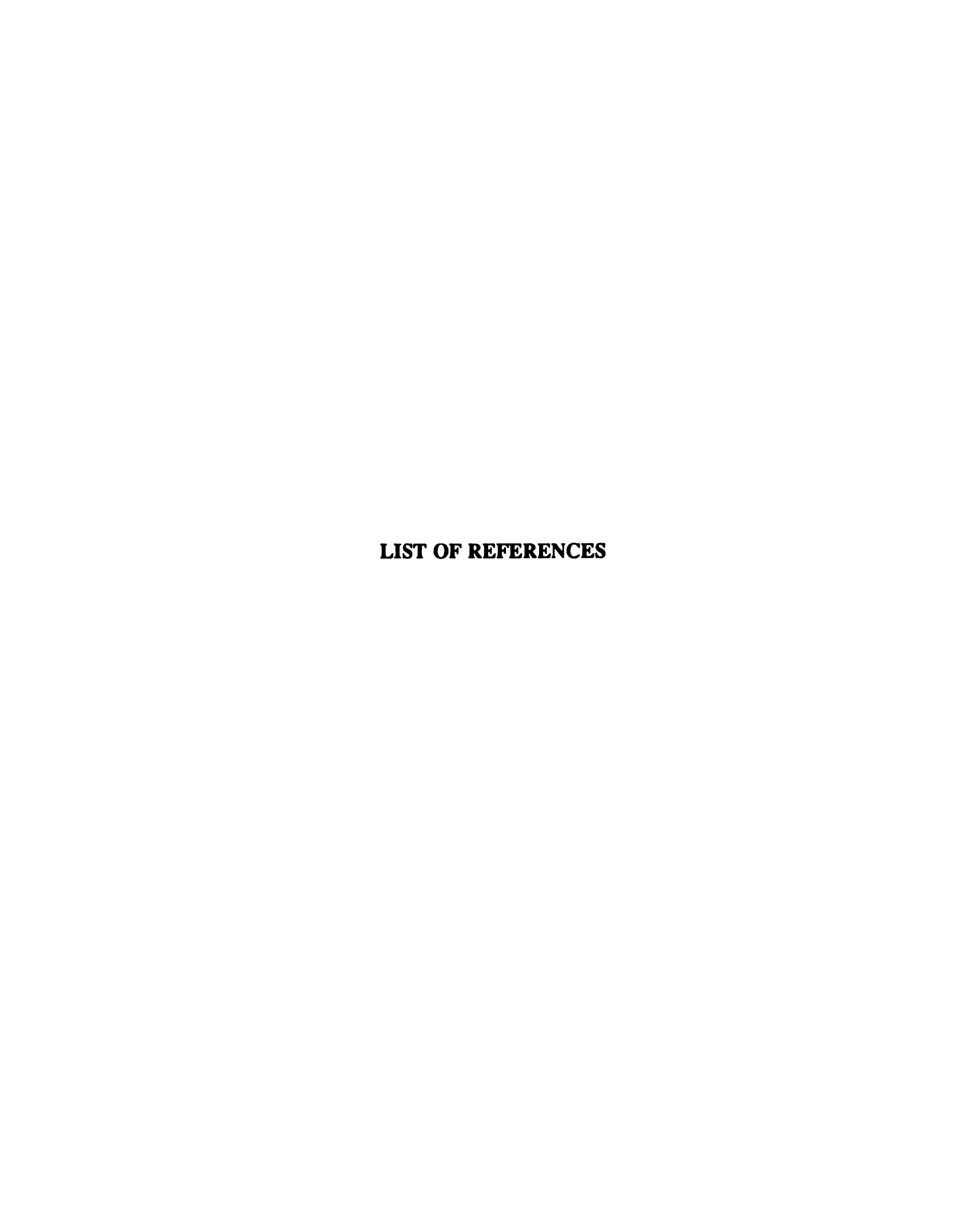


Figure II.30 Frequency dependence of the conductivity of Na+-fluorohectorite.

4. The near linear relationship between  $\varepsilon''$  and  $\varepsilon'$  indicates that  $\tan \delta = \varepsilon''/\varepsilon'$  is a constant. Here  $\delta$  is the phase angle between applied voltage and current in the measuring system. This is referred to as constant phase angle behavior. It is frequently observed at low frequencies and has not been completely explained. To date we have not found the appropriate model to give the correct frequency dependence, but the analytical possibilities are not all worked out



#### LIST OF REFERENCES

- Schwan, H. P.; Schwarz, G.; Maczuk, J.; Pauly, H. J. Phys. Chem. 1962, 66, 2626.
- 2. Frank, F. Water, A Comprehensive Tretise Vol 1. The Physics and Physical Chemistry of Water, Plenum Press: New York, 1972.
- 3. Sposito, G.; Prost, R. Chem. Rev. 1982, 82, 553.
- 4. Sen, P. N.; Chew, W. C. J. Microwave Power 1983, 18, 95.
- 5. Sen, P. N.; Chew, W. C.; Wilkinson, D. A. I. P. Conference Proceedings 1984, 107, 52.
- 6. Sen, P. N.; Scala, C.; Cohen, M. H. Geophysics 1981, 46, 781.
- 7. Kittel, C. Introduction to Solid State Physics 5th Ed.; New York, John Wiley.
- 8. Maxwell, J. C. A Treatise on Electricity and Magnetism, Ed.; New York, Dover Publication Inc. 1954.
- 9. Wagner, K. W. Erklarung der Dielektrischen Nachwirkungen auf Grund Maxwellscher Vosrtellungeni Arch. Electr. V2 p371.
- 10. Sen, P. N. Geophysics 1981, 46, 1714.

- 11. Kenyon, W. E. J. Appl. Phys. 1984, 55, 3153.
- 12. Bidadi, H.; Schroeder, P. A.; Pinnavaia, T. J. J. Phys. Chem. Solids 1988, 49, 1435.
- 13. Anderson, J. C. Dielectrics Reinhold Ed.; New York, 1964.
- 14. Day, D. R.; Lewis, T. J.; Lee, H. L.; Senturia, S. D. J. Adhesion 1985, 18, 73.
- 15. Chew, W. C.; Sen, P. N. J. Chem. Phys. 1982, 77, 4683.
- 16. O'Brien A. B.; White, L. R. J. Chem. Soc. Faraday Trans. II 1978 74 1607.
- 17. Fixman, M. J. Chem. Phys. 1981, 72, 5177.
- 18. Fixman, M. Macromolecules. 1981, 13, 711.
- 19. Delacey, E. H. B.; White, L. R. J. Chem. Soc. Faraday Trans. II 1981, 77, 2007.
- 20. Fixman, M. J. Chem. Phys. 1983, 78, 1483.
- 21. Fripiat, J. J.; Jelli, A.; Poncelet, G.; Andre, J. J. Phys. Chem. 1965, 69, 2185.
- 22.. Weiler, R. A.; Chaussiden, J. Clays Clay Miner. 1968, 16, 147.
- 23. Arulanandan, K.; Mitchell, J. K. Clays Clay. Miner. 1968, 16, 337.
- 24. Calvet, R. Clays Clay Miner. 1975, 23, 257.

- 25. Lockhart, N. C. J. Colloid Interface. Sci. 1980, 74, 509.
- 26. Lockhart, N. C. J. Colloid Interface. Sci. 1980, 74, 520.
- 27. Raythatha, R.; Sen, P. N. J. Colloid Interface. Sci. 1986,109, 301.
- 28. Scott, J. H.; Carroll, R. D.; Cunningham, D. R. J. Geophys. Res. 1967, 72, 5101.
- 29. Chew, W. C. J. Che. Phys. 1984, 80, 4541.
- 30. Sen, P. N. Phys. Lett. 1986, 39, 667.
- 31. Chew, W. C.; Sen P. N. J. Che. Phys. 1982, 77, 2042.
- 32. Eisenberg, D.; Kauzmann, W. The Structure and Preoperties of Water, Oxford University Press, 1969.
- 33. Farmer, V. C. The infrared Spectra of Minerals., The Mineralogical Society London; 1974.
- 34. Prost, R. Ann. Agron. 1975, 26, 400-463.
- 35. Farmer, V. C.; Russell, J. D. Trans. Faraday Soc. 1971, 67, 2737.
- 36. Prost, R. Proc. Int. Clay Conf. Mexico City, 1975, 351.
- 37. Mamy, J. Ann. Agron. 1968 19 175.
- 38. Clementz, D. M. Pinnavaia, T. J.; Mortland, M. M. J. Phys. Chem. 1973, 77, 197.

- 39. Calvet, R. Adsorption dipolaire et conductivite de l'eau adsorbee sur la montmorillonite calcique; Proc. Int. Clay Conf. Vol II. Madrid.
- 40. Freyman, A.; Soutif, M. La Spectroscopie Hertzienne appliquee a la Chimie. Dunod, Paris, 1960 37.
- 41. Ducross, P.; Dupont, M. Bull. Groupe France Argiles 1962, T8 8.
- 42. Van, O. H. J. Colloid. Sci. 1965 20 822.
- 43. Bradley, W. F. Clark, G. F.; Grim, R. E. Z Krist 1937 97 216.
- 44. Hofman, U.; Hausdorf, A. Z Krist 1942, 104, 265.
- 45. Barrer, R. M.; MacLead, D. M. Trans Faraday Soc. 1954, 50, 980.
- 46. Barrer, R. M.; Kelsay, K. Trans Faraday Soc. 1961, 57, 625.
- 47. Barrer, R. M.; Millington, A. D. J. Colloid. Interface Sci. 1967, 25, 359.
- 48. Barrer, R. M.; Reay, J. C. S. Trans Faraday Soc. 1957, 53, 1253.
- 49. Barrer, R. M.; Jones, D. L. J. Chem. Soc. A 1971, 1595.
- 50. Barrer, R. M.; Jones, D. L. J. Chem. Soc. A 1970, 1531.
- 51. Cotton, F. A.; Wilkinson, G. Advanced Inorganic Chemistry 1980 Forth Edition.

### CHAPTER III

### **ELECTROCHEMICAL PROPERTIES OF SMECTITE CLAYS**

### III.a Background

Electrode surface modification has been an active and exciting area of investigation in electrochemistry over the last two decades.<sup>1-7</sup> Studies of the modified electrodes have served to understand the electrode double layer and the effects of adsorbed species as well as chemical treatments on the double layer and the heterogeneous electron transfer rates. These fundamental studies have led to practical applications of electrode modifications in electrocatalysis<sup>8-17</sup>, organic synthesis<sup>18-24</sup>, biochemical analysis<sup>25-32</sup>, energy conversion<sup>33-42</sup>, electrochromic displays<sup>43-47</sup>, redox chemical sensors<sup>48-52</sup>, and in the area of semiconductors<sup>53-57</sup> and electronics.<sup>58-61</sup>

#### What is Electrode Modification?

A modified electrode differs from an ordinary electrode in that a thin film of some chosen material is deliberately coated on to the electrode surface in order to immobilize a chemical on the electrode surface so that the electrode thereafter displays the chemical, electrochemical, optical and other properties of the immobilized molecules (Figure III.1). For analytical purposes, target species can

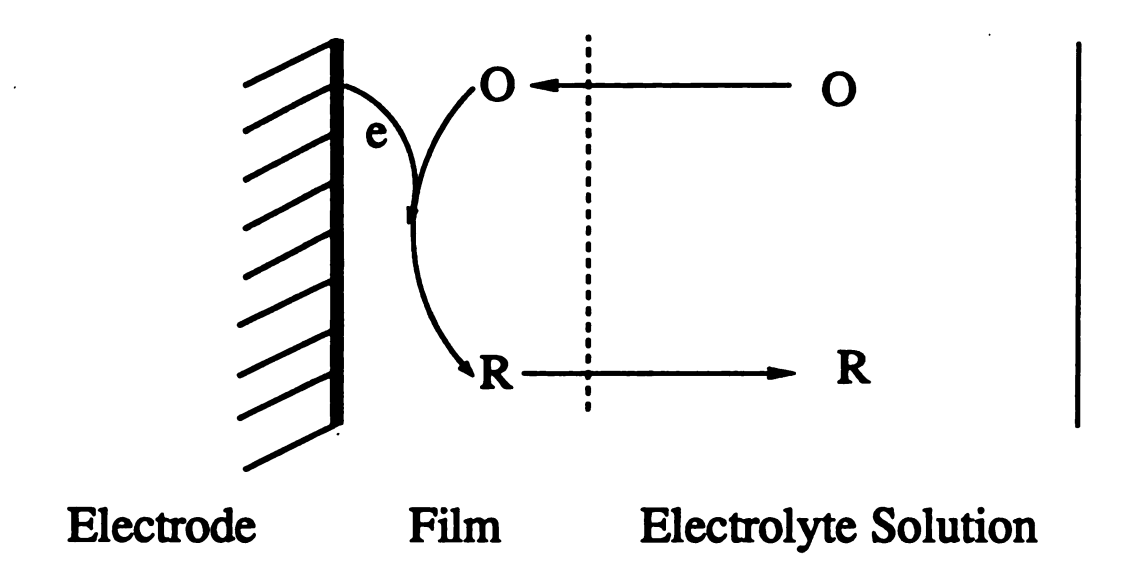


Figure III.1 A Simplified Model for a Surface Modified Electrode.

selectively be bound and hence surfaces of high specificity and sensitivity can be developed. The ability to vary the properties of the coating grants a new freedom in the design and construction of electrodes with desirable kinetic characteristics.

The electrode surface modification was first introduced by Hubbard and Lane<sup>62</sup> with an attempt to modify the electrode double layer by deliberately allowing the electrodes to adsorb an olefinic layer. Following this pioneering work, the subject of modified electrodes grew rapidly from organic monolayers to organic polymers and then to include crystalline inorganic materials. The primary driving force in casting of films on electrode surfaces is the adsorption and the covalent bond formation with guest materials. Depending on the nature of the electrode and the modifier, several techniques have been adopted for surface modification.

## Adsorption.

Adsorption is the oldest and the simplest technique for attaching redox centers to electrode surfaces. Many species are strongly and sometimes irreversibly adsorbed on an electrode surface. The extent of adsorption depends on the nature of the electrode material, the nature of the modifier and the solvent used. The strength of adsorption is usually a function of the type of compound being adsorbed. Many organic compounds are heavily adsorbed with increasing number of aromatic rings present in the molecule. For instance, hydrophobic organic species such as dicobalt

porphyrin dimers are often strongly adsorbed on metal or carbon surfaces from aqueous solutions.<sup>8,63-64</sup> The preparation simply involves cleaning the substrate material and immersing it in a solution containing the desired modifier species. However, the slow desorption has usually caused a loss of the modified surface.

#### Covalent Attachment.

To improve the stability of modified layers, species have been covalently bonded to electrodes. Condensation reactions were used to attach monolayers of modifiers on reactive SnO<sub>2</sub> surfaces.<sup>65</sup> Silanation, the best example of this type, of the electrode surfaces with different types of silane compounds is possible due to the sensitivity of these reagents to water. The silanation reaction can be used to modify any electrode that contain alkoxy-, chloro- or hydroxyl groups. When the technique is applied to platinum or carbon electrodes, prior oxidation of the surface is required.

## Polymerization of Monomers.

Films can be produced by inducing polymerization of the monomer on an electrode surface by electrochemical oxidation or reduction<sup>66-68</sup>, by plasma or glow discharge<sup>69-72</sup> polymerization. Free radicals, initiated by electrochemical techniques, have been employed to grow films on electrode surfaces.<sup>73-75</sup> Multilayers can also be prepared by electrodepositing an insoluble film.<sup>66</sup> These

electrochemical procedures use the changes in physical properties of the monomers, such as solubility, to generate thin films on electrode surfaces.

## Dip, Spin Coating and Droplet Evaporation.

Multilayered films are generally formed by dipping the electrode in a dilute solution of the polymer.<sup>76-77</sup> More reproducible films are formed by spinning the electrode. Spin coating and droplet evaporation methods require a solution or a suspension of the modifier species and are the most successful methods for crystalline materials.<sup>78-80</sup>

# Composite Electrodes.

Preparation of composite electrodes has recently been introduced by Dickstein and Curran. 81 Following this initial account several new methods for producing composite electrodes have been reported. 82-85 Usually conducting carbon powder is entrapped within an organo monomeric material and then polymerize to yield a uniform and strongly compacted composite. Inorganic crystalline materials have also been added in some of these preparations in order to make the composite robust and long lasting. Composite electrodes are very useful because of their ability to be polished to renew the surface reproducibility.

A large number of cationic as well as anionic exchange materials have been used as electrode surface modifiers: this includes both organic and inorganic materials. It essentially involves the incorporation of electroactive counter ions to an electrode modified with a polyionic film. This method, based on the principle of ion exchange for the incorporation of redox species, was introduced by Oyama and Anson.86-87 Their work was based on protonated polyvinylpyridine and deprotonated polyacrilic acids. This approach to electrode modification was extremely attractive due to its simplicity and broad scope. An increasing emphasis was placed for the immobilization of multi-ionically charged redox ions such as  $Fe(CN)_6^{3-}$ ,  $IrCl_6^{2-}$ ,  $Mo(CN)_8^{3-}$ ,  $Ru(CN)_6^{3-}$  and  $Co(CN)_6^{3-}$  which were incorporated into a variety of polycationic films including quaternized polyvinylpyridine<sup>88-90</sup> and polymeric viologens.<sup>91-92</sup> Polystyrene sulfonate, an anionically charged polymer, was one of the earliest to be employed as a cation exchange polymer in modified Numerous cationic species such as Ru(bpy)<sub>3</sub><sup>2+</sup>, electrodes. Co(bpy)<sub>3</sub><sup>2+</sup> and related materials have been studied.<sup>93-95</sup>

Perhaps the most widely used anionic polymeric material for modifying electrode surfaces has been the perfluoro sulfonate material Nafion (DuPont de Nemours, Inc.). Nafion is a cationic exchanger due to its sulfonate side chain; and its non-crosslinked nature makes its solvent swelling characteristics very dependent on the nature of the counter ion present. It has been found that Nafion exists in segregated phases or domains with hydrophilic (fluorocarbon) and hydrophilic (clusters of sulfonate sites) domains

being connected by an interfacial region. Nafion has been extensively employed in numerous studies especially by the groups of  $Anson^{97-99}$  and  $Bard^{100-103}$  and  $Martin.^{104-107}$  A variety of redox cations have been incorporated into Nafion including  $Ru(bpy)_3^{2+}$ ,  $Fe(bpy)_3^{2+}$ ,  $Os(bpy)_3^{2+}$ ,  $Co(bpy)_3^{2+}$ ,  $Co(terpy)_3^{2+}$ , methylviologen,  $Ru(NH_3)_6^{3+}$  and others. However, one of the problems with Nafion is that materials that are retained in the hydrophobic domains exhibit very sluggish transport rates. This can have very deleterious effects in an electrocatalytic cycle if the active component resides mainly in the hydrophobic domain.

A large number of crystalline inorganic materials have been used for electrode surface modifications. This include prussian blue and other analogous compounds of the general formula  $M_k[M'(CN)_6]_l$ ; where M and M' are transition metals with different formal oxidation numbers.  $^{108-112}$  Clays  $^{113-123}$ , zeolites  $^{124-128}$  and hydrotalcites  $^{129-130}$  have also been employed as media for incorporating redox couples by taking advantage of their ion exchange properties. Polyoxometalates  $^{131-133}$ , porous aluminum oxide  $^{134-135}$ , Zrphosphates  $^{136}$  and tungsten oxide bronzes  $^{137-138}$  have also been tested in electrode modifications.

The first example on the use of clays was by Ghosh and Bard<sup>113</sup> who employed sodium montmorillonite layers dispersed on polyvinyl alcohol and coated tin oxide electrode with it. Subsequently they incorporated redox ions such as  $Ru(bpy)_3^{2+}$ ,  $Fe(bpy)_3^{2+}$ ,  $Ru(NH_3)_6^{3+}$  and methyl viologen and characterized their electrochemical responses. Later on they recognized that polyvinyl

alcohol was not an essential ingredient for the electrode modification. Electrode surfaces modified with clay offer several advantages, the two most important being (i) high chemical and thermal stability and (ii) known and potentially controllable structural features. Moreover, clays are capable of catalyzing certain reactions 139-140 and of acting as catalyst supports. 141 Yamagishi and Amarata 142-143 showed that a clay discriminates the chirality of an adsorbate very distinctly when pre-exchange a chosen optically active metal complex. A diverse number of inorganic 113,117,120,122 and organic cations 114, 118, 119 as well as certain anions 117, 121, 123 have been reported to be electroactive in clay modified electrodes. species typically exhibit a depressed response in clay films due to the electrostatic repulsion by the negatively charged clay layers. 117,121 Polypyridyl metal complexes such as Fe(bpy)<sub>3</sub>2+ and  $Os(bpy)3^{2+}$  have played an important role in exploring the electrochemistry of clay modified electrodes. They bind in clays at about 100-fold excess over the concentration of the soaking solution. The experimentally determined diffusion coefficient of Ru(NH<sub>3</sub>)<sub>6</sub><sup>3+</sup> is a facto of 300 larger than that of polypyridyl metal complexes. 140 Quantitative studies have shown that only a small fraction (15-30%) metal complexes in films of the bipyridyl clav are Working with  $M(bpy)_3^{2+}$  pre-exchanged electroactive. 115,117 montmorillonite, King et al. 120 showed that tris bipyridyl metal complexes electrostatically bound at the gallery exchange sites of smectite clays are rigorously electroinactive. On immersion of the exchanged film into a bulk solution containing additional complex, electroactivity was observed that was consistent only with the

additional complex. Added  $Fe(bpy)_3^{2+}$  did not shuttle charge to the  $Os(bpy)_3^{2+}$  adsorbed to the clay surface at ion exchange sites, as might be postulated from reactions (1) and (2).

$$Fe(bpy)_3^{2+} \longrightarrow Fe(bpy)_3^{3+} + e^-$$
 (1)

The oxidation mechanism shown in equation (2) was not observed by King et al.  $^{120}$  It is consistent with the fact that tris bipyridyl metal complexes are strongly adsorbed by clay surfaces and not likely to be desorbed. The change in pre-exchange  $Os(bpy)_3^{2+}$  charge must be accommodated by anion adsorption, which the authors suggested is unlikely due to surface anion charge repulsion. Therefore, they concluded that all complexes adsorbed in amounts less than the cation exchange capacity are electronactive, even in the presence of a charge shuttle. The electroactivity observed when the clay modified electrode is dipped into a solution of  $M(bpy)_3^{2+}$  salts was attributed mainly to the presence of

physically adsorbed  $M(bpy)_3^2+/SO_4^2$  ion pairs in excess of the cation exchange capacity of the film and correlated with the number of edge sites present in the clay film. This was confirmed by increased magnitude and rate of development of the reduction peak associated with the uptake of the complex from solution into a claymodified electrode in the order fluorohectorite < montmorillonite < laponite. This series corresponds to changes in the edge site for an approximately constant total basal area. Similar results were observed for methyl viologen. Fitch et al. 122 have also found that  $Cr(bpy)_3^{3+}$  exchanged montmorillonite suspensions were electroinactive; and if a Na+-montmorillonite modified electrode was placed in Cr(bpy)3<sup>3+</sup>, extensive electroactivity was observed. Therefore, they have suggested that the method of film preparation plays an important role in clay modified electrodes. White and Bard<sup>118</sup> have reported that unlike the trisbypyridine complexes, the methyl viologen dimers, (MV+)2, adsorbed on the clay surfaces was found to be electroactive if a charge shuttle such as Fe(CN)6<sup>3</sup> was added to the solution as shown in equations (3) and (4).

$$Fe(CN)_6^{4-}$$
 Fe(CN)<sub>6</sub><sup>3-</sup> + e<sup>-</sup> (3)

$$Fe(CN)_6^{3-} + \frac{1}{2} (MV^+)_2 \longrightarrow MV^{2+} + Fe(CN)_6^{3-}$$
 (4)

These results suggest that complexes adsorbed on clay surfaces in amounts less than or equal to the cation exchange capacity are not directly electroactive. A charge shuttle is required to access these non desorbable species as in the case of methyl viologen dimer. Even in the presence of charge shuttle, electroactivity may not be observed for adsorbed tris bipyridyl metal complexes as in the case of  $Os(bpy)_3^2$  which was not oxidized in the presence of mobile  $Fe(bpy)_3^3$ .

Lee and Fitch<sup>144</sup> examined montmorillonite-modified electrodes for a variety of film preparation and electrolyte conditions in order to elucidate the role of swelling. The arrival of the Fe(CN)63anion at the electrode surface is constrained primarily by the available pore space and was chosen by Lee and Fitch<sup>144</sup> as the A spin-coated, clay-modified marker of the film structure effects. electrode gave a time invariant current for Fe(CN)63- reduction immediately upon exposure to 0.4 mM Fe(CN)<sub>6</sub><sup>3</sup>-. However, an ovendried or air-dried film generated a much smaller current and took a long time to reach the current given by the spin coated film. has been interpreted by the authors as the inhibition of swelling of the air-dried or the oven-dried electrode by the presence of edge-toface cross linking bonds. They also showed that concentration and type of the electrolyte affect the electroacivity of Fe(CN)63- at the clay modified electrode. In the presence of CsCl and KCl no current was observed for the reduction of Fe(CN)63-, whereas in the presence of LiCl and NaCl the current was dependent upon the concentration of the electrolyte. The explanation for this was the change in the faceto-face interlayer distance due to known differences in hydration of the electrolyte cation.

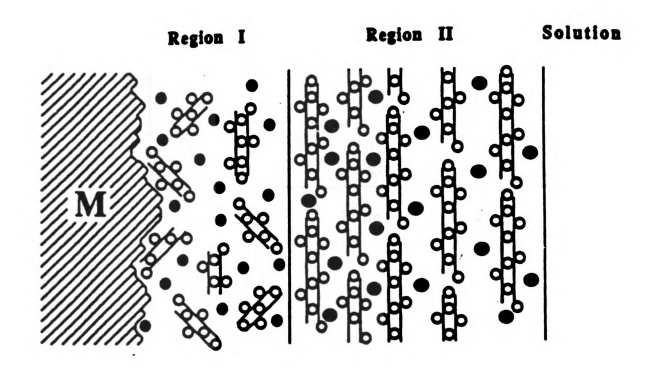
Inoue et al.<sup>145</sup> attempted to determine the effects of edge versus interlayer sites in the electrochemistry of montmorillonite films with respect to  $Ru(bpy)_3^{2+}$  and  $Fe(CN)_6^{3-}$  while working with a glassy carbon electrode. They found that the peak current for the oxidation of  $Ru(bpy)_3^{2+}$  dramatically decreased if the pH of the solution was below 4, while that of the  $Fe(CN)_6^{3-}$  increased. These results were interpreted as a consequence of the protonation of clay to give a positive charge to the platelets.  $Ru(bpy)_3^{2+}$  adsorption does not take place at protonated sites having positive charges. Positively charged voids increase the amount of adsorbed  $Fe(CN)_6^{3-}$  resulting a higher peak current for the reduction of  $Fe(CN)_6^{3-}$ . Therefore, they concluded that edge adsorption sites were more important in clay modified electrodes. However, no attempt has been made to control the total electrolyte concentration; hence the swelling changes discussed above might have affected the results.

King  $^{146}$  has studied the effects of film thickness on the electrochemistry of Fe(bpy) $_3^{2+}$  at montmorillonite-modified graphite electrodes. They have found that the amount of electrochemically active Fe(bpy) $_3^{2+}$  incorporated into montmorillonite films at a given concentration of Fe(bpy) $_3^{2+}$  is independent of film thickness and increases monotonically with the concentration of Fe(bpy) $_3^{2+}$  in the soaking solution and reaches a maximum at 5 mM. They have also noted that the roughness of the electrode surface increases the incorporation of electroactive Fe(bpy) $_3^{2+}$ . Pyrolytic graphite

electrodes give a much higher current densities than glassy carbon, tin oxide or platinum electrodes. Based on these observations the authors have concluded that electroactive Fe(bpy)<sub>3</sub><sup>2+</sup> in the clay film can be divided into two distinct regions as shown in Figure III.2. Only those ions in region I, defective or disordered zone, with access to the electrode surface either by direct contact or charge shuttling through open pathways display electroactivity. The increase order in region II reduces the basal volume and eliminates electrochemical pathways to the electrode surface thereby resulting in electrochemically isolated Fe(bpy)<sub>3</sub><sup>2+</sup> ions.

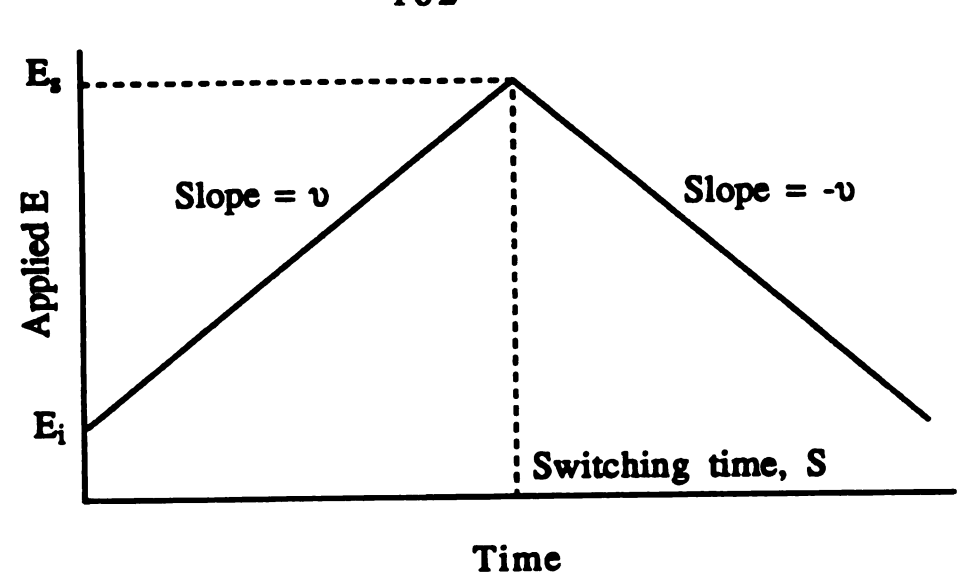
## Cyclic Voltammetry.

The current in an electrochemical experiment depends on three parameters: the diffusion coefficient, D; the accessible area of the underlying electrode; and the concentration of the species within the film. In cyclic voltammetry, the potential at the surface of the underlying electrode is swept linearly from an initial potential,  $E_i$ , to a switching potential,  $E_s$ , and back again to the  $E_i$  (Figure III.3). If a species is present whose standard electrode potential,  $E^o$ , lies between  $E_i$  and  $E_s$ , a current corresponding to the reduction of the species will be observed in the negative sweep, and a current corresponding to the oxidation of the reduced material will be observed in the positive sweep. The current versus potential curve will have a peak shape if linear diffusion to the electrode surface



- O Non-Electroactive ions
- . Electroactive ions
- Isolated potentially active ions

Figure III.2 Model proposed by  $King^{146}$  to explain the observed the electroactivity of  $Fe(bpy)_3^{2+}$  at clay modified electrodes.



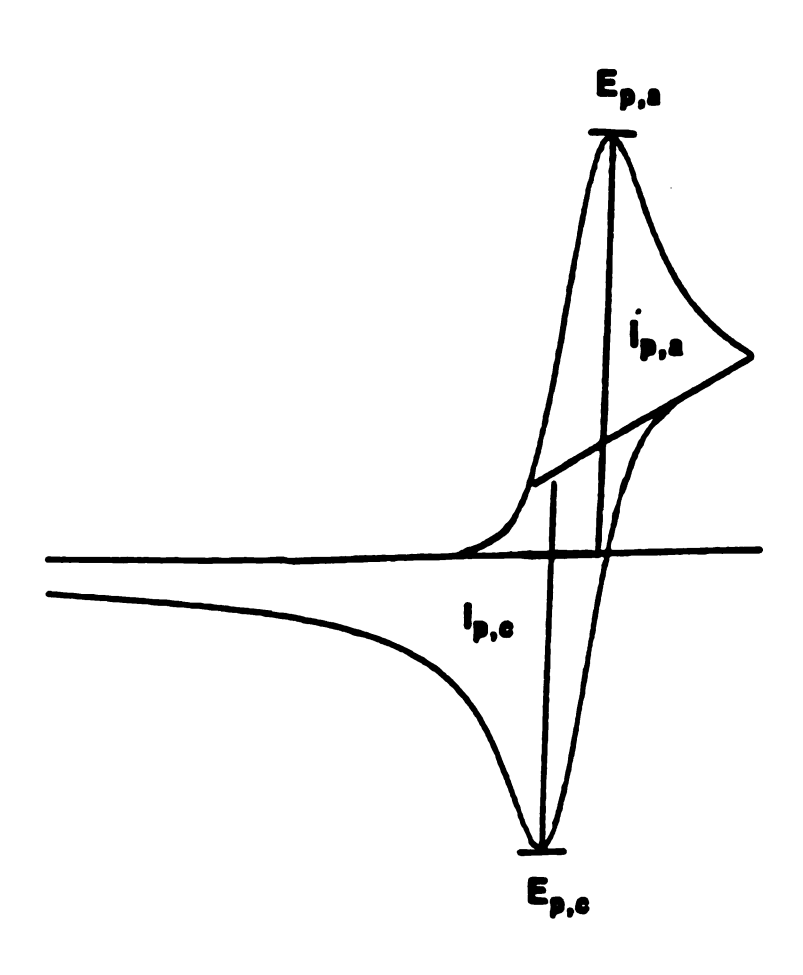


Figure III.3 (A) An idealized cyclic potential sweep and (B) the resulting cyclic voltammogram.

occurs. The peak current can be described by the following expression.

$$i_p = (2.69 \times 10^5) n^{3/2} D^{1/2} v^{1/2} AC_0^*$$

where  $i_p$  is the peak current observed in amperes, n is the number of electrons involved in the reduction process. A is the area of the electrode in cm<sup>2</sup>, D is the diffusion coefficient for the oxidized species in cm<sup>2</sup> sec<sup>-1</sup>, v is the rate at which the potential is swept in V sec<sup>-1</sup> and  $C_0^*$  is the concentration of the oxidized species before the electrochemical perturbation is applied, in mol cm<sup>-3</sup>.<sup>147</sup> For linear diffusion,  $E^0$  is midway between reduction and oxidation peaks.

If the electrochemical experiment is carried out at a modifying layer, the same relationships hold, except that the area of the conductive channels can now play an important role in defining the type of diffusion observed.  $^{148-150}$  Furthermore, if the distance sampled by the electrochemical experiment is smaller than the layer modifying the electrode, the experiment can be considered to be a normal electrochemical experiment within a new medium. Here, D,  $C_0^*$  and  $E_0$  will be determined by the chemistry of the modifying layer.

# Stirred-Solution Voltammetry.

Stirred solution voltammetry utilizes current-voltage relationships which are obtained at a stationary electrode immersed in a stirred solution. In this case, the potential of the working

electrode is swept linearly from an initial point,  $E_i$ , to a final point,  $E_f$ , while the solution is being stirred. If an electrochemically reducible/oxidizable species is present in the solution, whose standard electrochemical potential is in between the scanned points  $(E_i \text{ and } E_f)$ , the resulting current versus potential plot will look like the curve shown in Figure III.4. The current resulting from an applied potential is determined by the slope of the concentration-distance profile of the reactant at the electrode surface. A limiting current,  $i_1$ , is reached when the surface concentration of the electroactive species becomes effectively zero and is expressed by the following equation.

$$i_l = nFAD \frac{C_0^*}{\delta}$$

where  $i_l$  is the limiting current observed in amperes, n is the number of electrons involve in the reduction/oxidation reaction, F is the Faradaic constant, A is the area of the working electrode, D is the diffusion coefficient of the oxidized (or reduced) species involved in the process  $C_0^*$  is the bulk concentration or the concentration before the electrochemical process began and  $\delta$  is the thickness of the unstirred solution, ("diffusion layer thickness"), as shown in Figure III.5.

The origin of electroactivity and the location of electroactive ions with respect to tris(2 2'-bipyridine) metal complexes, at clay modified has been identified. However, those of metal complexes

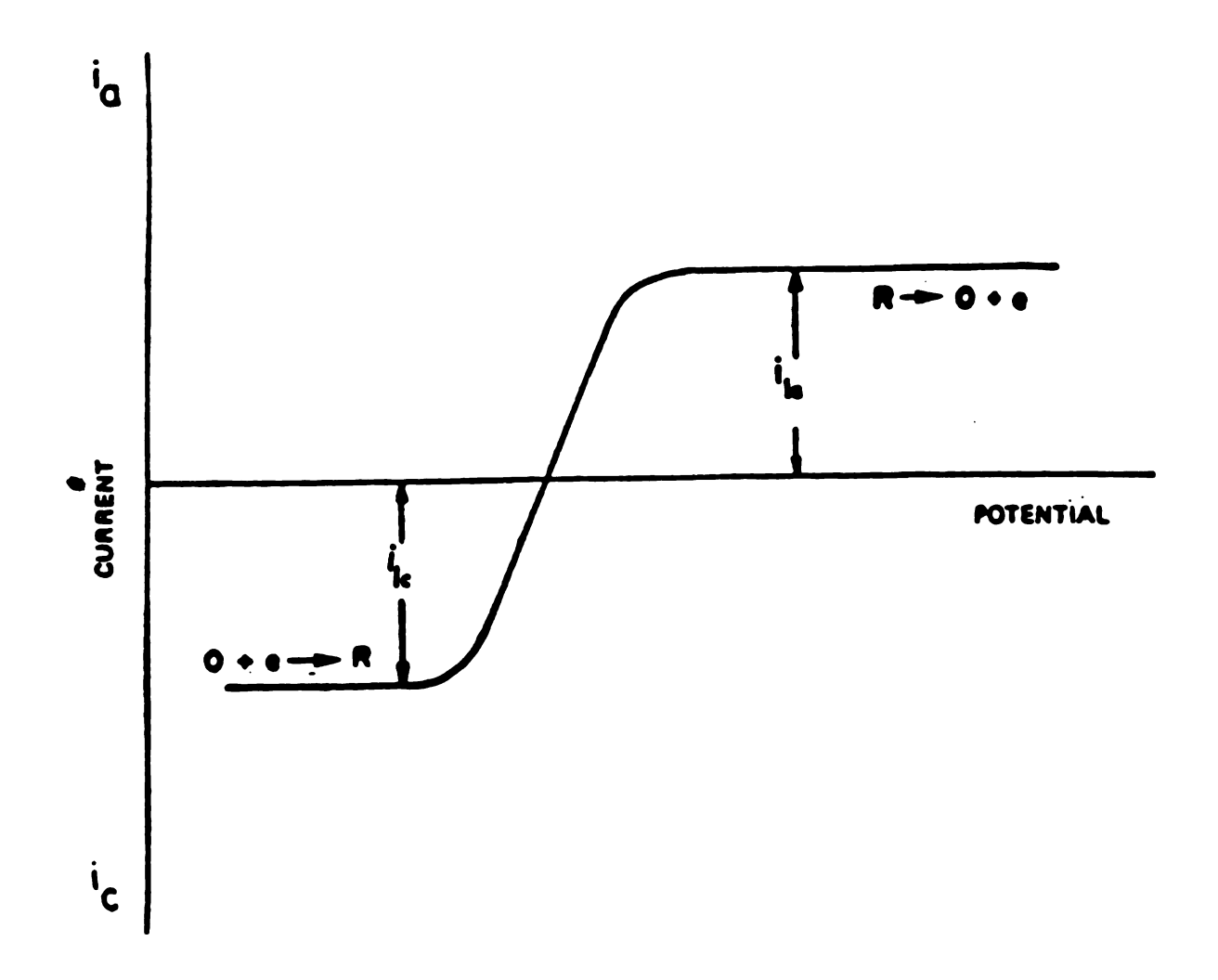


Figure III.4 Idealized current versus potential curve for stirred solution voltammetry.

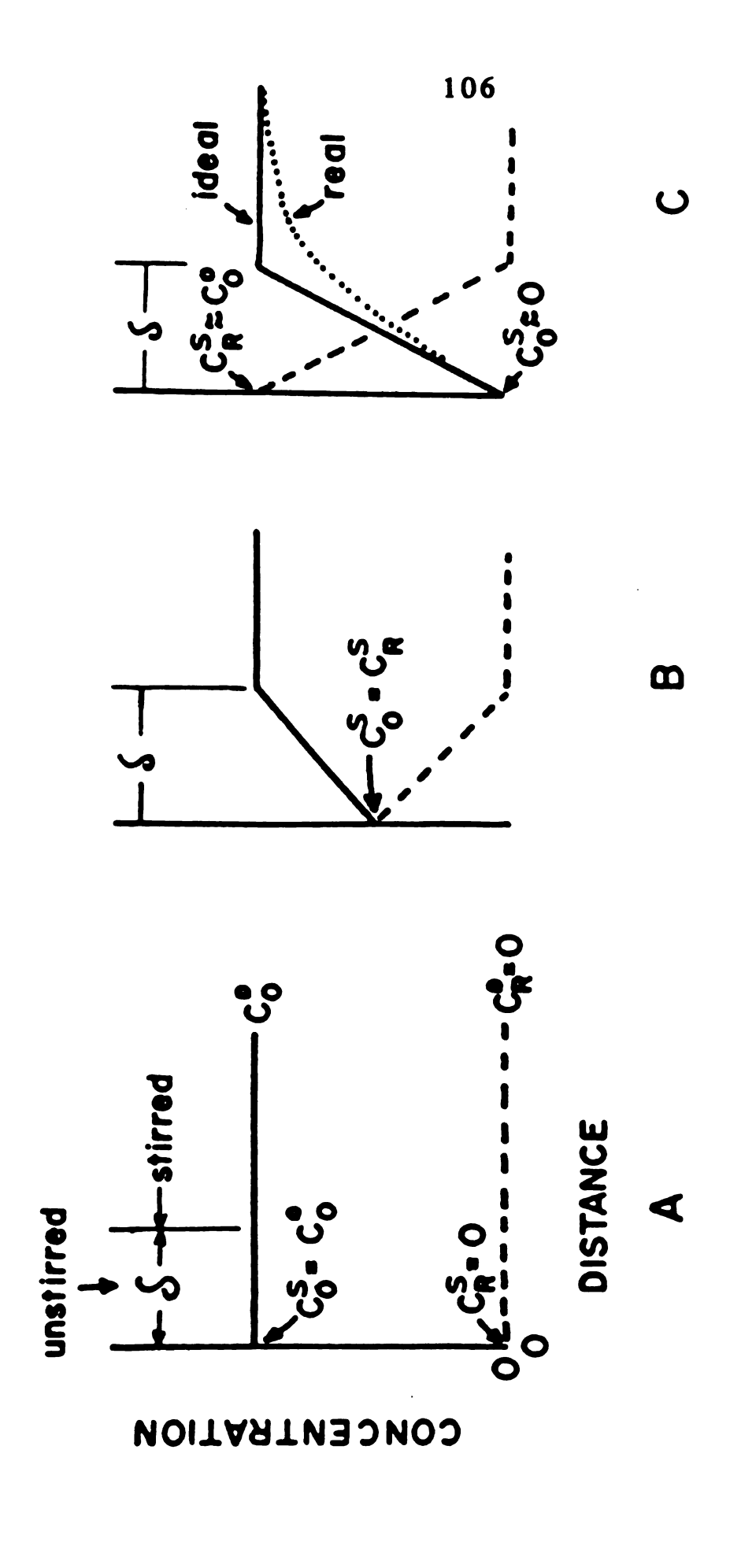


Figure III.5 An idealized concentration profiles in stirred solution voltammetry. (A) Unperturbed or Eapp << E0' (B)  $E_{app} = E^{0'}$  (C)  $E_{app} >> E^{0'}$ 

with simple ligands, such as NH<sub>3</sub>, are still to be elucidated. The charge transport properties within the clay films are also still in the process of being defined. Experiments were designed to investigate the electrochemistry of  $Ru(NH_3)_6^{3+}$ , the effects of supporting electrolyte cation, and its concentration on the electrochemistry of  $Ru(NH_3)_6^{3+}$  and  $Fe(bpy)_3^{2+}$ . Effects of the supporting electrolyte pH on the electrochemistry of  $Ru(NH_3)_6^{3+}$  and  $Fe(bpy)_3^{2+}$  cations have also been investigated. The understanding of these principle factors is essential in order to develop an electrocatalytic system or any other basic application from clay electrode modification.

## III.b Experimental

# Synthesis of Metal Complexes

Hexaamminoruthenium(III) chloride was purchased from Alfa Reaserch Chemicals and Materials. Tris(2 2'-bipyridine)iron(II) sulfate synthesized according to the was published procedures. 120, 152-153 An aqueous solution of ferrous sulfate was slowly added to an ethanolic solution containing 3.5 mol of 2 2'bipyridine, purchased from Baker Chemicals. The resulting mixture was stirred for 2 hrs and the red product was precipitated with acetone, filtered and finally washed with benzene to remove excess Crystalline solid [Fe(bpy)3]SO<sub>4</sub> was recovered from an ethanol/acetone mixture.

## Purification of Smectite Clays

Purification and preparation of the sodium form of montmorillonite, laponite and fluorohectorite was discussed in II.b. Nontronite was from Garfield, Washington; and was purified with the same procedure used for the purification of montmorillonite (section II.b).

## Supporting Electrolytes

Sodium acetate (Baker Chemicals), acetic acid (Mallinkrodt) were used as received. Alkali metal sulfates and all the quaternary alkylammonium salts were purchased from Aldrich Chemicals. Trichloroacetic acid was obtained from Baker Chemicals. Distilled deionized water was used as the solvent in preparation of all the soaking solutions and supporting electrolytes. Salts of Li<sup>+</sup>, Na<sup>+</sup>, K<sup>+</sup>, Rb<sup>+</sup>, Cs<sup>+</sup>, (CH<sub>3</sub>)<sub>4</sub>N<sup>+</sup>, (C<sub>2</sub>H<sub>5</sub>)<sub>4</sub>N<sup>+</sup> and (C<sub>4</sub>H<sub>9</sub>)<sub>4</sub>N<sup>+</sup> in the concentration range 0.01-0.1 M were used as the supporting electrolytes.

# Construction of Graphite Working Electrodes

Cylindrical rods with a diameter of 4.76 mm were machined from a block of pyrolytic graphite, purchased from the specialty products Division of Union Carbide Corporation (Cleveland, OH). The cylinder axis was collinear with the c-axis of the graphite block. A graphite cylinder was sealed with heat shrink tubing to a glass tube

containing a copper wire. Copper wire was also sealed to the other end of the glass tube entrapping mercury within the glass tube in order to make the electrical contact between the copper wire and the graphite. 154-155 A fresh surface was obtained for each experiment by cleaving a thin layer of the graphite with a razor blade.

## Preparation of Clay Modified Electrodes

Clay modified electrodes were prepared by allowing 10  $\mu$ L of a 1 % clay suspension to evaporate on the freshly cleaved pyrolytic graphite electrode surface. Density of clay on the graphite surface was found to be 5.61 x 10<sup>-5</sup> g cm<sup>-1</sup>. This coverage corresponds to a film thickness of 2.12  $\mu$ m. The electroactive ions were incorporated into the clay films either by soaking the modified electrode in an aqueous solution of the desired species or by pre-exchanging with the clay samples before the films were cast. Hexaammine-ruthenium(III) was intercalated into laponite by adding the required amount of Ru(NH<sub>3</sub>)<sub>6</sub><sup>3+</sup>, based on the cation exchange capacity of the clay, to a suspension of Na<sup>+</sup>-laponite. Resulting suspension was stirred for 1 hr and dialized for a week to remove the excess Na<sup>+</sup> cations.

#### Instrumentation

Voltammograms were recorded on a Bioanalytical System (BAS) 100A Electrochemical Analyzer. A conventional H-cell was

used with a KCl saturated Ag/AgCl reference electrode. Platinum gauze was the counter electrode and pyrolytic graphite electrodes were used as the working electrode (0.18 cm2). Either nitrogen or argon was used to purge the supporting electrolyte.

### III.c Results and Discussion

Electroactive  $Ru(NH_3)_6^{3+}$  Gallery Cations in Clay Modified Electrodes.

In contrast to the electrochemically inactive homoionic  $M(bpy)_3^{2+}$  and  $M(phen)_3^{2+}$  clays, homoionic  $Ru(NH_3)_6^{3+}$  smectites were found to be electroactive when cast as a thin film on a pyrolytic graphite electrode. Moreover, electroactivity was observed even when the cation was present in amounts less than the cation exchange capacity of the film. The series of cyclic voltammograms shown in Figure III.6 were recorded for  $Ru(NH_3)_6^{3+}$ -laponite at loadings from 10% to 100%, of the cation exchange capacity.  $Ru(NH_3)_6^{3+}$  exchanged into montmorillonite films also exhibited well defined cyclic voltammograms, suggesting that  $Ru(NH_3)_6^{3+}$  cations at ion exchange sites of the clay were electroactive. In order to obtain further verification of the electroactivity of  $Ru(NH_3)_6^{3+}$  at clay ion exchange sites, a comparative study was carried out using clay films impregnated with electroactive  $Fe(bpy)_3^{2+}$  /  $SO_4^{2-}$  ion pairs.

Figure III.7 shows the time-dependence for the peak currents for Na+-montmorillonite coated electrodes prepared by soaking for

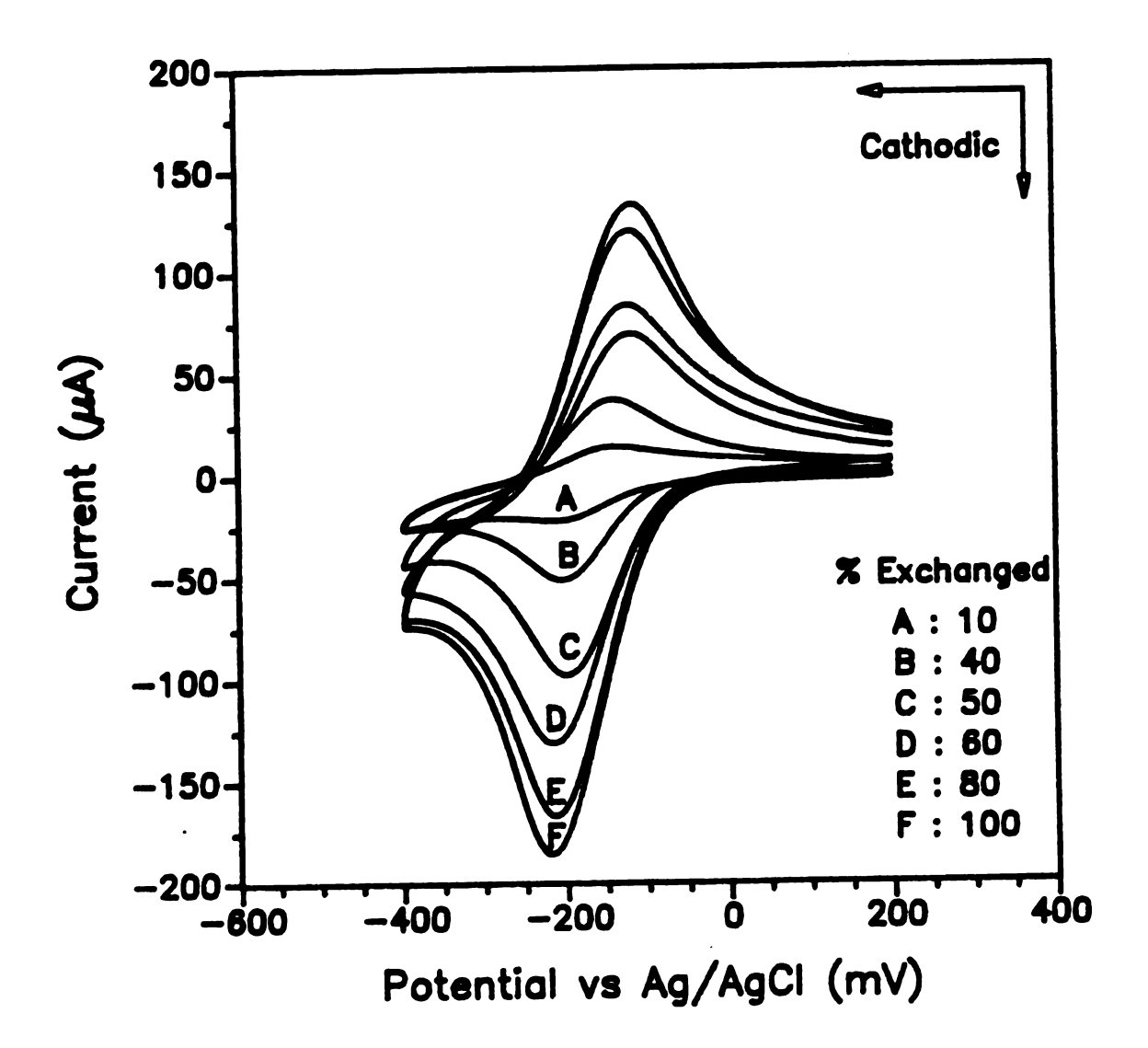


Figure III.6 Homoionic  $Ru(NH_3)_6^{3+}$  loaded by pre-exchange in Na<sup>+</sup>-laponite. Supporting electrolyte was 0.05 M Na<sub>2</sub>SO<sub>4</sub>. Scan rate 100 mV Sec<sup>-1</sup>.

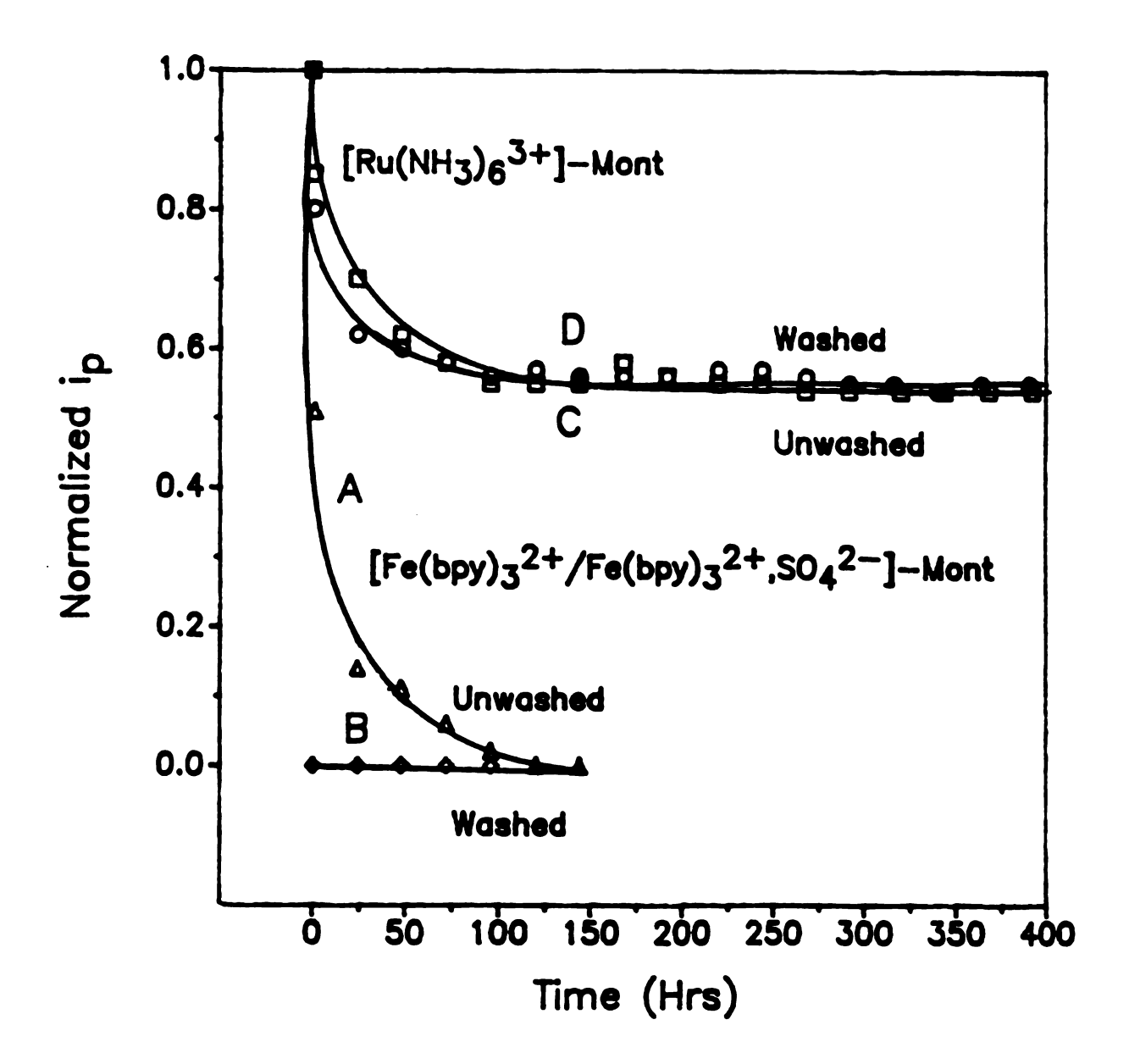


Figure III.7 Time dependency of normalized i<sub>pc</sub> of homoionic Ru(NH<sub>3</sub>)<sub>6</sub><sup>3+</sup> and ion paired Fe(bpy)<sub>3</sub><sup>2+</sup> at montmorillonite-modified electrodes in 0.05 M CH<sub>3</sub>CO<sub>2</sub>Na supporting electrolyte buffered at pH 3. Scan rate 100 mV sec<sup>-1</sup>.

24 hrs in 1 mM solutions of Ru(NH<sub>3</sub>)6<sup>3+</sup> and Fe(bpy)<sub>3</sub><sup>2+</sup> containing 0.05 M sodium acetate buffer at pH 3.0. The electroactivity of the film soaked in 1 mM Fe(bpy)<sub>3</sub><sup>2+</sup> decreased to zero within 4-5 days upon aging in pure supporting electrolyte (curve A). This loss in electroactivity occurs because all the electroactive Fe(bpy)<sub>3</sub><sup>2+</sup>/SO<sub>4</sub><sup>2-</sup> ion pairs are desorbed into the supporting electrolyte, leaving only the exchange ions that are rigorously electroinactive. When the electrode was allowed to age in deionized water for 4-5 days prior to the recording of the cyclic voltammograms, no electroactivity was observed even for the initial voltammogram (curve B). This result again was attributable to the desorption of loosely bound ion pairs from the film, leaving only the electrostatically bound inactive complex cations.

In contrast to the ion-paired  $Fe(bpy)_3^{2+}$  system, a Na+-montmorillonite graphite electrode prepared by soaking in 1 mM  $Ru(NH_3)_6^{3+}$  exhibited a steady state current upon aging in pure supporting electrolyte over 4-5 days (curve C in Figure III.7). Essentially the same behavior was observed for the washed film (curve D), indicating that there is little or no contribution to the total electroactivity in  $Ru(NH_3)_6^{3+}$  due to adsorbed ion pairs. Essentially all of the activity in the case of  $Ru(NH_3)_6^{3+}$  is due to ions bound at the exchange sites, both gallery sites and edge sites, of the clay layers. The initial decrease in electroactivity for  $Ru(NH_3)_6^{3+}$  montmorillonite with aging in the pure supporting electrolyte can be attributed to the ion exchange displacement of  $Ru(NH_3)_6^{3+}$  by the electrolyte cations. This hypothesis was confirmed by the effects of

supporting electrolyte cation size and concentration on the initial decrease of electroactivity of these two metal complexes.

Figure III.8 shows the depletion of electroactivity for a  $Ru(NH_3)_6^{3+}$ -montmorillonite electrode immersed in different concentrations of  $Na_2SO_4$  supporting electrolyte. In each case the electrode was prepared by soaking in 1 mM  $Ru(NH_3)_6^{3+}$  for 24 hrs. When the supporting electrolyte concentration was greater than 0.1 M, the electroactivity of  $Ru(NH_3)_6^{3+}$  was depleted within a few minutes. The same total loss of activity has been observed by Bard et al. However, when the supporting electrolyte concentration was below 0.1 M, the clay bound  $Ru(NH_3)_6^{3+}$  ions entered into equilibrium with the supporting electrolyte cations, and a steady state current was observed. The electroactive fraction of  $Ru(NH_3)_6^{3+}$  cation at steady state increased with decreasing electrolyte concentration.

In contrast to the behavior of the  $Ru(NH_3)6^{3+}$  clays, the depletion of electroactivity of a clay modified electrode containing  $Fe(bpy)3^{2+}/SO4^{2-}$  ion pairs was independent of the concentration of the supporting electrolyte. The electroactive fraction of  $Fe(bpy)3^{2+}$  remaining in the film after 24 hrs aging at different concentrations of  $Na_2SO_4$  as the supporting electrolyte is depicted in Figure III.9. It is clear that the fraction of  $Fe(bpy)3^{2+}$  leached from the film was not affected by the concentration of the supporting electrolyte. These latter results indicated that the binding of electroactive  $Fe(bpy)3^{2+}$  centers did not involve an ion exchange process as in the case of  $Ru(NH_3)6^{3+}$ .

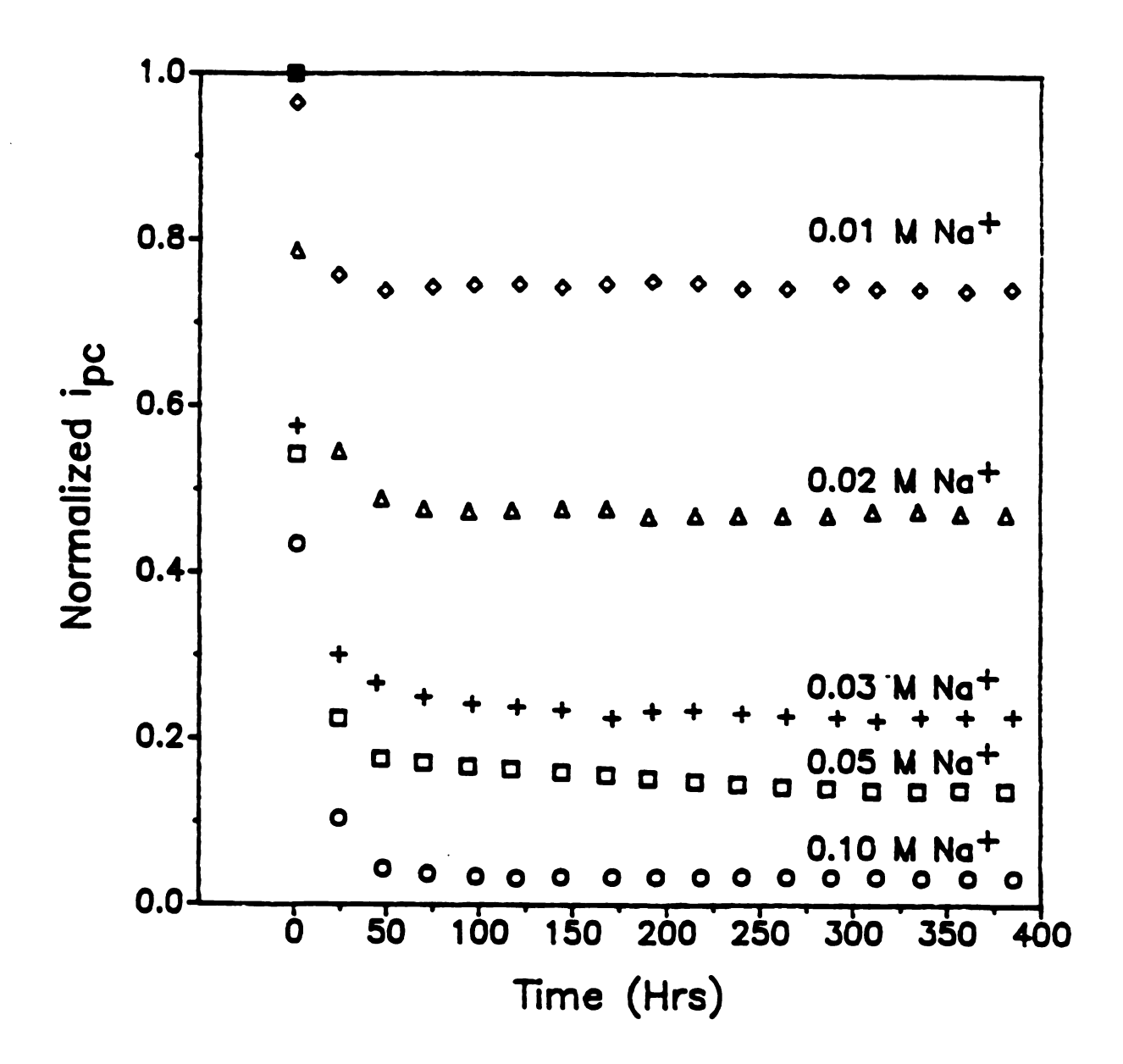


Figure III.8 Time dependency of normalized  $i_{pc}$  of homoionic  $Ru(NH_3)_6^{3+}$  in different concentrations of  $Na_2SO_4$  supporting electrolyte. Scan rate 100 mV sec<sup>-1</sup>.

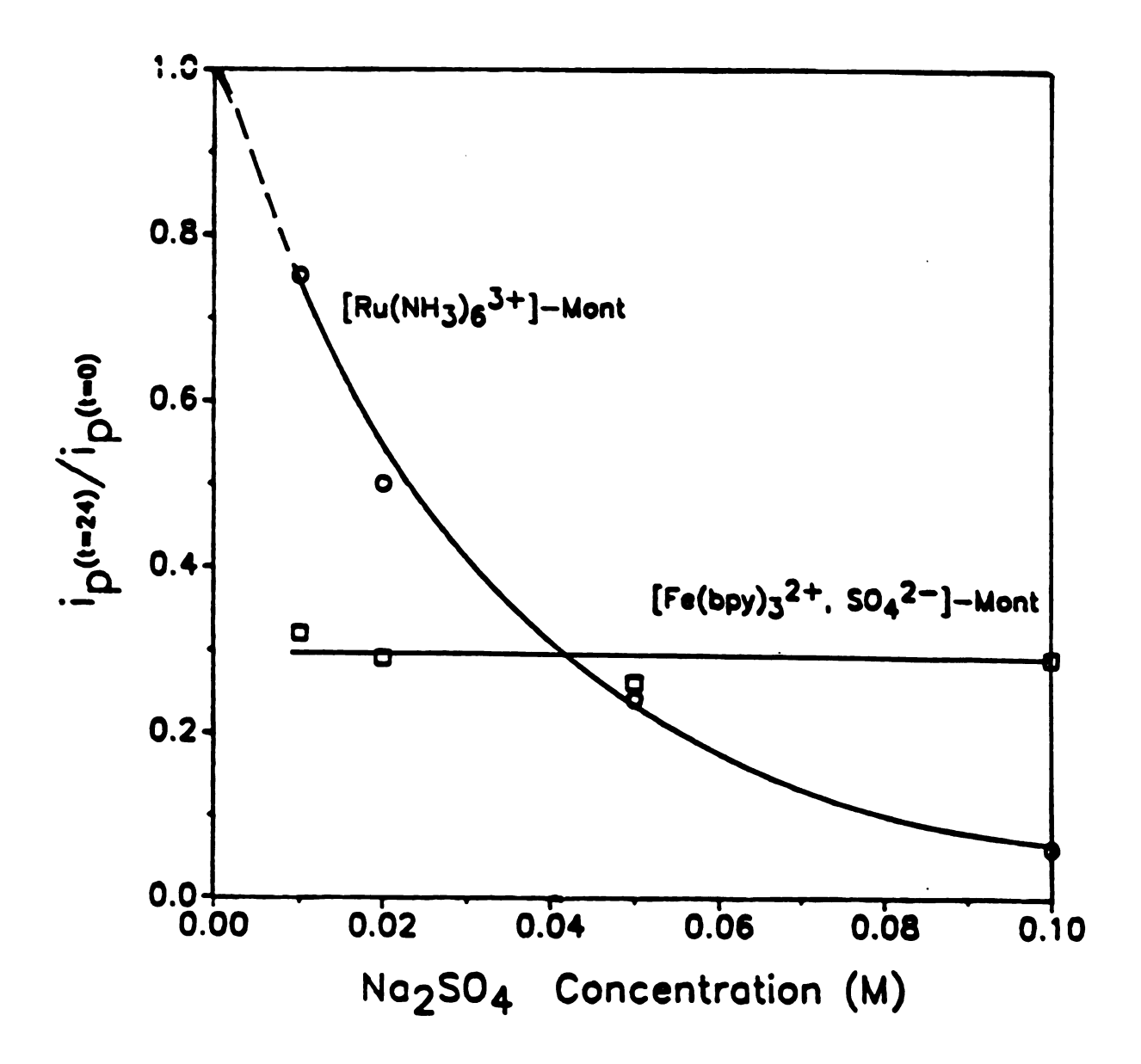


Figure III.9 Normalized peak current  $i_p(t=24) / i_p(t=0)$  of homoionic  $Ru(NH_3)_6^{3+}$  and ion paired  $Fe(bpy)_3^{2+}$  in different concentrations of  $Na_2SO_4$  supporting electrolyte. Scan rate 100 mV sec<sup>-1</sup>.

Figure III.10 shows the depletion of electroactivity for a homoionic Ru(NH<sub>3</sub>)<sub>6</sub><sup>3+</sup> montmorillonite modified electrode immersed in 0.01M solutions of Li<sub>2</sub>SO<sub>4</sub>, Na<sub>2</sub>SO<sub>4</sub>, K<sub>2</sub>SO<sub>4</sub>, Rb<sub>2</sub>SO<sub>4</sub> and Cs<sub>2</sub>SO<sub>4</sub>. The electroactive fraction of Ru(NH<sub>3</sub>)<sub>6</sub><sup>3+</sup> bound to the clay at steady state decreased in the order Li<sup>+</sup> > Na<sup>+</sup> > K<sup>+</sup> > Rb<sup>+</sup> > Cs<sup>+</sup>. The binding of these hydrated ions to the clay layers is favored in the order Li<sup>+</sup> < Na<sup>+</sup> < K<sup>+</sup> < Rb<sup>+</sup> < Cs<sup>+</sup>. <sup>156</sup> As expected, the equilibrium concentration of  $Ru(NH_3)_6^{3+}$  in the film followed the reverse order of electrolyte cation binding. The importance of the hydration energy of the electrolyte cation was confirmed by the results shown in Figure III.11 where the fraction of electroactive Ru(NH<sub>3</sub>)<sub>6</sub><sup>3+</sup> remaining after 24 hrs aging is plotted verses the cation hydration energy. figure shows that the depletion of electroactivity for ion paired Fe(bpy)<sub>3</sub><sup>2+</sup> within the same time period was independent of the supporting electrolyte cation. These observations confirm that the depletion of electroactivity of Ru(NH<sub>3</sub>)<sub>6</sub><sup>3+</sup> arises from the exchange of Ru(NH<sub>3</sub>)<sub>6</sub><sup>3+</sup> in the film with cations in the supporting electrolyte and that the loss of electroactivity for  $Fe(bpy)_3^2$  is due to the physical desorption of ion pairs.

The initial peak currents observed for homoionic  $Ru(NH_3)_6^{3+-1}$  montmorillonite also were dependent on the nature of the electrolyte cation. The order of initial  $i_{pc}$  was  $Li^+ < Na^+ < K^+ < Rb^+ < Cs^+$ . In contrast, the initial value of  $i_{pa}$  for ion-paired  $Fe(bpy)_{32}$  center showed a strong dependence on electrolyte anion. Table III.1 provides the initial peak currents observed for  $Ru(NH_3)_6^{3+}$  cations and ion-paired  $Fe(bpy)_3^{2+}$  centers in montmorillonite films

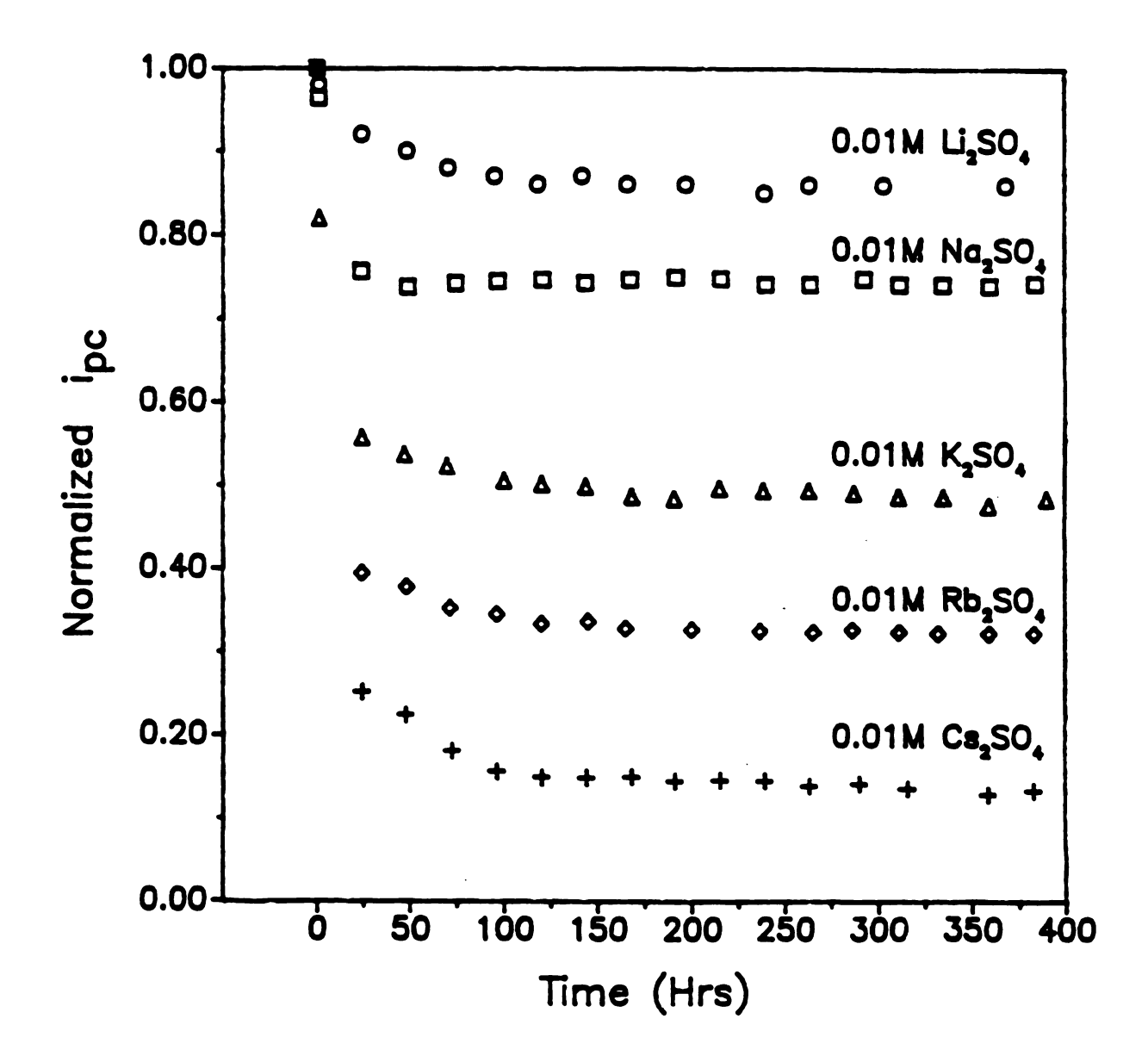
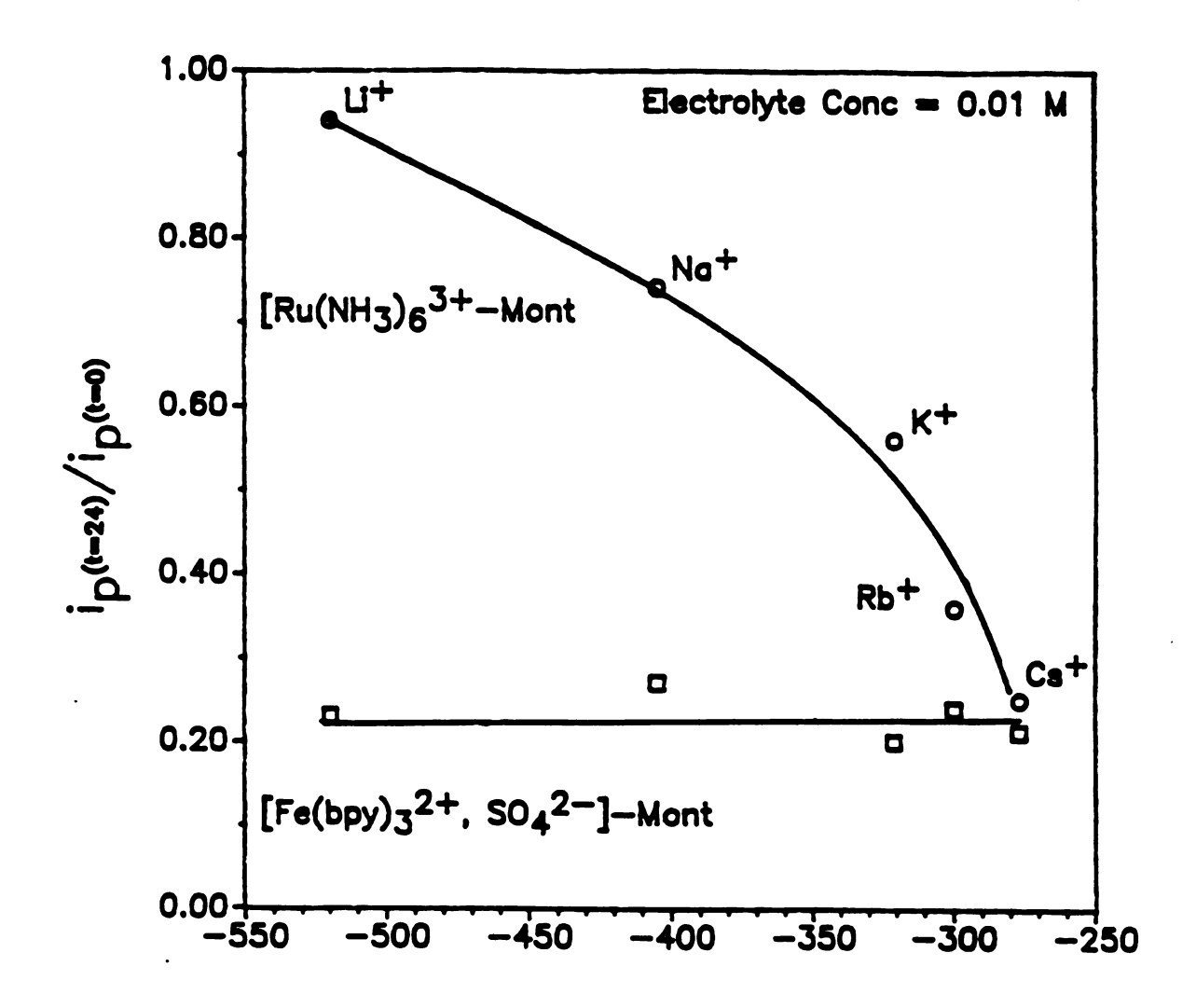


Figure III.10 Time dependency of normalized  $i_{pc}$  of homoionic  $Ru(NH_3)_6^{3+}$  in 0.01 M concentrations of different supporting electrolytes. Scan rate 100 mV sec<sup>-1</sup>.



Enthalpy of Hydration of the Electrolyte Cation

Figure III.11 Normalized peak current  $i_p(t=24) / i_p(t=0)$  of homoionic  $Ru(NH_3)_6^{3+}$  and ion paired  $Fe(bpy)_3^{2+}$  in 0.01 M concentrations of different supporting electrolytes. Scan rate 100 mV sec<sup>-1</sup>.

Table III.1 Dependance of initial peak current  $(\mu A)$  on supporting electrolytes for electroactive centers in montmorillonite-modified electrodes.

Electrolyte (0.1 M)	Homoionic Ru(NH <sub>3</sub> ) <sub>6</sub> <sup>3+</sup>	Homoionic Fe(bpy) <sub>3</sub> <sup>2+</sup>
CsCl*	221 ± 6	96 ± 2
[Me <sub>4</sub> N]Cl*	208 ± 7	97 ± 4
[Et <sub>4</sub> N]Cl*	187 ± 5	97 ± 3
[Bu <sub>4</sub> N]Cl*	95 ± 3	117 ± 3
Na[CH3CO2] <sup>§</sup>	$105 \pm 2$	76 ± 1
Na[C <sub>2</sub> H <sub>5</sub> CO <sub>2</sub> ] <sup>§</sup>	101 ± 3	69 ± 3
Na[C <sub>4</sub> H <sub>9</sub> CO <sub>2</sub> ] <sup>§</sup>	101 ± 3	52 ± 2
Na[C <sub>7</sub> H <sub>15</sub> CO <sub>2</sub> ] <sup>§</sup>	101 ± 2	33 ± 2

<sup>\*</sup> pH = 5.8 - 6.8

<sup>§</sup> Buffered at pH 7.0 with the corresponding acid.

immersed in different supporting electrolytes. It is clear that for homoionic Ru(NH<sub>3</sub>)<sub>6</sub><sup>3+</sup> -montmorillonite the initial peak current greatly depends on the nature of the electrolyte cation, but not on Conversely, the peak current for ion-paired Fe(bpy)<sub>3</sub><sup>2+</sup> centers varies with the electrolyte anion, but not with the cation. These results suggest the following interpretation. In the case of homoionic Ru(NH<sub>3</sub>)<sub>6</sub><sup>3+</sup> -montmorillonite, reduction of the ruthenium causes a negative charge build up within the clay film. In order to achieve electrical neutrality, a cation is adsorbed from the supporting The diffusion of ions, which depends inversely upon the hydrated radius, should be highest for Cs+ and lowest for Therefore, the tetrabutylammonium cation. initial inc for  $Ru(NH_3)6^{3+}$  - montmorillonite is expected to increase in the order  $[Bu_4N]^+ < [Et_4N]^+ < [Me_4N]^+ < Cs^+$ , as observed. In the case of the ionpaired Fe(bpy)<sub>3</sub><sup>2+</sup> centers on montmorillonite, a positive charge is built up within the clay film upon oxidation of the iron. Therefore, an anion, rather than a cation is adsorbed from the supporting electrolyte. As a result, the  $i_{pa}$  for ion paired Fe(bpy)<sub>3</sub><sup>2+</sup> centers is affected by the nature of the anion in the supporting electrolyte. current is expected to increase with decreasing size of the anion, in the order  $C_7H_{15}CO_2^- < C_4H_9CO_2^- < C_2H_5CO_2^- < CH_3CO_2^-$ , as observed. The proposed electrical neutrality mechanisms for the two types of clay modified electrodes are summarized in Scheme III.1.

The ion exchange inertness of homoionic  $M(bpy)_3^2$  and  $M(phen)_3^2$  clays toward common electrolyte salts appears to be the primary factor leading to their electrochemical inactivity. The

Scheme III.1 Electrical Neutrality Mechanism.

Homoionic Redox Centers, eg., Ru(NH<sub>3</sub>)<sub>6</sub><sup>3+</sup>

{ 
$$[Ru(NH_3)6^{3+}] }_{clay} + [M^+]_{soln}$$
  
{  $[Ru(NH_3)6^{2+}]$  ,  $[M^+] }_{clay} - e^-$ 

Ion-Paired Redox Centers, eg., [ Fe(bpy)32+, SO42-]

{ 
$$[Fe(bpy)_3^{2+}, SO_4^{2-}] }_{clay} + [X^-]_{soln}$$
  
{  $[Fe(bpy)_3^{2+}, SO_4^{2-}] , [X^-] }_{clay} + e^-$ 

binding of polypyridyl metal complexes to smectite clays has been extensively studied owing to their potential use in photocatalytic reactions and as microporous materials with high surface areas. 157-In addition to electrostatic interactions, other factors may also govern the binding of polypyridyl cations by clays. For instance, van der Waals interactions have been proposed as contributing to the binding of these centers to clay surfaces. 157 Polypyridyl metal complexes are expected to bind to clay gallery surfaces with their three-fold axis perpendicular to the layers. 157, 162 The unique equilateral triangular base of both phenanthroline and bipyridine complexes matches the geometry of the hexagonal holes on the surface of the clay. This should allow the positive charge of the cation to draw closer to the center of clay negative charge. 162 However, it recently has been shown that the  $C_3$  axis of Ru(phen)<sub>3</sub><sup>2+</sup> in montmorillonite is tipped by 25-30° from the vertical direction. 165 This orientation may be caused by physical adsorptive interactions between the polypyridyl ligands and the clay surface.

The difference in electrostatic and physical adsorptive interactions between the clay surface and  $Fe(bpy)_3^{2+}$ , and that with  $Ru(NH_3)_6^{3+}$  are clearly shown in Figures III.12 and III.13. Na<sup>+</sup>-montmorillonite dried in humidified air for 18 hrs. has a d-spacing of 12.5 Å, and upon soaking in 1 mM solutions of  $Fe(bpy)_3^{2+}$  and  $Ru(NH_3)_6^{3+}$  for 24 hrs. increased the d-spacing to 18.0 Å and 15.0 Å respectively, indicating the intercalation of these cations into the clay. If the above samples were immersed in a mixture of 1:1 water:glycerin, the d-spacing of  $Ru(NH_3)_6^{3+}$  -montmorillonite

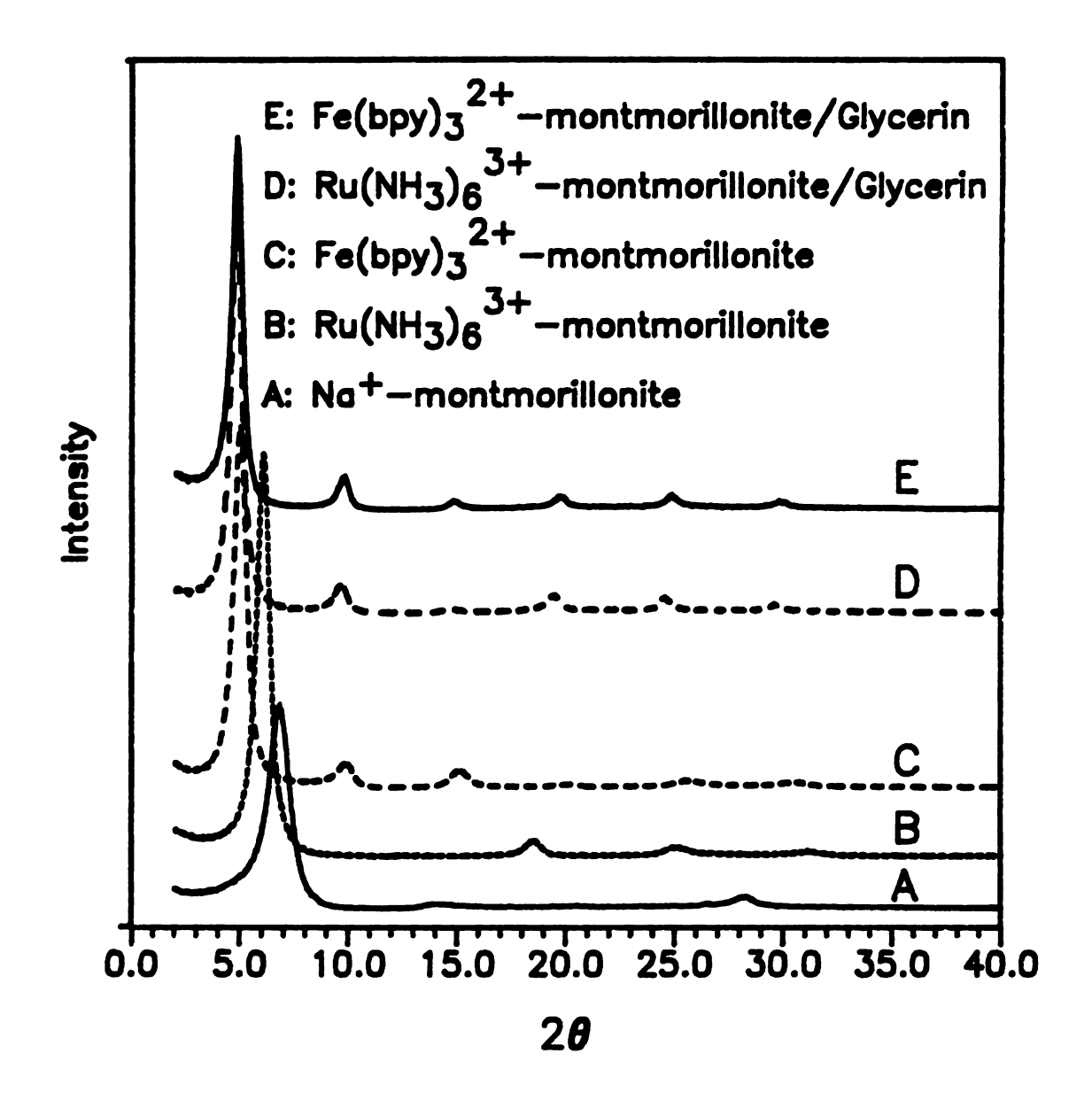


Figure III.12 X-ray diffraction patterns of homoionic montmorillonite. (A) Na<sup>+</sup>-montmorillonite; (B)  $Ru(NH_3)6^{3+}$ -montmorillonite; (C)  $Fe(bpy)3^{2+}$ -montmorillonite; (D)  $Ru(NH_3)6^{3+}$ -montmorillonite/glycerin; (E)  $Fe(bpy)3^{2+}$ -montmorillonite/glycerin.

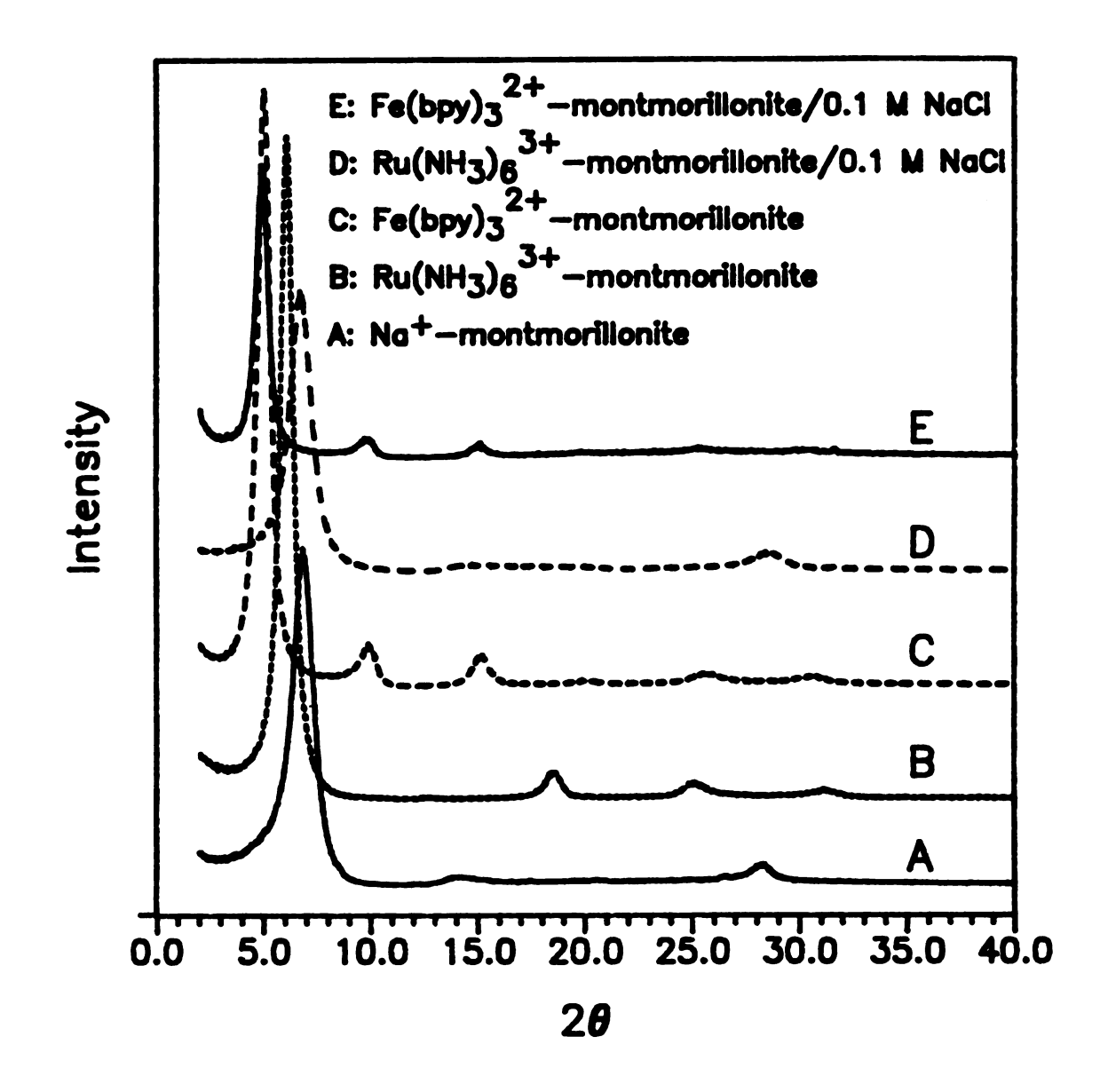


Figure III.13 X-ray diffraction patterns of homoionic montmorillonite. (A) Na<sup>+</sup>-montmorillonite; (B)  $Ru(NH_3)_6^{3+}$ -montmorillonite; (C)  $Fe(bpy)_3^{2+}$ -montmorillonite; (D)  $Ru(NH_3)_6^{3+}$ -montmorillonite/0.1 M NaCl; (E)  $Fe(bpy)_3^{2+}$ -montmorillonite/0.1 M NaCl.

increased to 18 Å; however the d-spacing of Fe(bpy)<sub>3</sub><sup>2+</sup> -montmorillonite remained the same. Similarly, if Ru(NH<sub>3</sub>)<sub>6</sub><sup>3+</sup> -montmorillonite and Fe(bpy)<sub>3</sub><sup>2+</sup> -montmorillonite slides were left in 0.1 M NaCl the d-spacing of Ru(NH<sub>3</sub>)<sub>6</sub><sup>3+</sup> -montmorillonite decreased to 12.5 Å indicating the exchange of Ru(NH<sub>3</sub>)<sub>6</sub><sup>3+</sup> with Na+ in 0.1 M NaCl. No change in the d-spacing of Fe(bpy)<sub>3</sub><sup>2+</sup> -montmorillonite was observed. These observations suggested the strong binding of Fe(bpy)<sub>3</sub><sup>2+</sup> to the montmorillonite surface and also the lability of Ru(NH<sub>3</sub>)<sub>6</sub><sup>3+</sup> in clay galleries.

# Confirmation of the Electrocatalytic Activity of Lattice Iron in Clay Modified Electrodes.

Ege et al.<sup>115</sup> have noted that the anode to cathode peak current ratio,  $i_{pc}/i_{pa}$ , of  $Ru(bpy)_3^{2+}$  incorporated into montmorillonite clays was greater than unity, at least in early scans. Also the number of coulombs passed during oxidation was much higher than for reduction. They have suggested that there is a chemical reaction between the electrogenerated  $Ru(bpy)_3^{3+}$  and lattice Fe(II) in the clay to regenerate  $Ru(bpy)_3^{2+}$ . Rudzinski and  $Bard^{140}$  have also observed a similar electrocatalytic effect in montmorillonite, hectorite and nontronite clays using  $Ru(NH_3)_6^{3+}$  and  $Ru(bpy)_3^{2+}$  as electroactive probe ions. On the basis of these observations they have suggested that the lattice iron in these clays was responsible for this catalytic behavior. Oyama and Anson<sup>139</sup> have described an electrocatalytic role for lattice iron in montmorillonite clay. In this

latter case the clay was found to catalyze the reduction of  $H_2O_2$  by  $Ru(NH_3)_6^{3+}$  formed by electrochemical reduction of  $Ru(NH_3)_6^{3+}$  at the clay electrode surface. The catalytic mechanism was attributed to the shuttling of electrons from  $Ru(NH_3)_6^{3+}$  to Fe(III) center in the clay to form Fe(II) which then reduced the adsorbed peroxide.

Although it is highly plausible that lattice iron can involve in the electrochemistry of clay modified electrodes, alternative mechanisms can be suggested. For instance, complexes such as  $Co(NH_3)6^{3+}$  are known to hydrolyze and to disproportionate on montmorillonite clay surface under certain conditions. 167 Even a very robust cobalt sepulchrate complex has been recently found to demetalate when adsorbed on the basal surface of the layered silicate magadiite. 168 Such decompositions of metal complexes on clay surfaces open up alternative explanations for the catalytic mechanism of clay modified electrodes. Therefore, we further studied the system by using non iron clays in order to determine whether such a clay can also participate in these reactions.

Here we confirm the importance of structural iron by using non iron smectite clays and relating the electrochemical activity to the lattice iron content. Both cyclic voltammetry and stirred solution voltammetry were used to elucidate the redox activity of lattice iron. A mechanism is suggested to explain the catalytic reaction when  $H_2O_2$  is introduced to the system.

Figure III.14 shows the observed wave currents for a series of

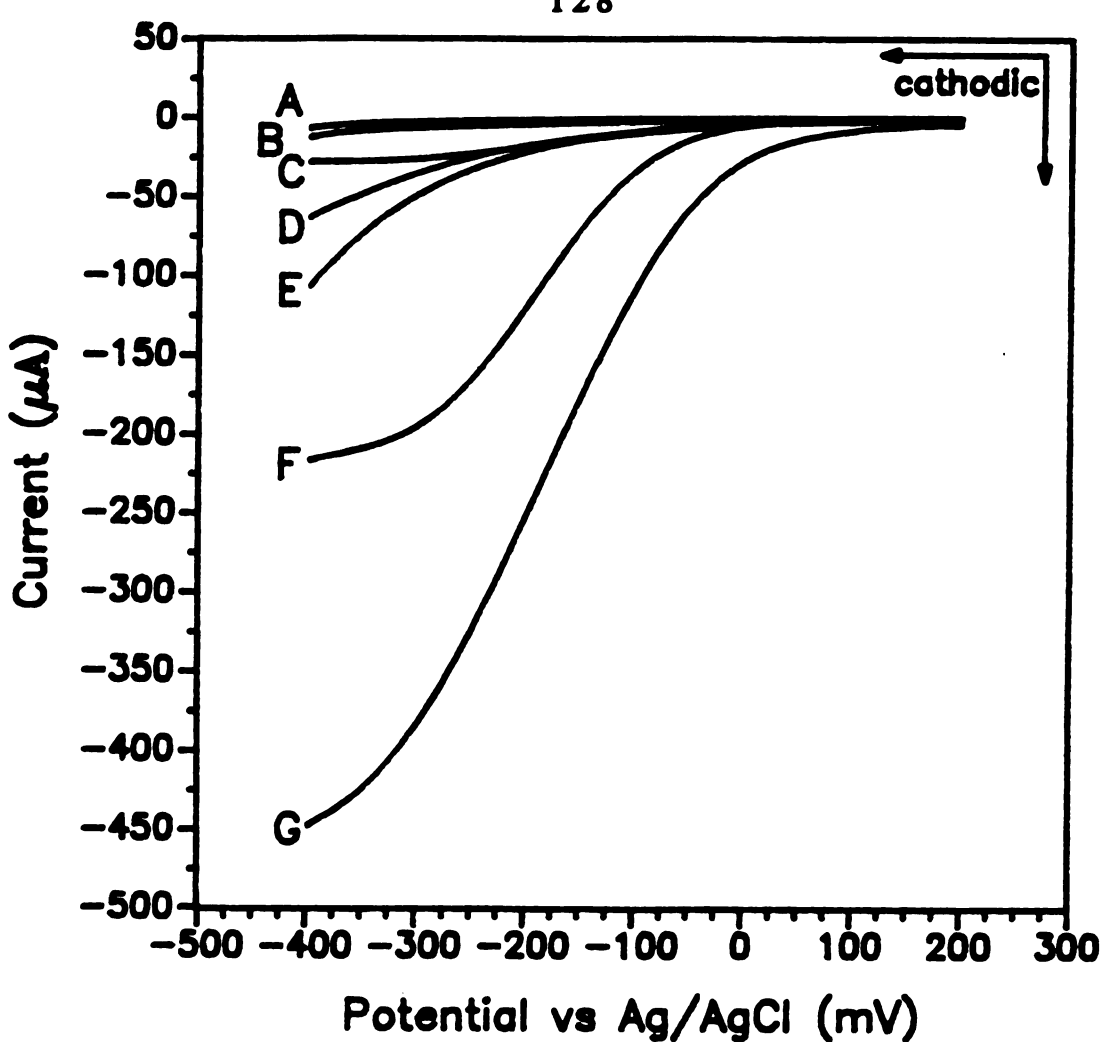


Figure III.14 Cathodic Limiting Currents for Stirred solution voltammograms: A) Bare graphite electrode in 0.05 M CH<sub>3</sub>CO<sub>2</sub>Na pH 3 buffer electrolyte containing 10<sup>-5</sup> M Ru(NH<sub>3</sub>)6<sup>3+</sup>. B) Bare graphite electrode in 0.05 M CH<sub>3</sub>CO<sub>2</sub>Na pH 3 buffer electrolyte containing 10<sup>-5</sup> M Ru(NH<sub>3</sub>)6<sup>3+</sup> and 0.1 M H<sub>2</sub>O<sub>2</sub>. C) Na<sup>+</sup>-montmorillonite coated graphite electrode in 0.05 M CH<sub>3</sub>CO<sub>2</sub>Na pH 3 buffer containing 10<sup>-5</sup> M Ru(NH<sub>3</sub>)6<sup>3+</sup>. D) Na<sup>+</sup>-laponite coated graphite electrode in 0.05 M CH<sub>3</sub>CO<sub>2</sub>Na pH 3 buffer containing 10<sup>-5</sup> M Ru(NH<sub>3</sub>)6<sup>3+</sup> and 0.1 M H<sub>2</sub>O<sub>2</sub>. E) Na<sup>+</sup>-montmorillonite coated graphite electrode in 0.05 M CH<sub>3</sub>CO<sub>2</sub>Na pH 3 buffer containing 0.1 M H<sub>2</sub>O<sub>2</sub>. F) Na<sup>+</sup>-montmorillonite coated graphite electrode in 0.05 M CH<sub>3</sub>CO<sub>2</sub>Na pH 3 buffer containing 10<sup>-5</sup> M Ru(NH<sub>3</sub>)6<sup>3+</sup> and 0.1 M H<sub>2</sub>O<sub>2</sub>. G) Na<sup>+</sup>-nontronite coated graphite electrode in 0.05 M CH<sub>3</sub>CO<sub>2</sub>Na pH 3 buffer containing 10<sup>-5</sup> M Ru(NH<sub>3</sub>)6<sup>3+</sup> and 0.1 M H<sub>2</sub>O<sub>2</sub>. G) Na<sup>+</sup>-nontronite coated graphite electrode in 0.05 M CH<sub>3</sub>CO<sub>2</sub>Na pH 3 buffer containing 10<sup>-5</sup> M Ru(NH<sub>3</sub>)6<sup>3+</sup> and 0.1 M H<sub>2</sub>O<sub>2</sub>.

stirred solution voltammetry experiments carried out with graphite/clay-modified electrodes. These data are similar to those of Omaya and Anson<sup>139</sup> with some exceptions. Our results contain additional information resulting from non iron clays, which can be used to prove the participation of lattice iron in a catalytic reaction.

Neither  $10^{-5}$  M Ru(NH<sub>3</sub>)6<sup>3+</sup> nor  $10^{-5}$  M Ru(NH<sub>3</sub>)6<sup>3+</sup> in 0.1 M H<sub>2</sub>O<sub>2</sub> shows an appreciable faradaic current at a bare graphite electrode surface (Figure III.14, curves A and B respectively). When the electrode was coated with clay, an increase in the observed current was seen in the presence of  $10^{-5}$  M Ru(NH<sub>3</sub>)6<sup>3+</sup> (curve C). Under these conditions ion exchange builds up the Ru(NH<sub>3</sub>)6<sup>3+</sup> ion concentration on the clay surfaces and a small faradaic current is manifested depending upon the time of soaking of the electrode in the electrolyte containing  $10^{-5}$  M Ru(NH<sub>3</sub>)6<sup>3+</sup> Also a relatively small current was obtained for a Na<sup>+</sup>-montmorillonite coated graphite electrode, when immersed in the supporting electrolyte containing only 0.1 M H<sub>2</sub>O<sub>2</sub> (curve E).

When 0.1 M H<sub>2</sub>O<sub>2</sub> was added to the electrolyte solution containing 10<sup>-5</sup> M Ru(NH<sub>3</sub>)<sub>6</sub><sup>3+</sup> a five-fold increase in the faradaic current was observed at the Na<sup>+</sup>-montmorillonite coated electrode (Figure III.14, curve F). However, when iron free clay, Na<sup>+</sup>-fluorohectorite or Na<sup>+</sup>-laponite, coated graphite electrodes were used instead of Na<sup>+</sup>-montmorillonite no significant increase in faradaic current was noticed (Figure III.14 curve D). For further verification of the dependence of faradaic current on lattice iron content of the clay, we investigated Na<sup>+</sup>-nontronite where the lattice iron content is

very high. Table I.1 indicates the unit cell formulae of laponite, montmorillonite, fluorohectorite and nontronite. In nontronite almost all the octahedral Al<sup>3+</sup> ions have been replaced by Fe<sup>3+</sup> ions. <sup>141,169</sup> When Na<sup>+</sup>-nontronite was employed as an electrode modifier the faradaic current increased the faradaic current increased by a factor of 7.3 (Figure III.14 curve G). The increment in current in the case of nontronite was 1.5 times greater than that of montmorillonite.

The cyclic voltammograms of Na<sup>+</sup>-laponite, Na<sup>+</sup>-montmorillonite and Na<sup>+</sup>-nontronite coated graphite electrodes soaked in 1 mM Ru(NH<sub>3</sub>)6<sup>3+</sup> (pH 3 acetate buffer) for 24 hrs are shown in Figures III.15 curves A, B and C respectively. For the Na<sup>+</sup>-laponite coated electrode the ratio of  $i_{pc}/i_{pa}$  was close to one. However, the Na<sup>+</sup>-montmorillonite coated electrode showed a higher deviation from unity,  $i_{pc}/i_{pa} = 1.9$ ; the ratio was even greater for the Na<sup>+</sup>-nontronite coated electrode  $i_{pc}/i_{pa} = 3.2$  as observed by Bard et al. 140

Figure III.16 shows cyclic voltammograms obtained for Na<sup>+</sup>-montmorillonite coated graphite electrodes that were pre-treated with reducing or oxidizing agents and then soaked in 1 mM Ru(NH<sub>3</sub>)<sub>6</sub><sup>3+</sup> solutions for 30 min. Treatment of the clay film with 0.1 M Na<sub>2</sub>S<sub>2</sub>O<sub>4</sub>, which served to reduce the lattice iron to the divalent state, decreased the i<sub>pc</sub>/i<sub>pa</sub> ratio, from a value of 1.9 for the pristine clay to a value of 1.1 for the reduced clay (Figure III.16 curves B and A respectively). On the other hand, when the iron in the clay film

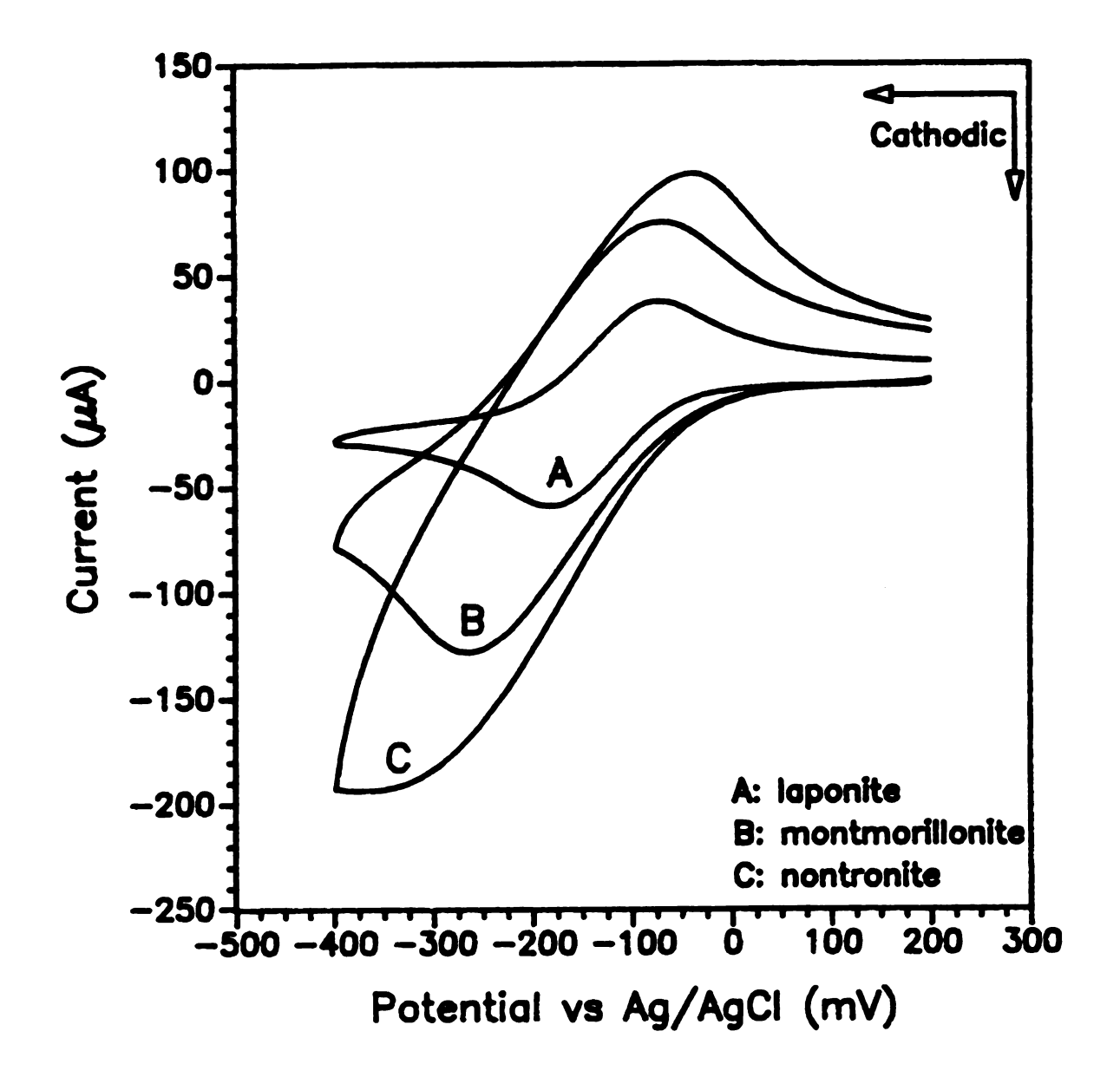


Figure III.15 Cyclic voltammograms of clay coated graphite electrodes soaked in 1 mM Ru(NH<sub>3</sub>)<sub>6</sub><sup>3+</sup> for 24 hrs and then rinsed with deionized water. The electrolyte was 0.05 M CH<sub>3</sub>CO<sub>2</sub>Na in a pH 3 buffer. a) Na<sup>+</sup>-laponite; b) Na<sup>+</sup>-montmorillonite and c) Na<sup>+</sup>-nontronite.

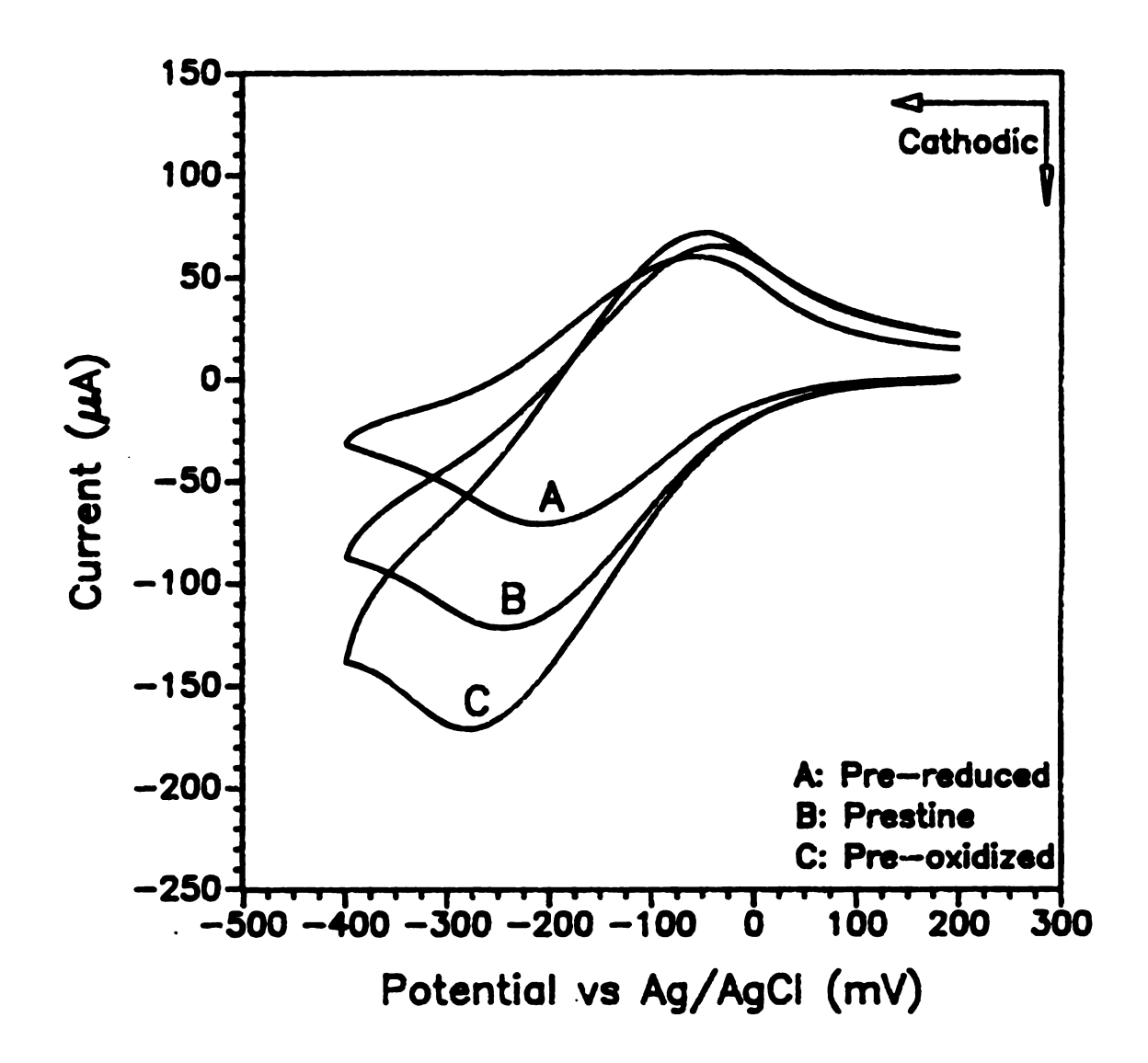


Figure III.16 Cyclic voltammograms of graphite electrodes coated with equivalent amounts of Na<sup>+</sup>-montmorillonite. a) pre-reduced with 0.1 M Na<sub>2</sub>S<sub>2</sub>O<sub>4</sub> and then soaked in 1 mM Ru(NH<sub>3</sub>) $_6$ <sup>3+</sup> for 30 mins. b) Pristine mineral without pre-reduction or pre-oxidation. c) pre-oxidized with 5 M H<sub>2</sub>O<sub>2</sub> and then soaked in 1 mM Ru(NH<sub>3</sub>) $_6$ <sup>3+</sup> for 30 mins. The electrolyte solution was 0.05 M CH<sub>3</sub>CO<sub>2</sub>Na in a pH 3 buffer.

was oxidized to the trivalent state with 5 M  $H_2O_2$  the  $i_{pc}/i_{pa}$  ratio increased to 7.7 (Figure III.16 curve C).

Because of the absence of lattice iron in either laponite or fluorohectorite, this catalytic reaction was not observed when any of these clays were used to modify the electrode surface. Taking into account all of the above and previous authors results possible catalytic sequence for  $H_2O_2$  decomposition in this acidic medium can be represented as given in Scheme III.2.

## Effects of the Electrolyte pH on the Electrochemistry at Clay Modified Electrodes.

Inoue et al.<sup>145</sup> reported that the peak current for the oxidation of  $Ru(bpy)_3^{2+}$  at montmorillonite modified electrodes is invariant in the pH range 10-4 but drastically decreases below pH 4. On the other hand peak current for the reduction of  $Fe(CN)_6^{3-}$  increases with decreasing the electrolyte pH below 4. They have additionally shown that the proton adsorption on montmorillonite also has a similar pH dependance. Therefore, they concluded that the pH dependence of the electroactivity  $Ru(bpy)_3^{2+}$  and  $Fe(CN)_6^{3-}$  is due to the protonation of the oxygen framework in clay to give the clay platelets a positive charge at pH values below 4.

Table III.2 indicates the peak currents for the oxidation of  $Fe(bpy)_3^{2+}$  and reduction of  $Ru(NH_3)_6^{3+}$  at montmorillonite coated modified electrodes at different pH ranging from 7 to 2.5. These

### Scheme III.2 Proposed scheme for the catalytic reaction

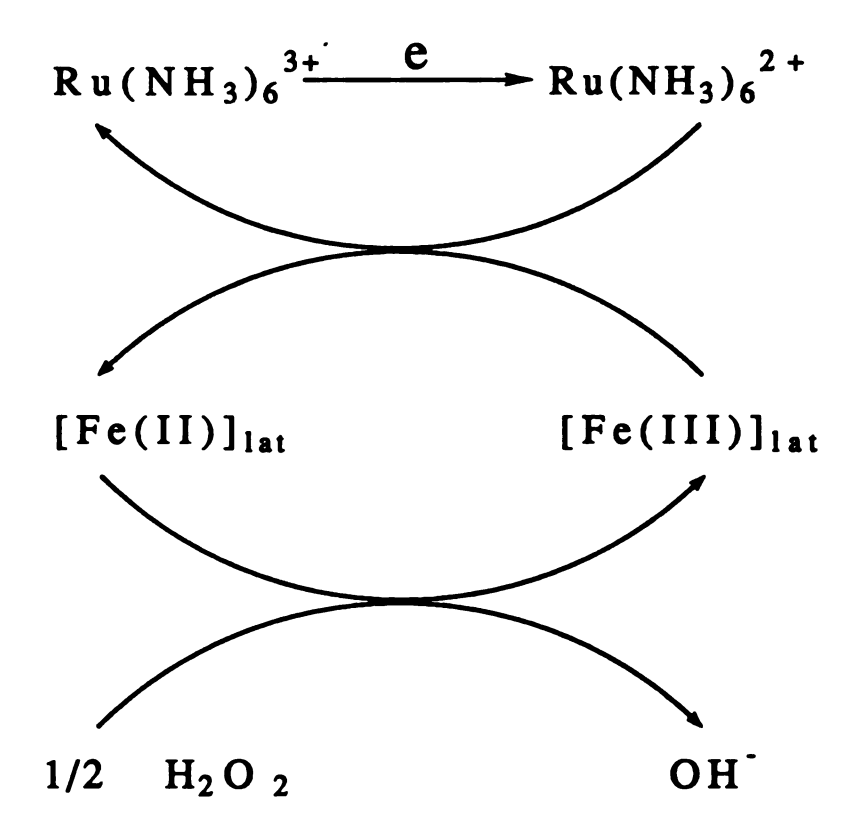


Table III.2 Dependance of initial peak current  $(\mu A)$  on pH of the supporting electrolyte, 0.1 M sodium acetate and acetic acid buffer, for electroactive centers in montmorillonite-modified electrodes.

Electrolyte pH*	Homoionic Ru(NH3)6 <sup>3+</sup>	Homoionic Fe(bpy)3 <sup>2+</sup>
7.0	226 ± 3	79 ± 5
6.0	221 ± 6	82 ± 4
5.0	225 ± 5	56 ± 3
4.0	226 ± 6	46 ± 3
3.0	211 ± 6	25 ± 3
2.5	<u>-</u>	0.0

<sup>\*</sup> Soaking solution also contains 0.1 M sodium acetate buffer.

electrodes were prepared by soaking the montmorillonite coated electrode in 1 mM solutions of Fe(bpy)<sub>3</sub><sup>2+</sup> and Ru(NH<sub>3</sub>)<sub>6</sub><sup>3+</sup> containing 0.1 M sodium acetate buffered at the desired pH. Cyclic voltammograms were recorded only in the supporting electrolyte containing 0.1 M buffered at the desired pH. It is clear that the peak current for the oxidation of Fe(bpy)32+ is dependant upon the pH of the electrolyte but the peak current for the reduction of Ru(NH<sub>3</sub>)<sub>6</sub><sup>3+</sup> is independent of pH. At pH 2.5 neither intersalation nor intercalation of Fe(bpy)3<sup>2+</sup> was noticed; that is the coated clay films remained colorless even after soaking in 1 mM Fe(bpy)<sub>3</sub><sup>2+</sup> containing 0.1 M sodium acetate buffered at pH 2.5 (0.1 M sodium acetate in glacial acetic acid) for 24 hrs. Ru(NH<sub>3</sub>)<sub>6</sub><sup>3+</sup> is not soluble in the above In contrast, the electrochemistry of  $Fe(bpy)_3^{2+}$  does not indicate any pH dependency as indicated by the peak currents summarized in Table III.3, where sodium trichloroacetate and trichloroacetic acid was used as the supporting electrolyte buffer. The decrease in the electroactivity of  $Fe(bpy)_3^2$  by the slow diffusion of trichloroacetate anion within the clay film, as discussed in section III.c.1. Therefore, a 0.1 M sodium acetate solution was used to record the cyclic voltammograms in order to resolve the true pH dependance, if there is any. These results are tabulated in Table III.4. Again, the anodic peak current for Fe(bpy)<sub>3</sub><sup>2+</sup> decreases below pH 3 while the cathodic peak current for Ru(NH<sub>3</sub>)<sub>6</sub><sup>3+</sup> remains These observations suggest that the decrease in invariant with pH. electroactivity of Fe(bpy)3<sup>2+</sup> at lower pH is not due to the protonation of the clay layers. If this were the case, the electroactivity of Ru(NH<sub>3</sub>)<sub>6</sub><sup>3+</sup> should also decrease at lower pH

Table III.3 Dependance of initial peak current  $(\mu A)$  on pH of the supporting electrolyte, 0.1 M sodium trichloroacetate and trichloroacetic acid buffer, for electroactive centers in montmorillonite-modified electrodes.

Electrolyte pH*	Homoionic Ru(NH <sub>3</sub> ) <sub>6</sub> <sup>3+</sup>	Homoionic Fe(bpy)3 <sup>2+</sup>
7.0	261 ± 7	48 ± 3
6.0	272 ± 5	48 ± 3
5.0	267 ± 7	49 ± 3
4.0	268 ± 6	46 ± 2
3.0	279 ± 5	47 ± 1
2.0	292 ± 7	49 ± 2
1.5	284 ± 8	46 ± 3

<sup>\*</sup> Soaking solution also contains 0.1 M sodium trichloroacetate buffer.

Table III.4 Dependance of initial peak current  $(\mu A)$  on pH of the soaking solution, 0.1 M sodium trichloroacetate and trichloroacetic acid buffer, for electroactive centers in montmorillonite-modified electrodes. Supporting electrolyte was always a 0.1 M sodium acetate and acetic acid buffered at pH 7.

pH of the Soaking Solution	Homoionic Ru(NH <sub>3</sub> ) <sub>6</sub> <sup>3+</sup>	Homoionic Fe(bpy)3 <sup>2+</sup>
7.0	290 ± 8	90 ± 4
6.0	288 ± 8	89 ± 6
5.0	294 ± 9	84 ± 4
4.0	291 ± 2	94 ± 2
3.0	322 ± 7	96 ± 6
2.0	282 ± 8	75 ± 5
1.5	288 ± 6	50 ± 1

because the electroactivity of  $Ru(NH_3)_6^{3+}$  arises from the exchanged  $Ru(NH_3)_6^{3+}$  and not from ion pairs.

The cyclic voltammogram of sodium montmorillonite coated graphite electrode soaked in 1 mM Fe(CN)63- for 24 hrs. and rinsed with deionized water is shown in Figure III.17. The supporting electrolyte was 0.1 M Na<sub>2</sub>SO<sub>4</sub>. This indicates that there is no appreciable quantity of electroactive Fe(CN)63- found within the Therefore, it is suggested that the electroactivity of Fe(CN)63at clay modified electrodes originates from the penetration of species in the electrolyte solution, perhaps through channels or cracks, as reported earlier. 115,116 Furthermore, no peak was observed for Fe(CN)6<sup>3-</sup> after soaking in 1 mM K<sub>3</sub>Fe(CN)6 containing 0.1 M CH<sub>3</sub>CO<sub>2</sub>Na buffer pH 4 or pH 3 for 24 hrs. However, a broad peak begins to appear about 400 mV more positive than that of the reported Fe(CN)6<sup>3-</sup> (210 mv Vs Ag/AgCl). This broad peak (at 620 mV) seems to agree with the reported potential for the complex known as Prussin Blue. 170,171 This complex may originate from the decomposition of Fe(CN)63- in these acidic media. This hypothesis was tested by similarly treating a bare graphite electrode in the above solutions. As shown in Figure III.18 bare graphite electrode also gives the very same cyclic voltammogram confirming the peak originates in these solutions are indeed from the deposition of the Prussian Blue on the electrode surface.

The pH dependency of the electroactivity of  $Fe(CN)_6^{3-}$  at a clay modified graphite electrode may be a result of the pH dependency

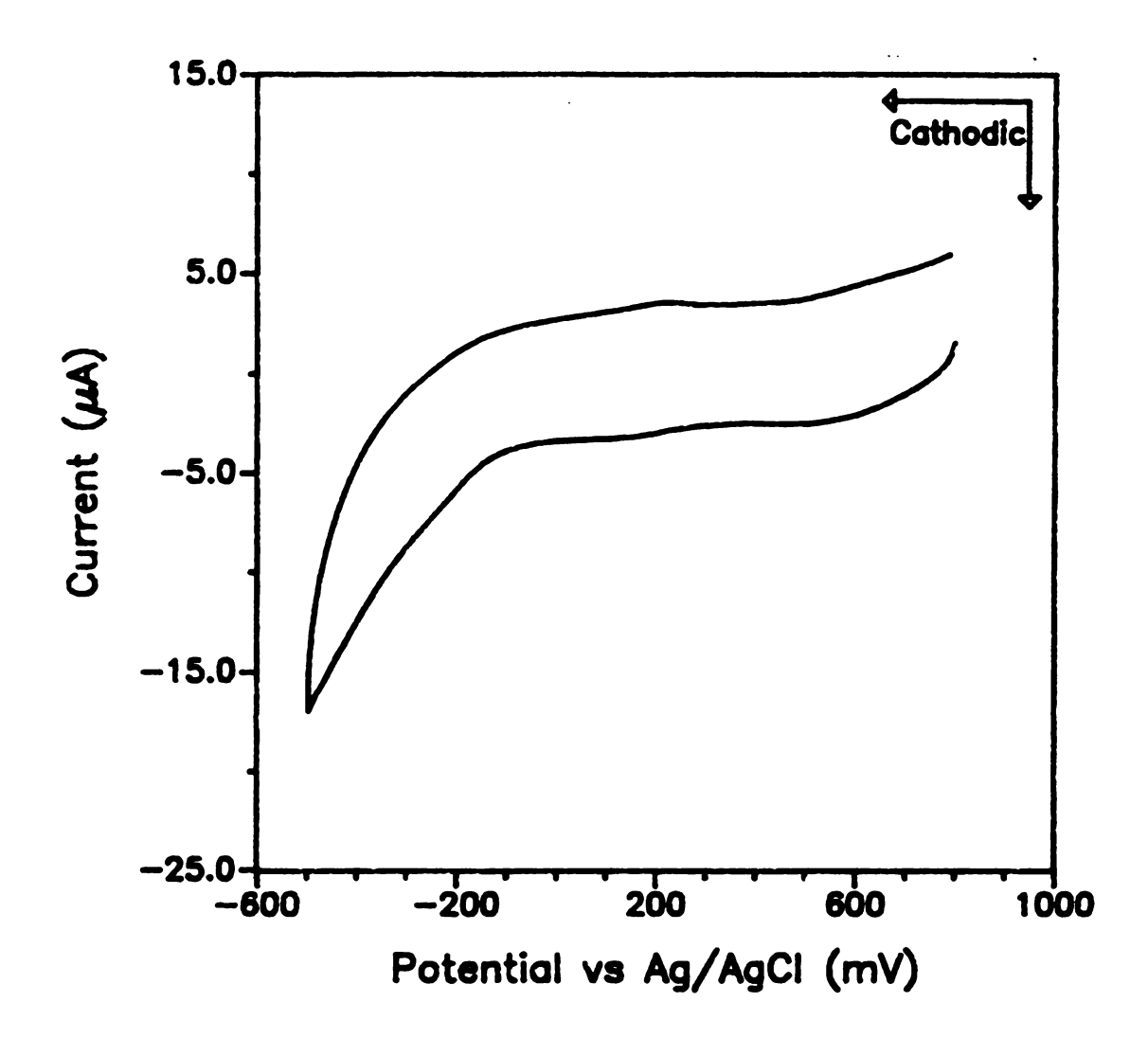


Figure III.17 Cyclic voltammogram of  $Fe(CN)_6^{3-}$  at a montmorillonite coated graphite electrode pre-soaked in 1 mM  $K_3Fe(CN)_6$  for 24 hrs. Supporting electrolyte was 0.05 M sodium sulfate pH 7.0. v=100 mV sec<sup>-1</sup>.

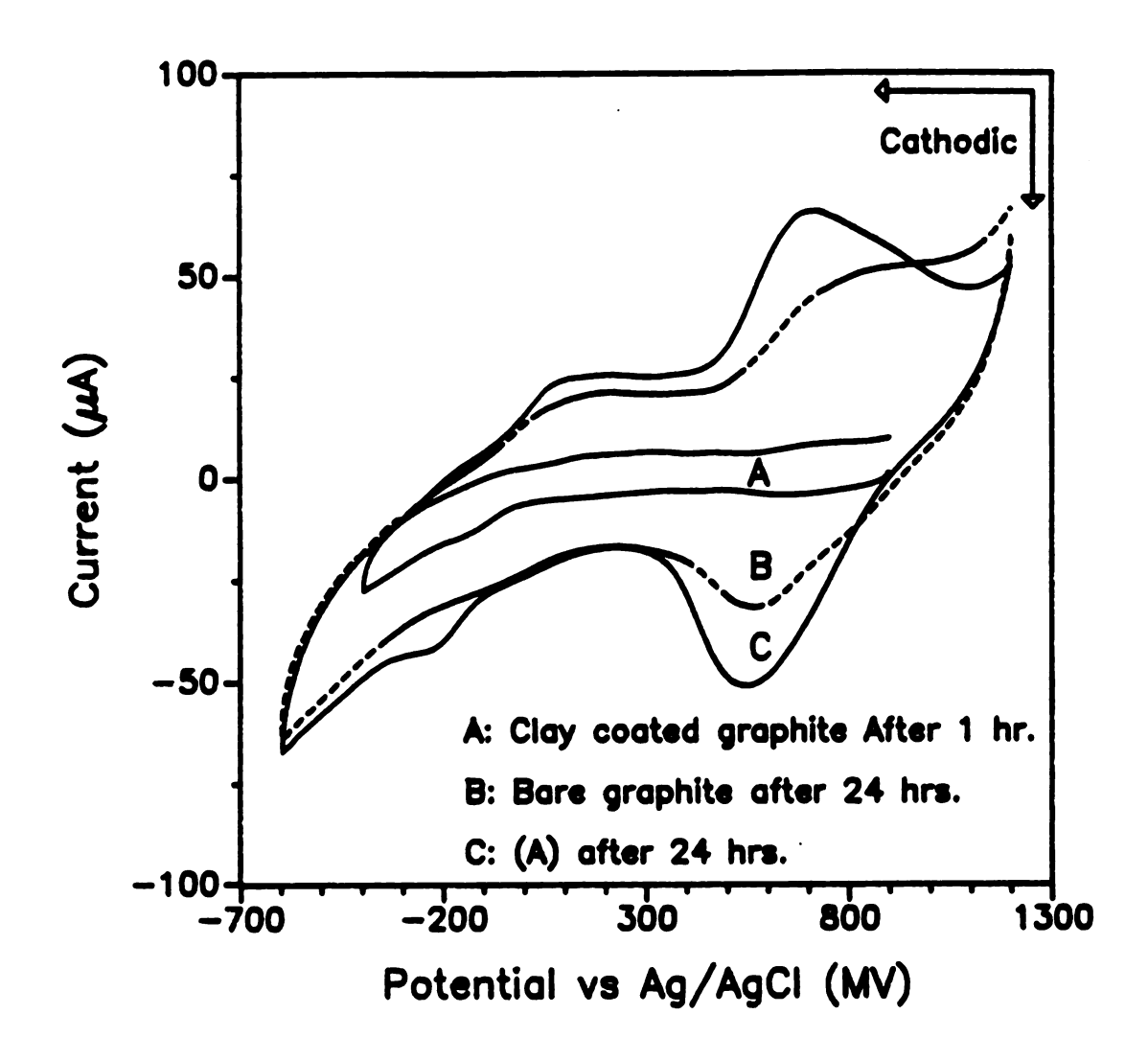


Figure III.18. Cyclic voltammograms of  $Fe(CN)_6^{3-}$  at (A) montmorillonite clay coated graphite electrode soaked in 1 mM  $Fe(CN)_6^{3-}$  containing 0.1 M  $CH_3CO_2Na$  pH 4 for 1 hr; (B) Bare graphite electrode soaked in 1 mM  $Fe(CN)_6^{3-}$  containing 0.1 M  $CH_3CO_2Na$  pH 4 for 24 hrs. (C) The same as (A) but soaked for 24 hrs.

of heterogeneous electron transfer rate constant which increases with decreasing pH.<sup>172</sup>

Effects of the Surface Density of Clay Coating on the Electrochemistry at Clay Modified Electrodes.

Working with Na+-montmorillonite and Fe(bpy)<sub>2</sub><sup>2+</sup> preexchanged montmorillonite, King found that the electroactivity of Fe(bpy)<sub>3</sub><sup>2+</sup> is independent from thickness of the clay coating.<sup>146</sup> Therefore, the author suggested a dual domain system to account for his observations (Section III.a and Figure III.2). Lee and Fitch<sup>144</sup> also reported that at low electrolyte concentrations, the electroactivity of Fe(CN)63- at montmorillonite-modified electrodes is independent of the thickness of the clay coating, but at higher electrolyte concentrations it is dependent upon the film thickness. These observations were explained on the basis of the difference in clay platelets arrangement at in these two ranges of supporting electrolyte. At higher electrolyte concentrations clay platelets tend to stack with face to face arrangement which inhibit penetration of the film by Fe(CN)6<sup>3-</sup> ions. However, at low concentrations clay platelets arrange with edge to face orientation. As a result of this the clay film become disordered allowing negatively charge Fe(CN)63- to penetrate the film.

The cathodic peak current of Ru(NH3)<sub>6</sub><sup>3+</sup> pre-exchanged into laponite against the weight of clay added per square centimeter (surface density of clay) is depicted in Figure III.19. The cathodic

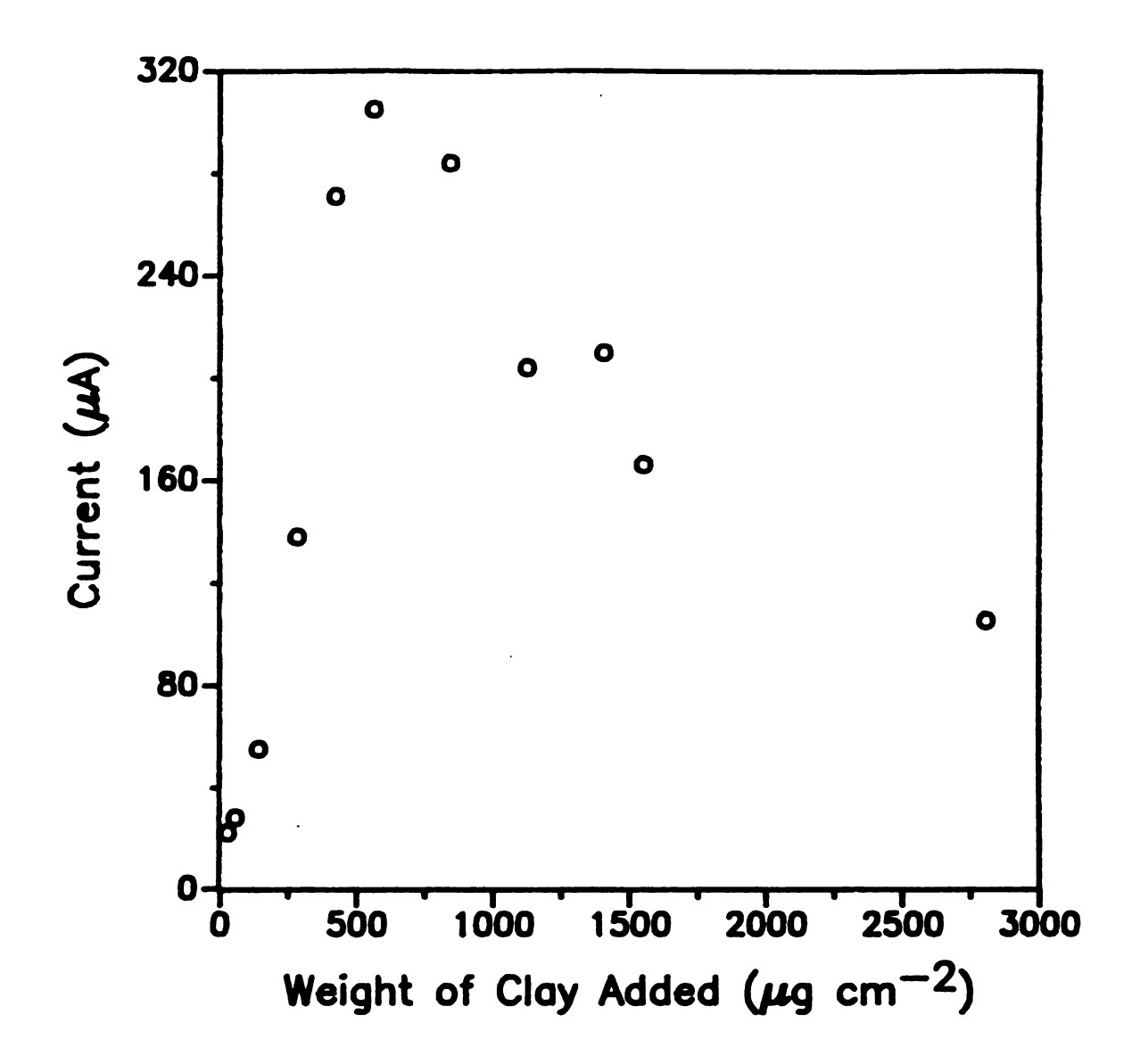


Figure III.19 Effect of the amount of clay added on cyclic voltammetry of  $Ru(NH_3)_6^{3+}$  pre-exchanged into laponite.

peak current sharply increases with increasing quantity of clay up to about 500 µm cm<sup>-2</sup> and then it starts to decrease slowly with further increase of the surface clay density. The number of coulombs passed upon electrolysis also increases with increasing surface clay density (Figure III.20). However, the number of coulombs passed reaches a maximum at a higher density, about 2000 µm cm<sup>-2</sup>. This may probably be due to the extended period of time involved in bulk electrolysis. During this extended period of time, the clay coating can adsorb water and swell to give a more disordered film thereby extending the electroactive clay density of the film. This suggestion is consistent with the fact that a pre-soaked electrode exhibits a higher electroactive clay density for the same species. possible that Ru(NH3)63+ located at a longer distance can reach the electrode surface because of the extended period of time involved. But cyclic voltammetry with different scan rates (50, 100, 200 mV sec-1) exhibited the same electroactive maximum, suggesting that this is not a diffusion limited process. Furthermore, if diffusion of Ru(NH3)<sub>6</sub><sup>3+</sup> controlled the electroactive clay fraction, a constant peak current could be expected for films contain surface density of clay more than 500 µm cm<sup>-2</sup>. However, the experimental data indicate that cathodic peak current decreases when the surface density of clay is higher than 500  $\mu$ m cm<sup>-2</sup>. This also suggests that it is not a simple diffusion limited process.

We have reported that the peak current of  $Ru(NH3)_6^{3+}$  is controlled by the diffusion of electrolyte cations within the clay film as a means of maintaining the electrical neutrality. This electrical

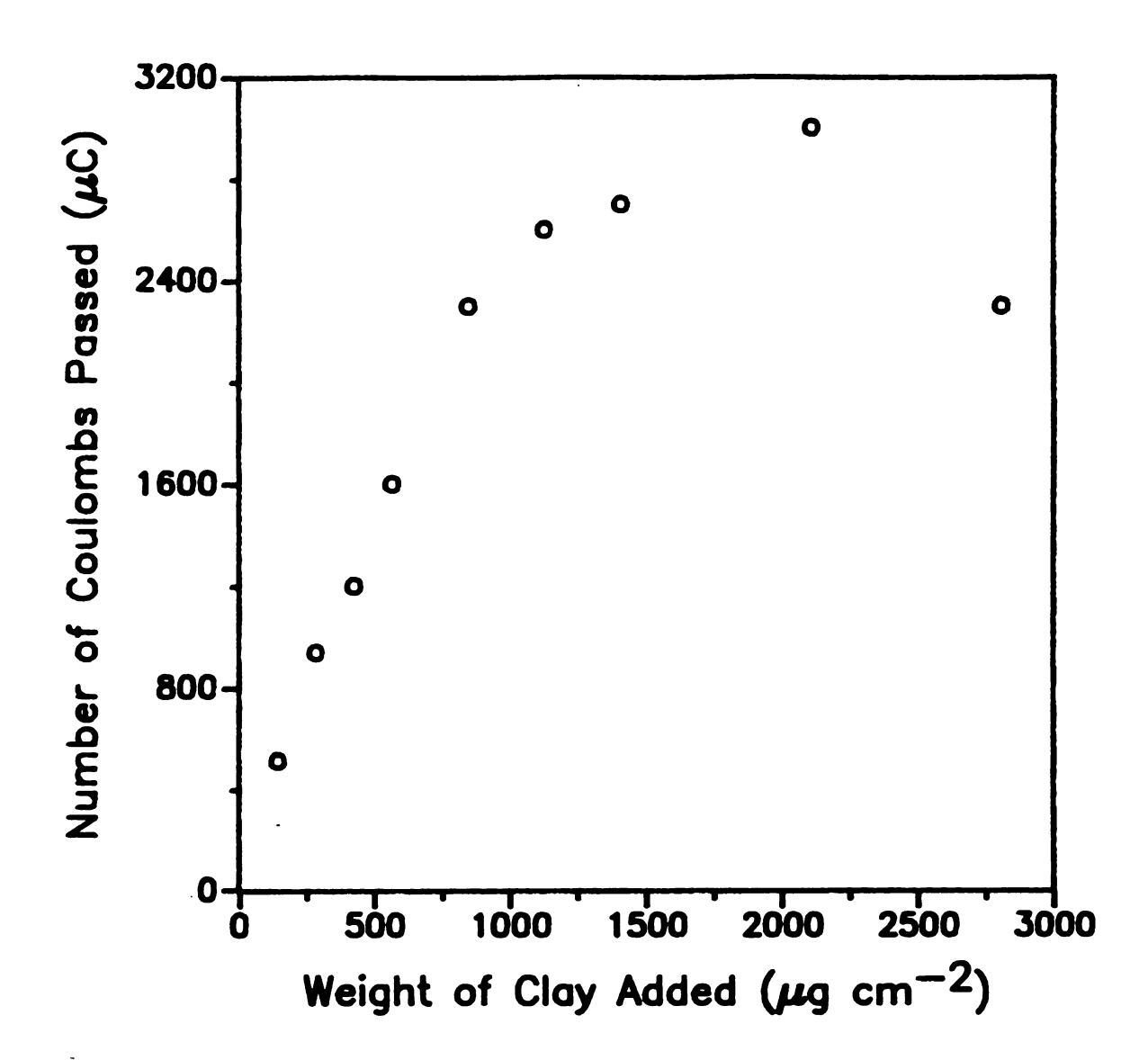


Figure III.20 Effect of the amount of clay added on bulk electrolysis of  $Ru(NH_3)6^{3+}$  pre-exchanged into laponite.

neutrality mechanism becomes more and more difficult with increasing surface density of clay at the electrode. As a result, cathodic peak current starts to decrease beyond a certain clay density at the electrode.

The variation of the peak current of clay coated electrodes soaked in 1 mM solutions of  $Ru(NH_3)_6^{3+}$  and  $Fe(bpy)_3^{2+}$  with the clay surface density is shown in Figure III.21. In contrast to the pre-exchanged  $Ru(NH_3)_6^{3+}$ , there is no maximum in the peak current of  $Ru(NH_3)_6^{3+}$ . This is most probably due to the disordering of the clay film upon prolong soaking. The peak current of  $Fe(bpy)_3^{2+}$  levels off after an initial increase, indicating that the electroactivity of  $Fe(bpy)_3^{2+}$  is restricted to the defect sites as suggested by King. 146

However, the assumption that the films are uniform, may not strictly accurate because of the higher possibility of accumulation of clay platelets at the edge of the electrode. Therefore, the observed maximum peak current for  $Ru(NH_3)_6^{3+}$  at about 500  $\mu$ m cm<sup>-2</sup> may not be strictly accurate.

#### III.d Conclusions

The difference in the electroactivity for  $Ru(NH_3)6^{3+}$  and  $Fe(bpy)_3^{2+}$  in clay modified electrodes has been elucidated. We have shown that  $Ru(NH_3)6^{3+}$  cations on the exchange sites of clays are electroactive, whereas  $Fe(bpy)_3^{2+}$  is electroactive when only coadsorbed as ion pairs. Chronocoulometry experiments carried out

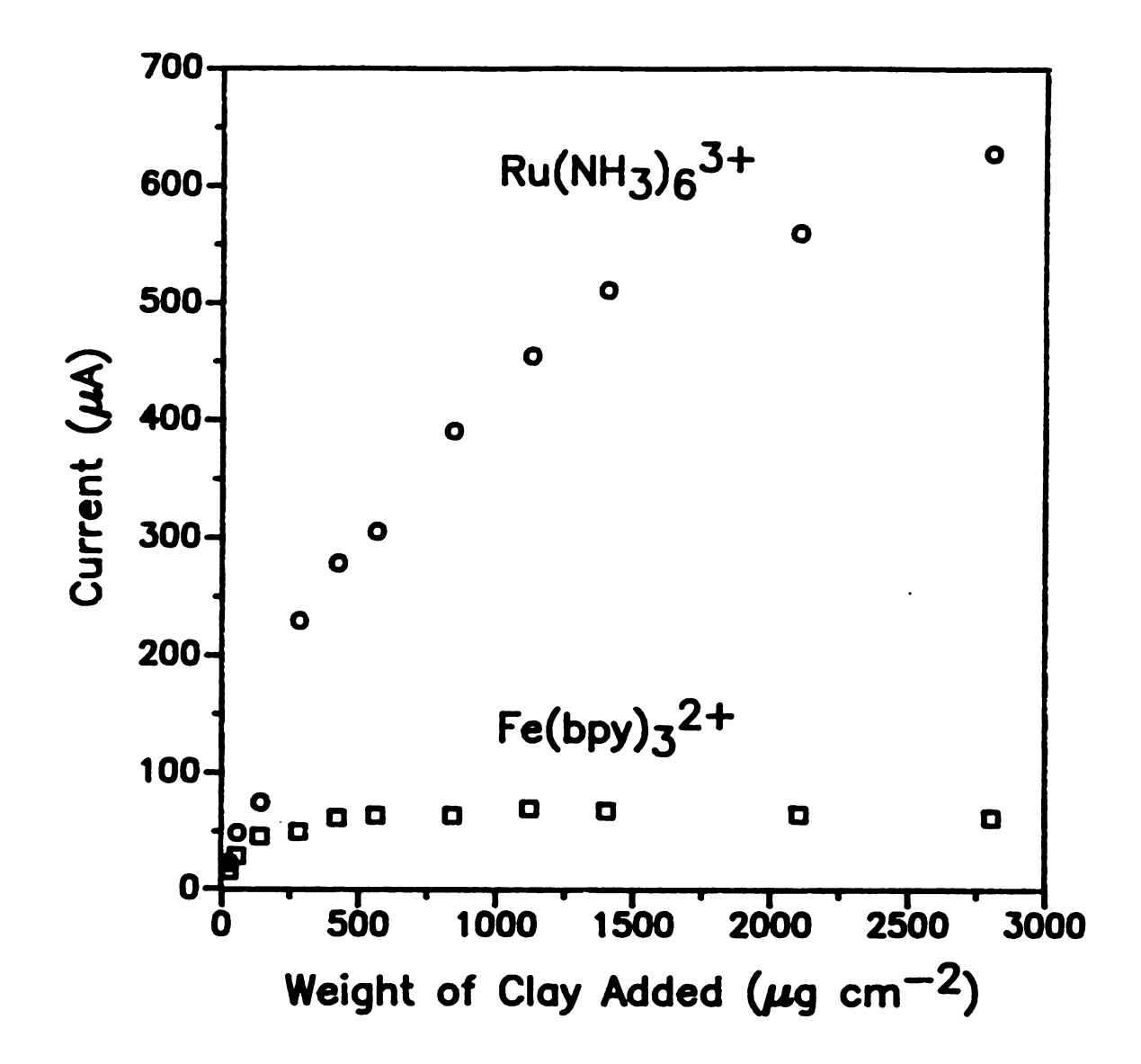


Figure III.21 Effect of the amount of clay added on cyclic voltammetry of  $Ru(NH_3)_6^{3+}$  and  $Fe(bpy)_3^{2+}$  at laponite coated graphite electrodes soaked in 1 mM solutions of  $Ru(NH_3)_6^{3+}$  and  $Fe(bpy)_3^{2+}$ .

with homoionic  $Ru(NH_3)6^{3+}$  laponite in 0.05 M  $Na_2SO_4$  as the supporting electrolyte indicated that more than 80% of the exchanged  $Ru(NH_3)6^{3+}$  cations are electroactive. To be electroactive the gallery exchange cations must be labile and allow for the coexchange of cations from the supporting electrolyte.  $Ru(NH_3)6^{3+}$  meets both conditions, but  $Fe(bpy)_3^{2+}$  is strongly bound and is not easily exchanged. The cation exchange inertness of polypyridyl metal complexes, which may result from special interactions with the clay surface, is consistent with the observation of earlier workers.  $^{122}$  Consequently, homoionic clays containing  $Fe(bpy)_3^{2+}$  and analogous polypyridyl complexes are electroinactive.

We have also shown that graphite electrodes modified with ferruginous clays, such as montmorillonite and nontrnite, can greatly enhance the faradaic current in stirred solution voltammetry in the presence of hydrogen peroxide. Furthermore, the anodic to cathodic peak current ratio,  $i_{pc}/i_{pa}$  in cyclic voltammograms of Ru(NH<sub>3</sub>)6<sup>3+</sup> exchanged into smectite clays, depends solely on the lattice iron content of the clay as well as its oxidation state. On the other hand, the absence of any enhancement in the faradaic current in stirred solution voltammetry and the cathodic to anodic peak current ratio of unity for iron free clays, such as laponite and fluorohectorite provide strong evidence that the catalytic activity truly originates from the lattice iron of the clay.

It was shown that the pH dependency of the electroactivity of  $M(bpy)_3^{2+}$  arises from the decrease in the formation of ion pairs and not due to the protonation of the clay layer oxygens. Electroactivity

at clay modified electrodes also depends to a certain degree upon the surface density of the clay at the electrode surface. In pre-exchanged clays, electroactivity decreases beyond a certain density of the clay coating probably due to the increasing difficulty to maintain the electrical neutrality within the clay film. However, electrodes presoaked in the electroactive species solutions did not show such a decrease within the range studied (~25-3000  $\mu$ g cm<sup>-2</sup>). This is probably due to the disordered structure of the clay coating upon prolong soaking.



### LIST OF REFERENCES

- 1. Murray, R. W. Acc. Chem. Res. 1980, 13, 135.
- 2. Murray, R. W. Electroanalytical Chemistry; ; Bard, A. J. Ed.; Dekker, New York, 1984 13 p191.
- 3. Snell, K. D.; Keenan, A. G. Chem. Soc. Rev. 1979, 8, 259.
- 4. Miller, J. S. Ed. Chemically Modified Surfaces in Catalysis and Electrocatalysis, American Chemical Society, Washington D. C., 1982 p1.
- 5. Albery, W. J.; Hillman, A. R. Ann Rev. C. R. Soc. Chem. London, 1981 377.
- 6. Faulkner, L. R. Chem. Eng. News. 1984 Feb 27 p28.
- 7. Abruna, H. D. Coord. Chem. Rev. 1988, 86, 135.
- 8. Collman, J. P.; Denisevich, P.; Konai, Y.; Marrocco, M.; Koval, C.; Anson, F. C. J Am. Che. Soc. 1980, 102, 6027.
- 9. Collman, J. P.; Kim, K. J. Am. Chem. Soc. 1986, 108, 7847.
- Evans, J. F.; Kuwana, T.; Henne, M. T.; Royer, G. P. J. Electroanal.
   Chem. 1977, 80, 409.

- 11. Chang, C. K.; Liu, H.-Y.; Abdalmuhdi, I. J. Am. Chem. Soc. 1984, 106, 2725.
- 12. Sullivan, B. P.; Meyer, T. J. J. Chem. Soc. Chem. Commun. 1984
  1244.
- 13. Cabrera, C. R.; Arbruna, H. D. J. Electroanal. Chem. 1986, 209, 101.
- 14. Stalder, C. J.; Chao, S.; Summers, D. P.; Wrighton, M. S. J. Am. Chem. Soc. 1983, 105, 6318.
- 15. Cosnier, S.; Deronzier, A.; Moutet, J.-C. J. Electroania. Chem. 1986, 207, 315.
- 16. Bettelheim, A.; Ozer, D.; Harth, R.; Murray, R. W. J. Electroanla. Chem. 1988, 246, 139.
- 17. Jiang, R.; Dong, S. J. Electroanla. Chem. 1988, 246, 101.
- 18. Firth, B. E.; Miller, L. L. J. Am. Chem. Soc. 1976, 98, 8272.
- 19. Komori, T.; Nonaka, T. J. Am. Chem. Soc. 1984, 106, 2656.
- 20. Yamagishi, A.; Amarata, A. J. Chem. Soc. Chem. Commun. 1984, 452.
- 21. Yamagishi, A.; Amarata, A. J. Chem. Soc. Chem. Commun. 1985, 449.
- 22. Tse, D. C. S.; Kuwana, T. Anal. Chem. 1978, 50, 1315.
- 23. Fijihira, M.; Yokozawa, A.; Kinoshita, H.; Osa, T. Chem. Lett. 1982, 1089.

- 24. Salmon, M.; Bidan, G. J. Electrochem. Soc. 1985, 132, 1897.
- 25. Castner, J. F.; Hawkridge, F. M. J. Electroanal. Chem. 1983 143 217.
- 26. Allen, P. M.; Hill, H. A. O.; Walton, O. J. J. Electroanal. Chem. 1984, 178, 69.
- 27. Chao, S.; Wrighton, M. S. J. Am. Chem. Soc. 1987, 109, 5886.
- 28. Chao, S.; Simon, R. A.; Mallouk, T. E.; Wrighton, M. S. J. Am. Chem. Soc. 1988, 110, 2270.
- 29. Dhesi, R.; Cotton, T. M.; Timkovich, R. J. Electroanal. Chem. 1983, 154, 129.
- 30. Elliot, C. M.; Martin, W. S. J. Electroanal. Che. 1982, 137, 377.
- 31. Ye, J.; Baldwin, R. P. Anal. Chem. 1988, 60, 2263.
- 32. White, B. A.; Murray, R. W. J. Am. Chem. Soc. 1987, 109, 2576.
- 33. Fruge, D. R.; Fong, G. D.; Fong, F. K. J. Am. Chem. Soc. 1979, 101, 3694.
- 34. White, H. S.; Arbruna, H. D.; Bard, A. J. J. Am. Chem. Soc. 1982, 104, 265.
- 35. Noufi, R. N. J. Electrochem. Soc. 1983, 130, 2126.
- 36. Dubois, D. L. Inorg. Chem. 1984, 23, 2047.
- 37. Cook, R. L.; Sammells, A. F. J. Electrochem. Soc. 1985, 132, 2429.

- 38. Yamamoto, T. J. Chem. Soc. Chem. Commun. 1981, 187.
- 39. Kaufman, J. H.; Chung, T. C.; Heeger, A. J.; Wudl, F. J. Electrochem. Soc. 1984, 131, 2091.
- 40. Simon, R. A.; Mallouk, T. E.; Daube, K. A.; Wrighton, M. S. *Inorg*. Chem. 1985, 24, 3119.
- 41. Hagemeister, M. P.; White, H. S. J. Phys. Chem. 1987, 91, 150.
- 42. Holdcroft, S.; Morrison, R.; Funt, L. B. J. Electroanal. Chem.; 1988, 245, 191.
- 43. Garnier, F.; Tourillon, G.; Gazard, M.; Dubois, J. C. J. Electroanal. Che, 1983, 148, 299.
- 44. Smith, D. K.; Lane, G. A.; Wrighton, M. S. J. Phys. Chem. 1988, 92, 2616.
- 45. Viehbeck, A.; DeBerry, D. W. J. Electrochem. Soc. 1985, 132, 1369.
- 46. Elliott, C. M.; Redepenning, J. G. J. Electroanal Chem. 1986, 197, 219.
- 47. Yashima, H.; Kobayashi, M.; Lee, K.-B.; Chung, D.; Heeger, A. J.; Wudl, F. J. J. Electrochem. Soc. 1987, 134, 46.
- 48. Thackeray, J. W.; White, H. S.; Wrighton, M. S. J. Phys. Chem. 1986, 90, 6674.
- 49. Chao, S.; Wrighton, M. S. J. Am. Chem. Soc. 1987, 109, 6627.

- 50. Marrese, C. A.; Blubaugh, E. A.; Durst, R. A. J. Electroanal. Chem. 1988, 243, 193.
- 51. Kasem, K. K.; Abruna, H. D. J. Electroanal. Chem. 1988, 242, 87.
- 52. Wang, J.; Zadeii, J. Anal. Chim. Acta. 1987 188 187.
- 53. Harrison, D. J.; Wrighton, M. S. J. Phys. Chem. 1984, 88, 3103.
- 54. Fan, F.-R. F.; Hope, G. A.; Bard, A. J. J. Electrochem. Soc. 1982, 129, 1647.
- 55. Noufi, R.; Frank, A. J.; Nozik, A. J. J. Am. Chem. Soc. 1981, 103, 1849.
- 56. Rosenblum, M. D.; Lewis, N. S. J. Phys. Chem. 1984, 88, 3103.
- 57. Nanthakumar, A.; Armstrong, N. R. J. Electroanal. Chem. 1988, 248, 349.
- 58. Chidsey, C. E. D.; Murray R. W. Science 1986, 231, 25.
- 59. Wilbourn, K.; Murray R. W. J. Phys. Chem. 1988, 92, 3642.
- 60. Wrighton, M. S. Science 1986, 231, 32.
- 61. Shu, C.-F.; Wrighton, M. S. J. Phys. Chem. 1988, 92, 5221.
- 62. Lane, R. F.; Hubbard, A. T. J. Phys. Chem. 1973, 77, 1401.
- 63. Collman, J. P.; Marrocco, M.; Denisevich, P.; Koval, C.; Anson, F. C. J. Electroanal. Chem. 1979, 101, 117.

- Collman, J. P.; Anson, F. C.; Bencosme, C. S.; Durand, R. R. Jr.; Kreh,
   R. P. J. Am. Chem. Soc. 1983, 105, 2710.
- 65. Moses, P. R.; Wier, L. Murray, R. W. Anal. Chem. 1975, 47, 1882.
- 66. Merz, A.; Bard, A. J. J. Am. Chem. Soc. 1978, 100, 3222.
- 67. Itaya, K.; Bard A. J. Anal. Chem. 1978, 50, 1487.
- 68. Rolison, D. R.; Umana, M.; Burgmayer, P. Murray, R. W. Inorg. Chem. 1981, 20, 2996.
- 69. Umana, M.; Rolison, R.; Nowak, R.; Daum, P.; Murray, R. W. Surf. Sci. 1980, 101, 295.
- 70. Nowak, R.; Schultz, F. A.; Umana, M.; Abruna, H. D.; Murray R. W. J. Electroanal. Chem. 1978, 94, 219.
- 71. Dautartas, M. F.; Mann, K. R.; Evans, J. F. J. Electroanal. Chem. 1980, 110, 379.
- 72. Heider, G. H.; Gelbert, M. B.; Yacynych, A. M. Anal Chem. 1982, 54, 322.
- 73. Abruna, H. D.; Denisevich, P.; Umana, M.; Meyer, T. J.; Murray, R. W. J. Am. Chem. Soc. 1981, 103, 1.
- 74. Diaz, A. F. Logan, J. A. J. Electroanal. Chem. 1980, 111, 111.
- 75. Pham, M.-C.; Lacaze, P.-C.; Dubois, J.-E. J. Electroanal. Chem. 1979, 99, 331.
- 76. Ghosh, P.; Spiro, T. G. J. Electroche. Soc. 1981, 128, 1281.

- 77. Oyama, N.; Anson. F. C. J. Am. Che. Soc. 1979, 101, 739.
- 78. Nakahama, S.; Murray R. W. J. Electroanal. Chem. 1983, 158, 303.
- 79. Omaya N.; Shigehara, K.; Anson, F. C. Inorg. Chem. 1981, 20, 518.
- 80. Schneider, J.; Murray R. W. Anal. Chem. 1982, 54, 1508.
- 81. Dickstein, H.; Curran, D. J. The Pittsburg Conference and Exposition on Analytical Chemistry and Applied Spectroscopy; Atlantic City, NJ, March 1987 Abs.No. 442.
- 82. Shaw, B. R.; Creasy, K. E. Anal. Chem. 1988, 60, 1241.
- 83. Kulesza, P. J.; Mlodnicka, T.; Haber, J. J. Electroanal. Chem. 1988, 255, 53.
- 84. Creasy, K. E.; Shaw, B. R. Anal. Chem. 1989, 61, 1460.
- 85. Leech, D.; Wang, J.; Smith, M. R. Analyst, London 1990,115, 1447.
- 86. Oyama, N.; Anson, F. C. J. Electrochem. Soc. 1980, 127, 247.
- 87. Oyama, N.; Anson, F. C. J. Electrochem. Soc. 1980, 127, 249.
- 88. Oyama, N.; Shimomura, T.; Shigehara, K.; Anson, F. C. J. Electrochem. Soc. 1980, 112, 271.
- 89. Oyama, N.; Anson, F. C. J. Electrochem. Soc. 1980, 127, 640.
- 90. Facci, J.; Murray, R. W. J. Phys. Chem. 1981, 86, 2870.
- 91. Mortimer, R. J.; Anson, F. C. J. Electroanal. Chem. 1982, 138, 325.

- 92. Bruce, J. A.; Wrighton, M. S. J. Am. Chem. Soc. 1982, 104, 74.
- 93. Majda, M. Faulkner, L. R. J. Electroanal. Chem. 1984, 169, 77.
- 94. Majda, M.; Faulkner, L. R. J. Electroanal. Chem. 1984, 169, 97.
- 95. Shaw, B. R.; Haight, G. P. Jr.; Faulkner, L. R. J. Electroanal. Chem. 1982, 140, 147.
- 96. Eisenberg, A.; Yeager Eds.; Perfluoro Sulfonate Ionomer Membranes, A. C. S. Symposium Series 180; American Chemical Society, Washington, DC, 1982.
- 97. Buttry, D. A.; Anson, F. C. J. Am. Chem. Soc. 1982, 104, 4824.
- 98. Buttry, D. A.; Anson, F. C. J. Am. Chem. Soc. 1983, 105, 685.
- 99. Anson, F. C.; Saveant, J.-M. J. Am. Chem. Soc. 1984, 178, 113.
- 100. Rubinstein, I.; Bard, A. J. J. Am. Chem. Soc. 1980, 102, 6641.
- 101. White, H. S.; Leddy, J.; Bard, A. J. J. Am. Chem. Soc. 1982, 104, 4811.
- 102. Martin, C. R.; Rubinstein, I.; Bard, A. J. J. Am. Chem. Soc. 1982, 104, 4817.
- 103. Henning, T. P.; Bard A. J. J. Electrochem. Soc. 1983, 130, 613.
- 104. Szentirmay, M. N.; Martin, C. R. Anal. Chem. 1984, 56, 1898.
- 105. Martin, C. R. Anal. Chem. 1982, 54, 1639.
- 106. Martin, C. R.; Dollard, K. A. J. Electroanal. Chem. 1983, 159, 127.

- 107. Penner, R. M.; Martin, C. R. J. Electrochem. Soc. 1985, 132, 514.
- 108. Neff, V. D. J. Electrochem. Soc. 1978, 125, 886.
- 109. Bocarsly, A. B.; Sinha, S. J. Electroanal. Chem. 1982, 137, 157.
- 110. Humphrey, B. D.; Sinha, S.; Bocarsly, A. J. Phys. Chem. 1984, 88, 736.
- 111. Joseph, J.; Gomathi, H.; Rao, G. P. J. Electroanal. Chem. 1991, 304, 263.
- 112. Itaya, K.; Shibayama, K.; Akahoshi, H.; Toshima, S. J. Appl. Phys. 1982, 53, 1498.
- 113. Ghosh, P. K.; Bard, A. J. J. Am. Chem. Soc. 1983, 105, 5691.
- 114. Kamat, P. V. J. Electroanal. Chem. 1984, 163, 389.
- 115. Ege, D.; Ghosh, P. K.; White, J. R.; Equey, J.-R.; Bard. A. J. J. Am. Chem. Soc. 1985, 107, 5644.
- 116. Itaya, K.; Bard, A. J. J. Phys. Chem. 1985, 89, 5565.
- 117. Liu, H.-Y.; Anson, F. C. J. Electroanal. Chem. 1985, 184, 411.
- 118. White, J. R.; Bard, A. J. J. Electroanal. Chem. 1986, 197, 233.
- 119. Mauricio, C.-A. C.; Fan, F.-R. F.; Bard, A. J. J. Electroanal. Chem. 1987, 234, 347
- 120. King, R. D.; Nocera, G. D.; Pinnavaia, T. J. J. Electroanal. Chem. 1987, 236, 43.

- 121. Fitch, A.; Fausto, C. L. J. Electroanal. Chem. 1988, 257, 299.
- 122. Fitch, A.; Lavy-Feder, A.; Lee, S. A.; Kirsh, M. T. J. Phys. Chem. 1988, 92, 6665.
- 123. Rong, D.; Kim, Y. I.; Mallouk, E. T. Inorg. Chem. 1990, 29, 1531.
- 124. Murray, G. C.; Nowark, R. J.; Rolison, D. R. J. Electroanal. Chem. 1984, 164, 205.
- 125. Gemborys, H. A.; Shaw, B. R. J. Electroanal. Chem. 1986, 208, 95.
- 126. Iwakura, C.; Miyazaki, S.; Yoneyama, H. J. Electroanal. Chem. 1988, 246, 63.
- 127. El Murr, N.; Kerkeni, M.; Sellami, A.; Taarit, Y. B. J. Electroanui. Chem. 1988, 246, 461.
- 128. Li, Z.; Mallouk, T. E. J. Phys. Chem. 1987, 91, 643.
- 129. Itaya, K.; Chang, H.-C.; Uchida, I. Inorg. Chem. 1987, 26, 624.
- 130. Shaw, B. R.; Creasy, K. E. J. Electroanal. Chem. 1988, 243, 209.
- 131. Keita, B.; Nadjo, L.; Haeussler, J. P. J. Electroanal. Chem. 1988, 243, 481.
- 132. Renneke, R.-F.; Hill, C. L. J. Am. Chem. Soc. 1986, 108, 3528.
- 133. Mizumo, N.; Watanabe, T.; Misono, M. J. Phys. Chem. 1985, 89, 80.
- 134. Miller, C. J.; Majda, M. J. Electroanal. Chem. 1986, 207, 49.

- 135. Miller, C. J.; Widrig, C. A.; Charych, D. H.; Majda, M. J. Phys. Chem. 1988, 92, 1928.
- 136. Lee, H.; Kepley, L. J.; Hong, H.-G.; Akhter, S.; Mallouk, T. E. J. Phys. Chem. 1988, 92, 2597.
- 137. Kulesza, P. J.; Faulkner, L. R. J. Am. Chem. Soc. 1988, 110, 4905.
- 138. Kulesza, P. J.; Faulkner, L. R. J. Electroanal. Chem. 1988, 248, 305.
- 139. Oyama, N.; Anson, F. C. J. Electroanal. Chem. 1986, 199, 467.
- 140. Rudzinski, W. E.; Bard, A. J. J. Electroanal. Chem. 1986, 199, 323.
- 141. Pinnavaia, T. J. Science 1983, 220, 365.
- 142. Yamagishi, A.; Amarata, A. J. Chem. Soc. Chem. Commun. 1984, 452.
- 143. Yamagishi, A.; Amarata, A. J. Electroanal. Chem. 1985, 191, 449.
- 144. Lee, S. A.; Fitch, A. J. Phys. Chem. 1990, 94, 4998.
- 145. Inoue, H.; Haga, S.; Iwakura, C.; Yoneyama, H. J. Electroanal. Chem. 1988, 249, 133.
- 146. King, R. D. Ph. D. Dissertation, Michigan State University.
- 147. Bard, A. J.; Faulkner, L. R. Electrochemical Methods
  Fundamentals and Applications; Wiley, New York, 1980.

- 148. Amatore, C.; Saveant, J. M.; Tessier, D. J. Electroanal. Chem. 1983, 146, 37.
- 149. Amatore, C.; Saveant, J. M.; Tessier, D. J. Electroanal. Chem. 1983, 147, 39.
- 150. Sabatani, E.; Rubenstein, I. J. Phys. Chem. 1987, 91, 6663.
- 151. Kissinger, P. T.; Heineman, W. R. Laboratory Techniques in Electroanalytical Chemistry, Marcel Dekker, Inc. New York.
- 152. Stalnaker, N. D.; Solenberger, J. C.; Wahl, A. C. J. Phys. Chem. 1977, 81, 601.
- 153. Burstall, F. H.; Nyholm, R. S. J. Chem. Soc. 1952, 3570.
- 154. Oyama, N.; Anson F. C. J. Am. Chem. Soc. 1979, 101, 3450.
- 155. McQuillan, A. J.; Reid, M. R. J. Electroanal. Chem. 1985 194 237.
- 156. Raythatha, R.; Sen, P. N. J. Colloid. Interface. Sci. 1986, 109, 301.
- 157. Berkheiser, V. E.; Mortland, M. M. Clays Clay Miner. 1977, 25, 105.
- Traynor, M. F.; Mortland M. M.; Pinnavaia T. J. Clays Clay Miner.
   1978 26 318.
- 159. Krenske, D.; Abdo, S.; Van Damme, H.; Cruz, M.; Fripiat, J. J. *Phys. Chem.* 1980, 84, 2447.
- 160. Abdo, S.; Canesson, P.; Cruz, M.; Fripiat, J. J.; Van Damme, H. J. Phys. Chem. 1981, 85, 797.

- 161. Yamagishi, A.; Soma M. J. J. Am. Chem. Soc. 1981, 103, 4640.
- 162. Yamagishi, A. J. Phys. Chem. 1982, 86, 2472.
- 163. Yamagishi, A. J. Chem. Soc. Dalton Trans. 1983, 679.
- 164. Yamagishi, A. Inorg. Chem. 1983, 21, 3393.
- 165. Taniguchi, M.; Yamagishi, A.; Iwamoto, T. *Inorg. Chem.* 1991, 30, 2462.
- 166. Thomas, J. K. Acc. Chem. Res. 1988, 21, 275.
- 167. Fripiat, J. J.; Helsen, J. Clays and Clay Miner. 1966, 14, 163.
- 168. Dailey, J.; Pinnavaia, T. J. J. Inclusion Phenom. 1991, Submitted.
- 169. Stucki, J. W.; Golden, D. C.; Roth, C. B. Clays and Clay Miner. 1984, 32, 350.
- 170. Itaya, K.; Uchida, I. Inorg. Chem. 1986, 25, 389.
- 171. Itaya, K.; Uchida, I.; Neff, V. D. Acc. Chem. Res. 1986, 19, 162.
- 172. Deakin, M. R.; Stutts, K. J.; Wightman, R. M. J. Electroanal. Chem. 1985, 182, 113.

#### CHAPTER IV

### LAYERED DOUBLE HYDROXIDE MODIFIED ELECTRODES.

### IV.a Background

Itaya et al showed that the layered double hydroxides can be used to modify an electrode surface. Mo(CN)8<sup>4-</sup>, Fe(CN)6<sup>3-</sup>, and IrCl6<sup>2-</sup> have been incorporated into the hydrotalcite films coated on tin oxide electrodes by soaking the electrodes in solutions of the desired anion. Reversible steady state waves for all the three anions were reported with an initial decrease in the peak current as in the case of clay modified electrodes. After this initial report, Shaw and Creasy have reported electrochemistry of catechol oxidation at layered double hydroxide composite electrodes. An improvement in the chemical reversibility and the charge transfer kinetics were observed at LDH composite electrodes compared to that of an unmodified electrode.<sup>2</sup>

# Polyoxometalates (POMs)

Polyoxometalates are a large group of compounds with the general formula  $[X_x M_m O_y]^{q-}$ ; where X is generally a non metal ion and X < M. When x = 0, the anions are called isopolyoxometalates and compounds with x > 0 are called heteropolyoxometalates. The familiar Keggin-type polyoxometalates are based on a central

tetrahedron  $XO_4$  which is surrounded by twelve  $MO_6$  octahedra arranged in four groups of three edge shared octahedra,  $M_3O_{13}$ . These groups are linked by sharing corners to each other and to the central  $XO_4$  tetrahedron (Figure IV.1).<sup>3</sup> Most of the polyoxometalates have either the Keggin structure  $[XM_{12}O_{40}]^{n-}$  or structures derived from fragments of that structure. They are stable only at low pH and begin to decompose at pH higher than 5.

Under appropriate oxidation states, the ability of polyoxometalates to catalyze various reactions such as hydrogenation of olefins<sup>3-6</sup>, reduction of nitrite and nitric oxide to ammonia<sup>7</sup>, have been reported. It has also been demonstrated that polyoxometalates can be used to modify electrode surfaces to obtain very durable and robust modified materials and to reduce oxygen efficiently in acidic media.<sup>8-12</sup> Keita and Nadjo have effectively immobilized [SiW<sub>12</sub>O<sub>40</sub>]<sup>4-</sup> and [P<sub>2</sub>W<sub>18</sub>O<sub>62</sub>]<sup>6-</sup> in polymeric metrices.<sup>13</sup> [SiW<sub>11</sub>O<sub>39</sub>]<sup>8-</sup>, known as the lacunary form, and its iron substituted form exhibit very well developed reversible multi-step and multi-electron transfer reactions with catalytic properties.<sup>7,14</sup>

### IV.b Experimental

Preparation of Polyoxometalate Intercalated Layered Double Hydroxides.

Intercalation of polyoxometalates into the galleries of layered double hydroxides generates a new class of compounds with

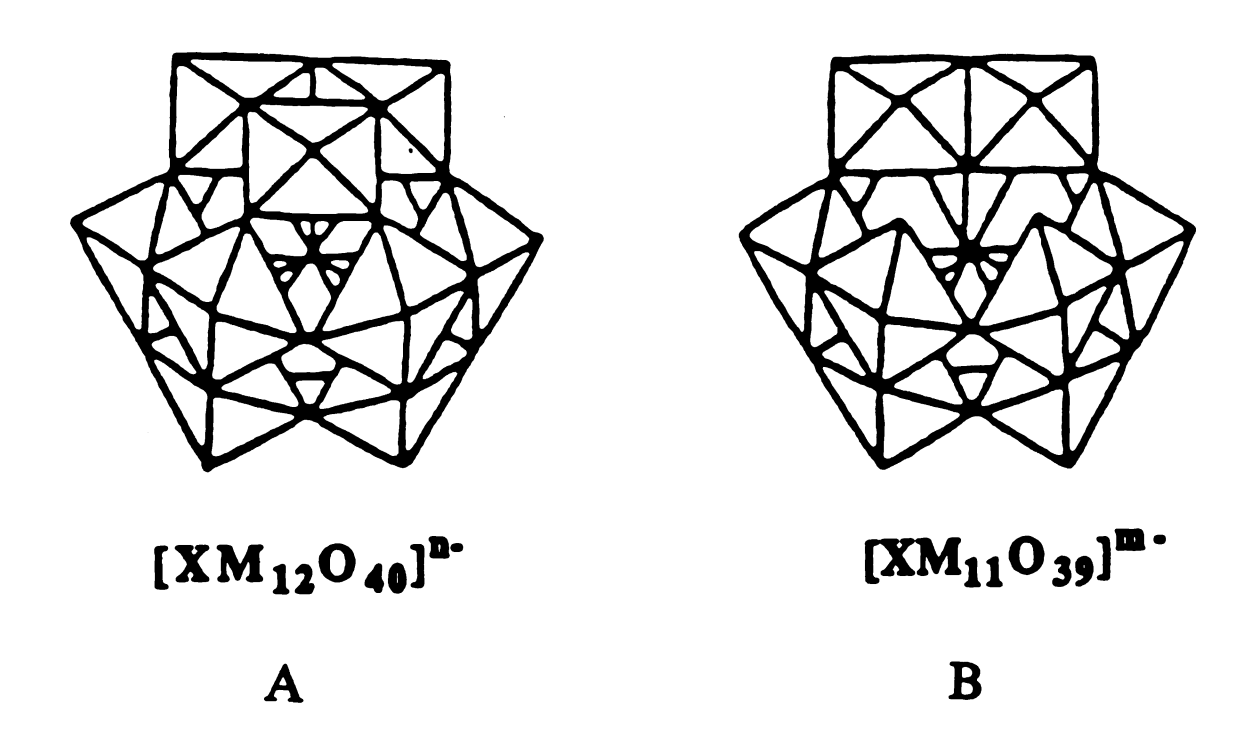


Figure IV.1 Structure of (A) Keggin-type and (B) lacunary Keggin-type polyoxometalates.

microporocity and selective catalytic properties.<sup>15-16</sup> These features can be utilized to generate new electrochemical and electrocatalytic systems in order to achieve selective oxidation reduction reactions.

Hydrotalcite-like, [Mg<sub>1-x</sub>Al<sub>x</sub>]-CO<sub>3</sub>, LDHs are known to decompose to magnesium-aluminum oxide solid solutions by heating to 400-800 °C. The resulting oxides readily rehydrate and adsorb anions to reconstruct the original LDHs.<sup>17-20</sup> This thermal decomposition and subsequent reconstruction property of the LDH was utilized to prepare the LDHs pillared by  $\alpha$ -[SiW<sub>11</sub>O<sub>39</sub>]<sup>8</sup>- and  $\alpha$ -[SiV<sub>3</sub>W<sub>9</sub>O<sub>40</sub>]<sup>7</sup>-. The parent layered double hydroxide, [Zn<sub>0.67</sub>  $Al_{0.33}$  (OH)<sub>2</sub>] (CO<sub>3</sub>)<sub>0.17</sub> 0.33(H<sub>2</sub>O), was formed by coprecipitation reaction of Zn<sup>2+</sup>, Al<sup>3+</sup> and CO<sub>3</sub><sup>2-</sup> at pH 6.2.<sup>21</sup> The LDH was then calcined in air at 500 °C for 3 hrs to form a mix oxide. Restructuring of the oxide into a POM-pillared LDH accomplished by adding the calcined product in small portions to a 10 mM POM solution with vigorous stirring at a POM/Al mol ratio of 1.0. The dropwise addition of 0.2 M HNO<sub>3</sub> maintained the pH at the desired value and prevented POM hydrolysis. Upon addition of the oxide, the mixture was allowed to stir for 30 min. All the reactions were carried out under argon to avoid possible reaction of the calcined oxide with CO<sub>2</sub>. The final products were washed with water and dried in air at 90 °C.22

# Preparation of LDH Modified Electrodes

A method similar to that described by Itaya was used to prepare the modified electrodes.<sup>1</sup> One gram of hydrotalcite, (HT),

chloride was dispersed in 100 ml of distilled deionized water and centrifuged at 2000 rpm for 1 hr. The white precipitate was discarded and the supernatant was used for film preparation. Films were cast by allowing 10  $\mu$ L of the suspension to evaporate at room temperature under humidified air for 18 hrs. Electroactive species were intercalated either by soaking in a solution of the desired species or by pre-exchange as described in the intercalation procedure.

### IV.c Results and Discussion

A cyclic voltammogram recorded for a 20 mM solution of SiW<sub>11</sub>O<sub>30</sub>8-, in 0.1 M CH<sub>3</sub>CO<sub>2</sub>Na buffered at pH 5, with a bare graphite electrode is shown in Figure IV.2. Two distinct two-electron reversible waves were obtained as reported in the literature.7,14 These responses have been assigned to the addition and removal of electrons from predominantly non-bonding orbitals within the four tungsten-oxide triads within the polyanion.<sup>3</sup> However, if an electrode coated with hydrotalcite chloride was employed, no electroactivity was observed even if the electrode was allowed to be in the solution for 24 hrs (Figure IV.3). Cyclic voltammogram for the SiW<sub>11</sub>O<sub>39</sub><sup>8</sup>- pre-exchanged into hydrotalcite is depicted in Figure Again no electroactivity was detected for the intercalated SiW<sub>11</sub>O<sub>39</sub>8-. In contrast to the SiW<sub>11</sub>O<sub>39</sub>8-, electroactivity for intercalated Fe(CN)63- was observed as reported by Itaya et el.1 Figure IV.5 shows the electrochemical responses of Fe(CN)63-

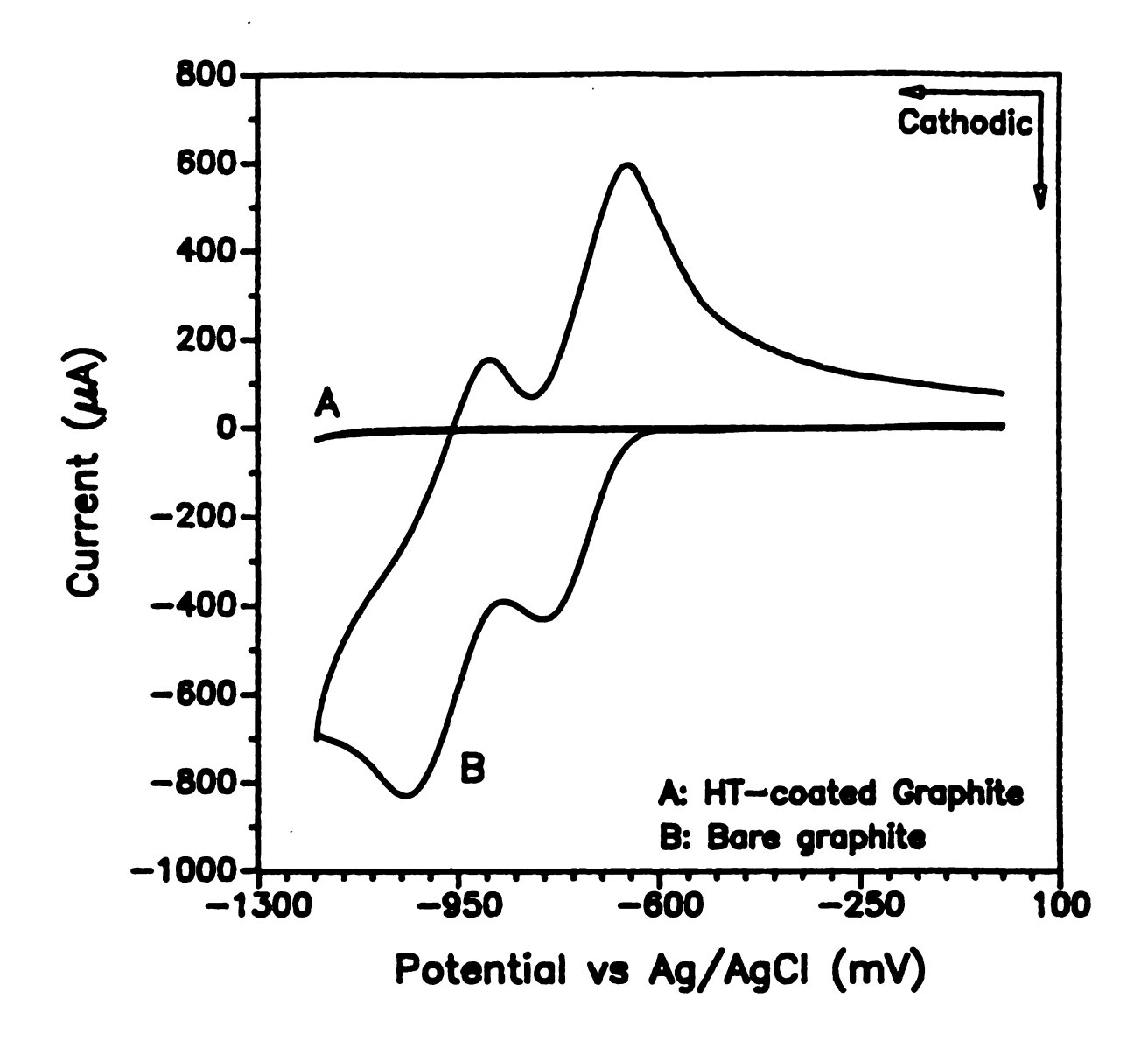


Figure IV.2 Cyclic voltammogram of  $SiW_{11}O_{39}^{8-}$  at a bare graphite and a hydrotalcite coated graphite electrode. Supporting electrolyte was 0.1 M sodium acetate buffer pH 5. v=100 mV sec<sup>-1</sup>.

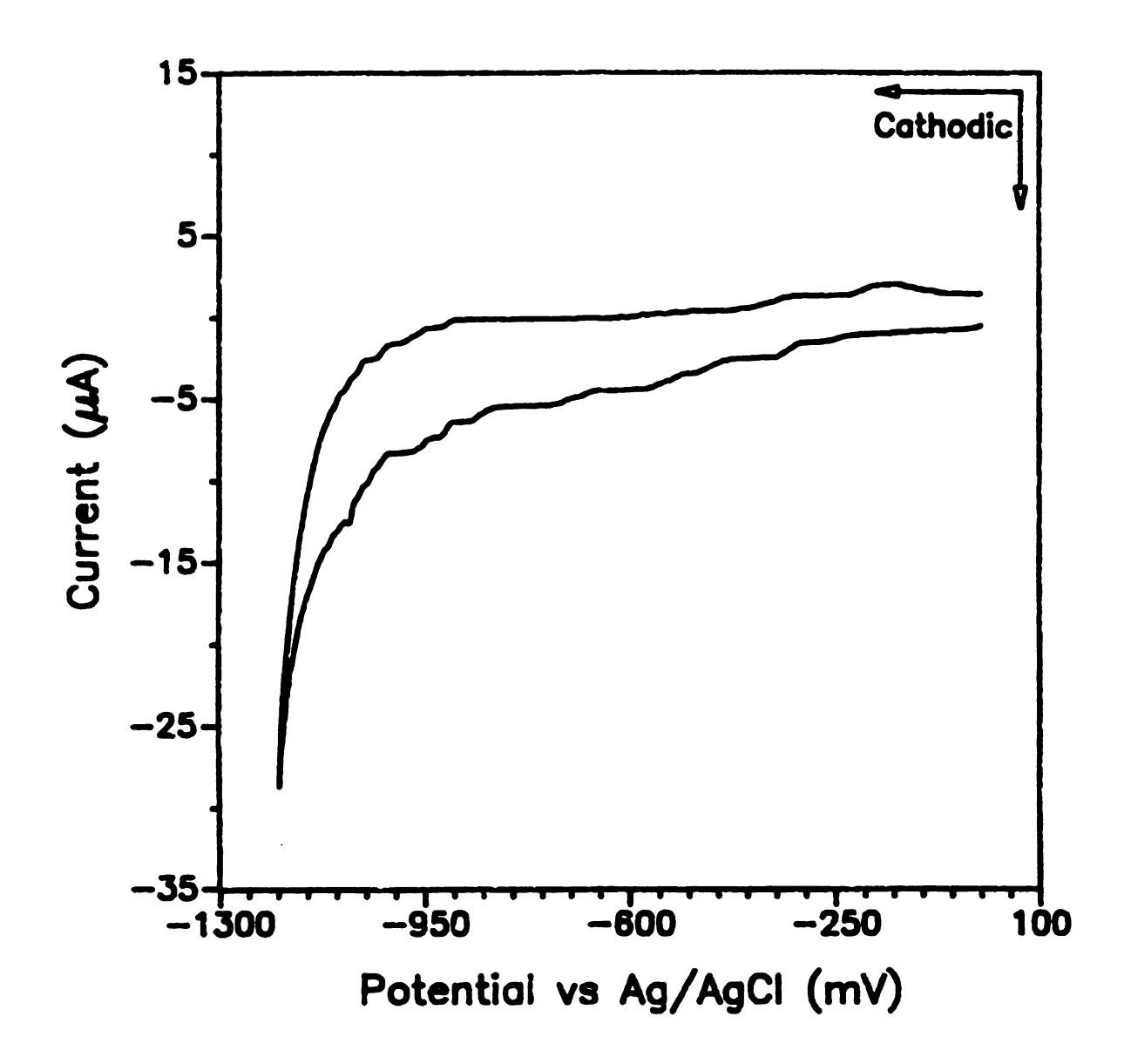


Figure IV.3 Cyclic voltammogram of  $SiW_{11}O_{39}^{8-}$  at a hydrotalcite coated graphite electrode (pre-soaked). Supporting electrolyte was 0.1 M sodium acetate buffer pH 5. v=100 mV sec<sup>-1</sup>.

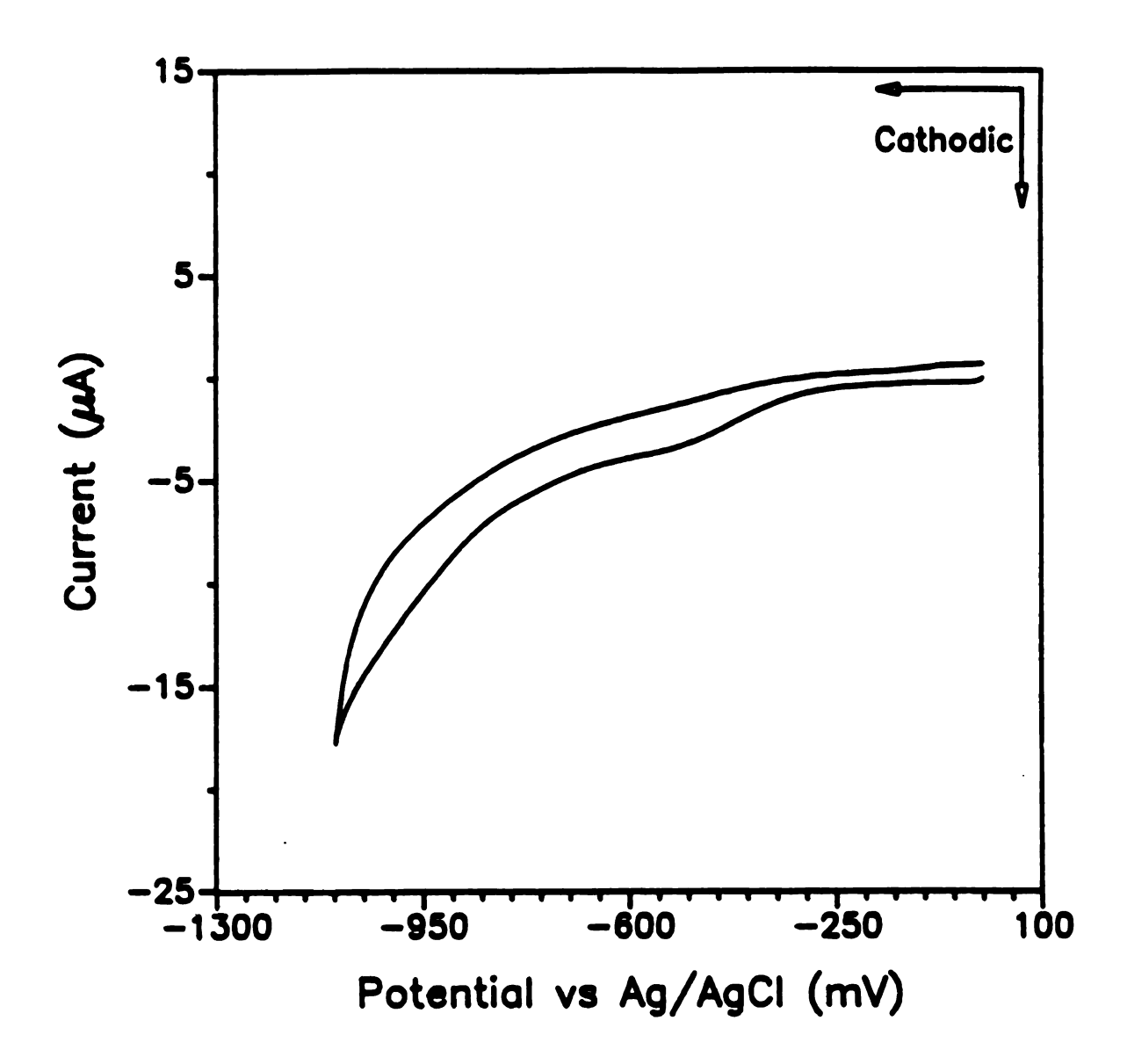


Figure IV.4 Cyclic voltammogram of  $SiW_{11}O_{39}^{8-}$  at a hydrotalcite coated graphite electrode (pre-exchanged). Supporting electrolyte was 0.1 M sodium acetate buffer pH 5. v=100 mV sec<sup>-1</sup>.

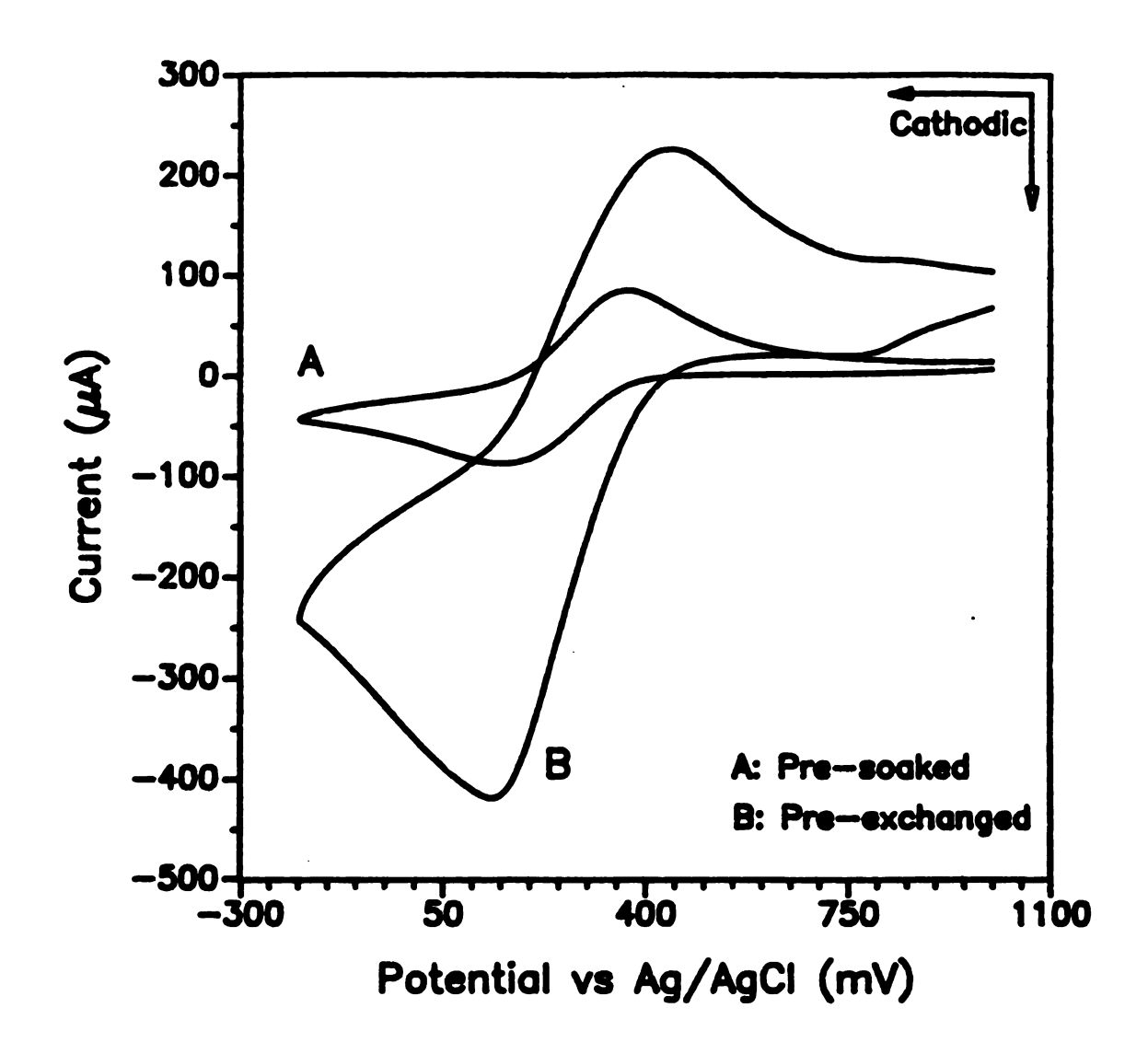


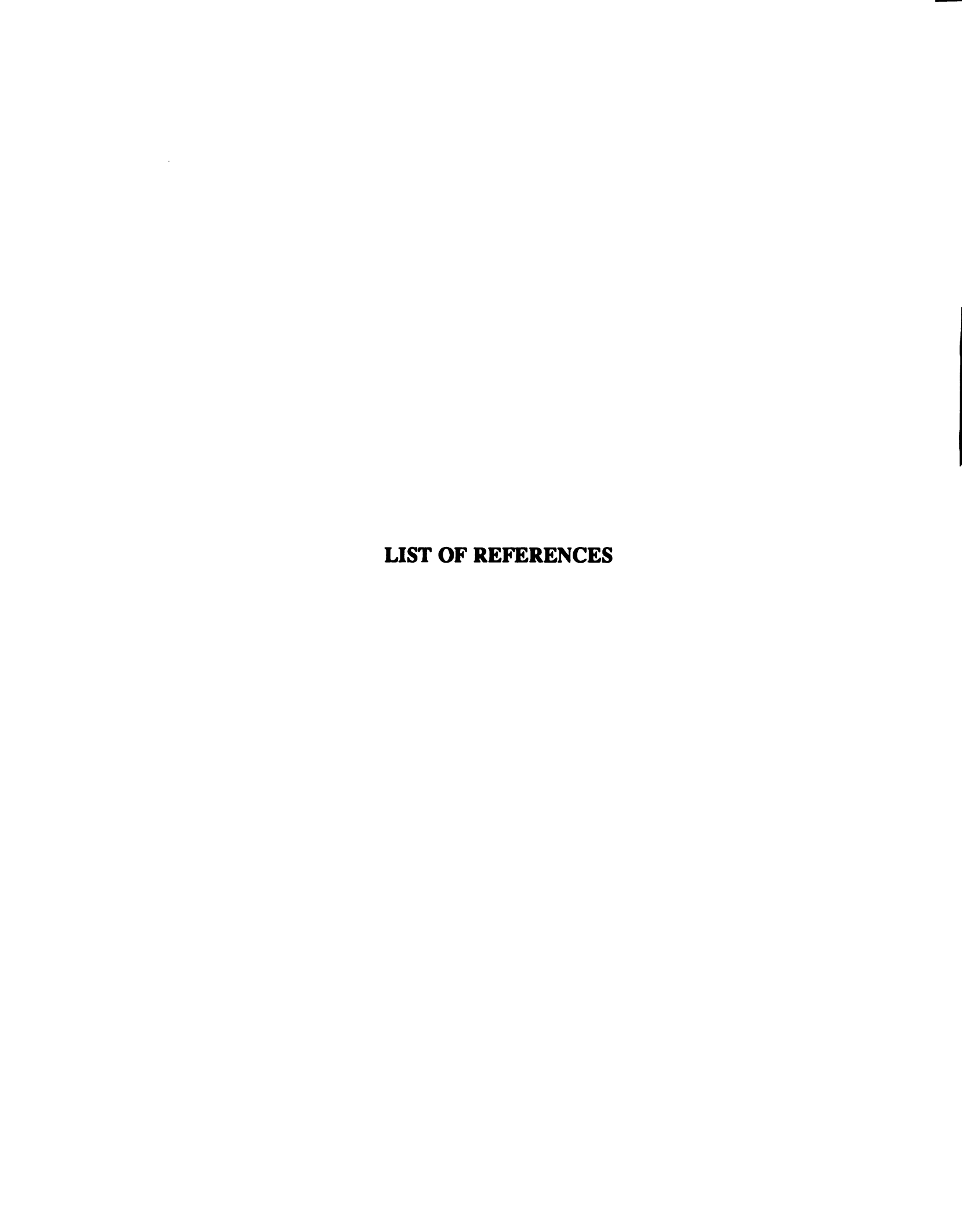
Figure IV.5 Cyclic voltammogram of  $Fe(CN)_6^{3-}$  at a hydrotalcite coated graphite electrode (pre-exchanged). Supporting electrolyte was 0.05 M sodium sulfate. v = 100 mV sec<sup>-1</sup>.

intercalated both by pre-exchanging and by soaking in a 20 mM  $Fe(CN)_6^{3-}$ .

These observations indicate that  $SiW_{11}O_{39}^{8-}$  is electroinactive in the galleries or the anion exchange sites of the hydrotalcite layers; whereas  $Fe(CN)_6^{3-}$  exhibit electroactivity when they are in hydrotalcite anion exchange sites. This may be because the  $SiW_{11}O_{39}^{8-}$  anions are tightly bound to the layered double hydroxide as in the case of trispolypyridyl metal complexes with silicate clays. On the other hand unlike trispolypyridyl metal complexes,  $SiW_{11}O_{39}^{8-}$  do not seem to form ion pairs. Therefore, the electroactivity for soaked electrodes were not also possible. The reason for the electroactivity of  $Fe(CN)_6^{3-}$  in hydrotalcite films is probably due to the mobility of these anions within the hydrotalcite layers as in the case of  $Ru(NH_3)_6^{3+}$  in clay modified electrodes.<sup>25</sup>

#### IV.d Conclusions

Polyoxometalates do not exhibit electroacivity in hydrotalcite layers probably due to immobility of these large anions within these films. However,  $Fe(CN)_6^{3-}$ , being a small anion, can easily diffuse to the electrode surface, through the layered double hydroxide film, to exhibit the electron transfer.



### LIST OF REFERENCES

- 1. Itaya, K.; Chang, H.-C.; Uchida, I. Inorg. Chem. 1987, 26, 624.
- 2. Shaw, B. R.; Creasy, K. E. J. Electroanal. Chem. 1988, 243, 209.
- 3. Pope, M. T. Heteropoly and isopoly Oxometalates, Springer, Berlin, Heidelberg, 1983.
- 4. Urabe, K.; Tanaka, Y.; Izumi, Y. Chem. Lett. 1985, 1595.
- 5. Renneke, R. F.; Hill, C. L. J. Am. chem. Soc. 1986, 108, 3528.
- 6. Izumi, Y.; Urabe, K. Chem. Lett. 1981, 663.
- 7. Toth, J. E.; Anson, F. C. J. Am. Che. Soc. 1989, 111, 2444.
- 8. Keita, B.; Nadjo, L. J. Electroanal. Chem. 1985, 191, 441.
- 9. Keita, B.; Nadjo, L.; Krier, G.; Muller, J.F. J. Electroanal. Chem. 1987, 223, 287.
- 10. Keita, B.; Nadjo, L. J. Electroanal. Chem. 1986, 199, 229.
- 11. Keita, B.; Nadjo, L.; Haeussler, J. P. J. Electroanal. Chem. 1987, 230, 85.
- 12. Keita, B.; Nadjo, L. J. Electroanal. Chem. 1987, 227, 265.

- 13. Keita, B.; Nadjo, L. J. Electroanal. Chem. 1988, 240, 325.
- 14. Toth, J. E.; Anson, F. C. J. Electroanal. Chem. 1988, 256, 361.
- 15. Miyata, S.; Kumura, T. Chem. Lett. 1973, 843.
- 16. Kwon, T.; Tsigdinos, G. A.; Pinnavaia, T. J. J. Am. Chem. Soc. 1988, 110, 3653.
- 17. Chibwe, K.; Jones, W. Chem. Matter. 1989, 1, 489.
- 18. Sato, T.; Wakabayashi, T.; Shimada, M. Ind. Eng. Chem. Prod. Res. Dev. 1986, 25, 89.
- 19. Chibwe, K.; Jones, W. J. Chem. Soc. Chem. Commun. 1989, 926.
- 20. Narita, E.; Yamagishi, T. Proc. 9th Int. Clay Conf. 1989 in press.
- 21. Miyata, S. Clays and Clay Miner. 1980, 28, 50.
- 22. Narita, E.; Kaviratna, P. DeS.; Pinnavaia, T. J. Chem. Lett. 1991, 805.
- 23. Kaviratna, P. DeS.; Pinnavaia, T. J. J. Electroanal. Chem. 1991 submitted.